

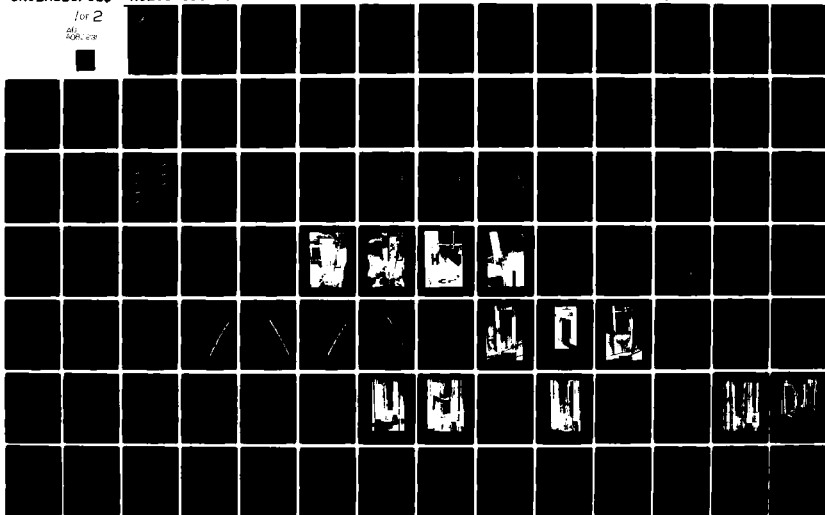
AD-A082 231

HERCULES INC CUMBERLAND MD ALLEGANY BALLISTICS LAB F/6 11/4  
DESIGN, PROTOTYPE FABRICATION AND MANUFACTURING TECHNIQUES FOR --ETC(U)  
NOV 79 W B STEWART DAAG46-77-C-0069  
A0296-610-03-009 AMMRC-TR-79-55 NL

UNCLASSIFIED

for 2

46  
206,000



ADA 082231



*B.S.*

AD

AMMRC TR 79-55

DESIGN, PROTOTYPE FABRICATION AND MANUFACTURING  
TECHNIQUES FOR A COMPOSITE BOX BEAM

NOVEMBER 1979

W. B. STEWART  
Hercules Aerospace Division  
Hercules Incorporated  
Allegany Ballistics Laboratory  
Cumberland, MD 21502

Final Report DAAG46-77-C-0069

Approved for public release; distribution unlimited.

DTIC  
MAR 24 1980

A

Prepared for

ARMY MATERIALS AND MECHANICS RESEARCH CENTER  
Watertown, Massachusetts 02172

DDC FILE COPY

80 3 21 013

The findings in this report are not to be construed as an official Department of the Army position, unless so designated by other authorized documents.

Mention of any trade names or manufacturers in this report shall not be construed as advertising nor as an official indorsement or approval of such products or companies by the United States Government.

**DISPOSITION INSTRUCTIONS**

Destroy this report when it is no longer needed.  
Do not return it to the originator.

UNCLASSIFIED

SECURITY CLASSIFICATION OF THIS PAGE (When Data Entered)

REPORT DOCUMENTATION PAGE		READ INSTRUCTIONS BEFORE COMPLETING FORM	
1. REPORT NUMBER AMMRC 79-55	2. GOVT ACCESSION NO. TR-99-55	3. RECIPIENT'S CATALOG NUMBER 9	
4. TITLE (and Subtitle) DESIGN, PROTOTYPE FABRICATION AND MANUFACTURING TECHNIQUES FOR A COMPOSITE BOX BEAM.		5. TYPE OF REPORT & PERIOD COVERED Final Report, Oct 1977 - Jun 1979	
7. AUTHOR(s) W. B. Stewart		6. PERFORMING ORG. REPORT NUMBER A0296-610-03-009	
9. PERFORMING ORGANIZATION NAME AND ADDRESS Hercules Aerospace Division Hercules Incorporated Allegany Ballistics Laboratory Cumberland, MD 21502		10. PROGRAM ELEMENT, PROJECT, TASK AREA & WORK UNIT NUMBER D/A Project: 1L2631020071 AMCMS Code: 623102 0710012 Agency Accession: DAOG 4804	
11. CONTROLLING OFFICE NAME AND ADDRESS Army Materials and Mechanics Research Center Watertown, Massachusetts 02172		12. REPORT DATE Nov 1979	
14. MONITORING AGENCY NAME & ADDRESS (if different from Controlling Office)		13. NUMBER OF PAGES 12/122	
		15. SECURITY CLASS. (of this report) Unclassified	
16. DISTRIBUTION STATEMENT (of this Report)  Approved for public release; distribution unlimited.		15a. DECLASSIFICATION/DOWNGRADING SCHEDULE	
17. DISTRIBUTION STATEMENT (of the abstract entered in Block 20, if different from Report)			
18. SUPPLEMENTARY NOTES			
19. KEY WORDS (Continue on reverse side if necessary and identify by block number)  Composite materials; fiber composites; filament wound composites; composite beams; static tests; buckling failure.			
20. ABSTRACT (Continue on reverse side if necessary and identify by block number)  Several composite systems were evaluated and the most appropriate was selected to fabricate two geometric half-scale versions of a full scale traversing launch beam. One beam was subsequently tested in four-point- bending.			

DD FORM 1473 1 JAN 73 EDITION OF 1 NOV 65 IS OBSOLETE

UNCLASSIFIED

SECURITY CLASSIFICATION OF THIS PAGE (When Data Entered)

401824

JOB

## SUMMARY

The U. S. Army is investigating advanced concepts for mobile assault bridging. One bridging concept which is being featured in the "Bridging for the Eighties" trilateral program is a vehicle mounted folding bridge which is positioned across an obstruction by means of a multi-segmented traversing (launch) beam. The launch beam is a weight/size and flexural modulus critical system element, suited to the advantages of fibrous composite design and fabrication.

Hercules/ABL was contracted by Army Materials and Mechanics Research Center (AMMRC) to investigate the merits of advanced composites as materials of construction for the launch beam. The principal initial program objectives were (1) to design a composite beam segment capable of carrying the anticipated system loads established by AMMRC, and (2) to investigate fabrication techniques via the construction of subscale beam segments.

AMMRC recognized that an important requirement of the multi-segment traversing beam as ultimately used will be moment and shear resistant connections at the beam ends, allowing unitized construction and beam folding for transportation. However, such joints represent a significant design challenge, beyond the scope and resources of this feasibility investigation, and were not included as a feature in this design/fabrication program, except that the beam designs were to be amenable to the eventual incorporation of joints.

Subsequent to program initiation, additional objectives were identified and work funded for their investigation. These included (1) determination of the flexural and shear strength and beam rigidity of the subscale

Availability Codes	
Dist.	Avail and/or special
A	

units fabricated, and (2) the design, fabrication, and testing of tension and compression specimens representative of the pin end joints/connections.

The approach taken to achieve the above objectives was: (1) design a full scale traversing beam segment (12.11 in. x 25 in. x 21 ft, 3 in.), without end connectors, to resist specified loading, including 460 kip-feet of moment, within a 20 lb/ft weight constraint, for a 7 meter span and with a flexural rigidity exceeding that of a baseline aluminum design, (2) characterize and select materials for the design which will provide adequate margins of safety, (3) design and fabricate two half-scale prototype traversing beams of the full scale design, (4) structurally test one of the half-scale prototype beams in a four-point-bending arrangement, to establish flexural strength, and then test a short undamaged section in three-point-bending to determine shear and web buckling strengths, and (5) design, fabricate, and test four pin-bearing end connectors for the top and bottom flanges of the full scale beam; two in tension and two in compression.

Based upon the initial trade studies and preliminary design calculations, the materials which exhibited the best potential ability to withstand the load, environment, and fatigue life requirements, and stay within the 20 lb/ft weight constraint were identified as AS graphite fiber and HBRF-55A epoxy. Other materials considered were HMS graphite and Kevlar-49 fibers and epoxy resins. The optimum cross sectional configuration was established as a box and the selected materials were used to fabricate two half-scale prototype box beams.

One of the half-scale beams was destructively tested in four-point-bending and the other, along with small undamaged sections from the tested

beam was delivered to AMMRC for further examination.

The results of the structural test were below anticipated with a failure load of only 25,000 lb ( $5.30 \times 10^5$  in.-lb) as compared to a value of 43,000 lb ( $0.91 \times 10^6$  in.-lb) predicted. The low failure load appeared to be due to a load pad crushing of the upper flange. The principal cause of premature failure was the inability to load the beam cross section in the manner for which it was designed; namely, as a segment highly moment loaded at the ends via moment resistant joints. To produce the design moments in the fabricated half-scale beam, which did not have moment resistant joints, required a series of large concentrated loads. The half-scale constant cross section beams were not designed to resist large concentrated loads, particularly in the web-to-flange transition regions which crushed out prematurely causing beam collapse. In scaling from the full-size to half-size box beam, shear strength is reduced by only the square of the scale ratio whereas flexural strength is reduced by the cube of this ratio. The unfavorable scaling of shear to flexural strength further complicated bend testing to produce a flexural failure. Mathematical calculations, however, yielded very good correlation between experimental and predicted results for flexural rigidity, strains, and deflections, up to the failure load.

In the short beam test, which was intended to determine the web shear buckling strength, failure occurred at a load of ~28,500 lb. The failure was, again, due to crushing in the web-to-flange transition region but occurred at a load well above the critical web shear buckling prediction of 20,000 lb based on classical orthotropic plate buckling theory.

Materials identical to those used to fabricate the box beams were then used to fabricate four pin-bearing end connectors; two of which were tested

in tension and two in compression. One damaged compression specimen was also shipped to AMMRC.

The tensile tests resulted in failure loads of 92,000 lb and 103,500 lb, respectively. These values are 29% and 20% below the predicted theoretical 100% efficient strength of 130,000 lb, respectively. In the first test, failure was attributed to a separation of the gage length material and also to the stress riser induced by the curvature of the material around the pin connector. Prior to testing, the second specimen was clamped to prevent separation of the gage section. The constraint provided by clamping is more consistent with constraint conditions in an actual overwrapped joint, and the increased strength observed in this specimen is probably more representative of the actual joint configuration. Therefore, these tests show that there is a strength reduction of about 20% due to the pin-wrapped design, when compared to the ultimate composite material strength.

The compression specimens failed well below the compressive strength of the material, buckling at loads of 20,000 and 21,000 lb, respectively. Two different phenomena related to buckling contributed to the low failure levels. First, the Euler buckling load of the specimen configuration may have been reached. However, the complexity of the specimen cross section of this configuration makes it difficult to predict the buckling load with a reasonable degree of accuracy. Second, a fabrication induced prestress, which created uneven stresses in the composite material on the two sides of the specimen, produced a slight pre-test curvature of the specimen. This undoubtedly contributed to the low buckling loads observed.

In summary, the initial program objectives of designing a composite traversing beam cross section which meets envelope, weight, and strength

requirements, and demonstrating fabricability with subscale constant cross section beams were achieved. Other objectives, based on testing the fabricated subscale beams to demonstrate strength levels, were only partially successful, primarily due to the difficulty of loading the half-scale units in the manner for which the full-scale beam was designed. Good correlation between analytical prediction and actual performance was established for beam rigidity and for strain/load relationships in the subscale box beam tests.

The program demonstrated the complexities associated with the use of composites in the traversing beam function. There is strong indication that the traversing beam design goals can be met with high performance composites such as those employed here, but the design of such complex structures in composites will require careful attention to the effects of the full load regime as well as to details such as end joints and manner of introducing concentrated loads.

## PREFACE

The work described in this report was performed by Hercules Incorporated at the Allegany Ballistics Laboratory (ABL) in compliance with Army Material and Mechanics Research Center Contract DAAG46-77-C-0069, ABL Authorization Code 296. This final report covers the work period from October 1, 1977, to June 15, 1979. Technical direction of this project was Dr. John M. Slepetz, AMMRC. At ABL, the program was controlled by Mr. C. M. Minke with Dr. A. A. Vicario, Dr. P. R. Evans, and Mr. W. B. Stewart performing the design, analysis, and testing.

## TABLE OF CONTENTS

	<u>Page</u>
SUMMARY	1
PREFACE	6
LIST OF FIGURES	9
LIST OF TABLES	11
INTRODUCTION	12
PROGRAM DETAILS	13
I.    FULL SCALE BEAM	13
A.    Design	13
B.    Analysis	18
II.   MATERIAL CHARACTERIZATION	18
III.  HALF SCALE PROTOTYPE BEAM	21
A.    Design and Analysis	21
B.    Fabrication	24
IV.  HALF SCALE BEAM TESTING	33
A.    Test Configuration and Procedure	37
B.    Results	42
1.    Full Half Scale Beam	42
2.    Short Half Scale Beam	54
V.   PIN BEARING END CONNECTORS	63
A.    Full Scale Design	63
B.    Full Scale Fabrication Including End Connectors	67
C.    Test Specimens	67
1.    Design	67
2.    Fabrication	70
3.    Tension Tests	70
4.    Compression Tests	77

TABLE OF CONTENTS (Cont'd)

	<u>Page</u>
DISCUSSION	81
CONCLUSIONS	85
RECOMMENDATIONS	87
REFERENCES	88
APPENDIX A	89
APPENDIX B	94

LIST OF FIGURES

<u>Figure No.</u>	<u>Title</u>	<u>Page</u>
1	Buckling Load vs. Winding Angle	16
2	Box Beam Fabrication Sequence	26
3	Half Scale Beam	28
4a	Half Scale Box Beam Winding Mandrel Assembly	30
4b	Winding Mandrel and Shroud	31
5	Half Scale Box Beam Cure Arrangement	32
6	Graphite Box Beam Cross Sections	34
7	Relative Moment/Shear Relationships Between a Traversing Beam, a Traversing Beam Segment, and a Half Scale Segment	36
8	Schematic of Four-Point-Bending Beam Test	38
9	Strain Gage Locations	40
10	Schematic of Interior and Exterior Web Bracing	41
11	Test Configuration	43
12	Test Set-up with the Inclusion of Web Bracing	44
13	Upper Flange Crush Failure	45
14	Upper Flange Point Load Crush Failure	46
15	Computer Printout of Load vs. Time	47
16	Load vs. Strain for Gage S8 (Top Flange)	49
17	Load vs. Strain for Gage S12 (Bottom Flange)	50
18	Load vs. Deflection at Mid-Span (Gage L1)	52
19	Load vs. Deflection at Load Point (Gage L3)	53
20	Load vs. Strain - Gage S5 Proof Tests	55
21	Load vs. Strain - Gage S6 Proof Tests	56
22	Load vs. Strain - Gage S17 Proof Tests	57
23	Load vs. Strain - Gage S18 Proof Tests	58

LIST OF FIGURES (Cont'd)

<u>Figure No.</u>	<u>Title</u>	<u>Page</u>
24	Schematic of the Three-Point-Bending Short Beam Test	59
25	Three-Point-Bending Test Configuration	60
26	Short Beam with the Inclusion of Wooden Bulkheads	61
27	Failure Mode of Short Beam Segment	62
28	End Connector Configuration	64
29	Fabrication Scheme Including End Connectors	68
30	End Connector Test Specimen	69
31	Tensile Test Configuration - Unit #1	72
32	Failure of Unit #1	73
33	Tensile Test Configuration - Unit #2	75
34	Stress vs. Strain - Tensile Unit #2	76
35	Failure of Unit #2	78
36	Compression Test Configuration	79

LIST OF TABLES

<u>Table No.</u>	<u>Title</u>	<u>Page</u>
1	Box Beam Design Requirements	13
2	Mobile Bridge Box Beam Design Study Results	15
3	Comparison of ABL Composite and Baseline Aluminum Design	17
4	Box Beam Margins of Safety	19
5	Nominal Static Composite Properties	20
6	Degradation Factors and Design Allowables	22
7	Design Summary of Full and Half Scale Designs	23
8	Half Scale Box Beam Margins of Safety at Failure	25
9	Strain Gage Types and Positions	39
10	Tensile Test Results - Unit #1	71
11	Tensile Test Results - Unit #2	74
12	Compression Test Results	77

## INTRODUCTION

The U. S. Army is pursuing improved mobile bridging via the most advanced technologies available, including structural fibrous composites. One Bridging concept being featured in the "Bridging for the Eighties" trilateral program is a vehicle mounted three-section folding bridge which is positioned across the obstruction by means of a launch beam. The launch beam is cantilevered during deployment and functions as a simply supported beam upon reaching the obstruction far side. The bridge structure is rolled into position over the launch beam. The launch beam is a weight and flexural modulus critical system element, suited to the advantages of fibrous composite design and fabrication. Accordingly, Army Materials and Mechanics Research Center selected Hercules Incorporated/Allegany Ballistics Laboratory to conduct a design, fabrication, and testing program on a simple box beam of a size and load capacity consistent with current launch beam development efforts.

The initial program features (1) the design of a full scale 7 meter box beam segment without end joints, and (2) the fabrication of two geometric half-scale beams. A subsequent contract modification provided for (3) the structural testing of one of the half-scale beams, and (4) the fabrication and testing of simplified pin wrapped joints simulating tensile and compressive specimens.

## PROGRAM DETAILS

### I. FULL SCALE BEAM DESIGN

#### A. Design

The beam design requirements selected by AMRC are summarized in Table 1. The requirements are representative of beam configurations and loadings being considered by various U. S. Army agencies at the time of the program. The nominal 7 meter beam length is an element of a multi-segment beam built-up by joining several elements end-to-end with moment resistant connectors. Incorporation of the end connectors was not considered within the scope of this program other than requiring that the beam design not preclude eventual incorporation of integrally fabricated joints.

TABLE 1

#### BOX BEAM DESIGN REQUIREMENTS

Element	Requirement
Cross Section Envelope	12.11 in. x 25.00 in.
Length	21 ft, 3 in.
Maximum Weight	20 lbs/linear foot
Minimum Bending Moment Capacity	$5.52 \times 10^6$ in.-lbs
Minimum Shear Force Capacity	20,000 lbs
Flexural Rigidity	Maximum; greater than comparable aluminum beam
Operating Temperature	-65°F to +165°F
Humidity	98% RH
Fatigue Life	$10^4$ cycles
Margin of Safety	> 0.33 for tension, compression, shear and buckling

Various geometric configurations, fibrous materials, and fiber plying angle combinations were considered and several satisfactory preliminary designs resulted (Table 2). Materials considered include AS and HM graphite, and Kevlar-49. When technical risk and estimated production costs were considered, in conjunction with a modified requirement to maximize beam flexural rigidity, the simple hollow box cross section constructed from AS graphite/epoxy was selected for final design optimization.

The design was considered to be optimized when the flexural rigidity was maximized within the nominal 18-18.5 lb/ft limit (allowing 1.5 to 2 lb/ft for a wear surface on the top flange) and all strength margins of safety exceeded 0.33. Allowable stresses were determined by degrading the nominal static laminate strengths for material variation and cyclic fatigue (Section II).

The highest flexural rigidity consistent with weight limitations and beam fabrication considerations occurs when the maximum possible amount of  $0^\circ$  (longitudinal) fiber is placed in the flanges. The webs consist of  $\pm 45^\circ$  windings, which also carry through the flanges. A winding angle of  $45^\circ$  was determined to be the most efficient, taking into account buckling considerations (Ref. 1), as shown in Figure 1.

The webs are sized to carry the 20 kip shear load and to be adequate in web or flexural/shear buckling. This allows the remaining material within the weight limitation to be  $0^\circ$  material in the flanges. The resulting final design is compared with a structurally adequate (but overweight) aluminum beam in Table 3. The webs of the composite beam are 0.264 in. thick  $\pm 45^\circ$  graphite/epoxy (fiber volume -55%) and the flanges contain 0.370 in. of  $0^\circ$  (fiber volume -55%) material in addition to the  $\pm 45^\circ$  web material which is continuous through the flanges. The beam weight, including a 1.0 lb/ft

TABLE 2

MOBILE BRIDGE BOX BEAM DESIGN STUDY RESULTS

	1		2		3		4		5		6	
	Baseline Type AS Graphite	0.32 @ 145° AS 0.21 @ 0° AS 0.32 @ 145° AS	Type IM-S Graphite	Type IM-S Graphite	Kevlar-49 Type IM-S Hybrid	Type AS/Foam Sandwich Design	Type AS/Foam Sandwich Design	Type AS/Foam Sandwich Design	Type AS/ Stiffener Design	Type AS/ Stiffener Design	Type AS/ Stiffener Design	Double Box Type AS Design
Flange Thickness (in.)	0.32 @ 145° AS 0.21 @ 0° AS	0.32 @ 145° AS 0.21 @ 0° IM-S	0.32 @ 145° AS 0.21 @ 0° IM-S	0.40 @ ±30° Kevlar 0.18 @ 0° IM-S	0.32 @ ±30° AS 0.18 @ 0° AS 0.25 Foam Sand.	0.32 @ ±30° AS 0.18 @ 0° AS 0.25 Foam Sand.	0.32 @ ±30° AS 0.18 @ 0° AS 0.25 Foam Sand.	0.32 @ ±30° AS 0.18 @ 0° AS 0.25 Foam Sand.	0.32 @ ±30° AS 2"x2"x0.25 Box Stiff @ ±10°	0.32 @ ±30° AS 2"x2"x0.25 Box Stiff @ ±10°	0.32 @ ±30° AS 2"x2"x0.25 Box Stiff @ ±10°	0.32 @ ±30° AS 2"x2"x0.25 Box Stiff @ ±10°
Web Thickness (in.)	0.32 @ 145° AS	0.32 @ 145° AS	0.32 @ 145° AS	0.40 @ ±30° Kevlar	0.32 @ ±30° AS	0.32 @ ±30° AS	0.32 @ ±30° AS	0.32 @ ±30° AS	0.32 @ ±30° AS			
Weight (lb/ft)	18.3	18.3	18.3	19.9	18.3	18.3	18.3	18.3	17.5	17.5	17.5	17.5
EI (lb-in.) (10) <sup>10</sup>	2.10	2.47	2.47	2.05	2.33	2.33	2.33	2.33	2.22	2.22	2.22	1.62
Avg. Bending Stress	31.5	32.0	32.0	27.1	24.9	24.9	24.9	24.9	27.0	27.0	27.0	29.2
Compression Flange (ksi)	31.5	32.0	32.0	27.1	37.4	37.4	37.4	37.4	47.3	47.3	47.3	29.2
Tension Flange (ksi)	31.5	32.0	32.0	27.1	37.4	37.4	37.4	37.4	47.3	47.3	47.3	29.2
Avg. Shear Stress (ksi)	1.2	1.3	1.3	1.3	1.7	1.7	1.7	1.7	0.80	0.80	0.80	1.1
Minimum Margin of Safety	10.52	10.77	10.77	10.22	10.33	10.33	10.33	10.33	10.33	10.33	10.33	10.01
Buckling Stress	43.4	47.9	47.9	36.2	60.0	60.0	60.0	60.0	3.8(1)	3.8(1)	3.8(1)	90.0
Flange (ksi)	34.9	36.6	36.6	4.1(1)	3.8(1)	3.8(1)	3.8(1)	3.8(1)	3.8(1)	3.8(1)	3.8(1)	34.9
Web (ksi)	34.9	36.6	36.6	4.1(1)	3.8(1)	3.8(1)	3.8(1)	3.8(1)	3.8(1)	3.8(1)	3.8(1)	34.9
Minimum Margin of Safety	10.40	10.50	10.50	10.34	11.40	11.40	11.40	11.40	11.40(2)	11.40(2)	11.40(2)	11.40
Flange	12.64	13.30	13.30	12.23	1.25	1.25	1.25	1.25	1.75	1.75	1.75	12.64
Web	12.64	13.30	13.30	12.23	1.25	1.25	1.25	1.25	1.75	1.75	1.75	12.64
Risk	1.00	1.10	1.10	1.50	1.50	1.50	1.50	1.50	1.75	1.75	1.75	1.30
Cost Factors	1.00	1.10	1.10	0.90	1.20	1.20	1.20	1.20	1.40	1.40	1.40	1.80
Labor	1.00	1.45	1.45	1.73	1.06	1.06	1.06	1.06	0.95	0.95	0.95	0.95
Materials	1.00	1.00	1.00	1.00	1.00	1.00	1.00	1.00	1.80	1.80	1.80	1.50
Tooling	1.00	1.00	1.00	1.00	1.00	1.00	1.00	1.00	1.80	1.80	1.80	1.50
Unit Cost (\$/MM In/ft)	\$4,040	\$5,530	\$5,530	\$6,220	\$4,220	\$4,220	\$4,220	\$4,220	\$4,290	\$4,290	\$4,290	\$4,620

(1) Based on Buckling Load

(2) Near Buckling

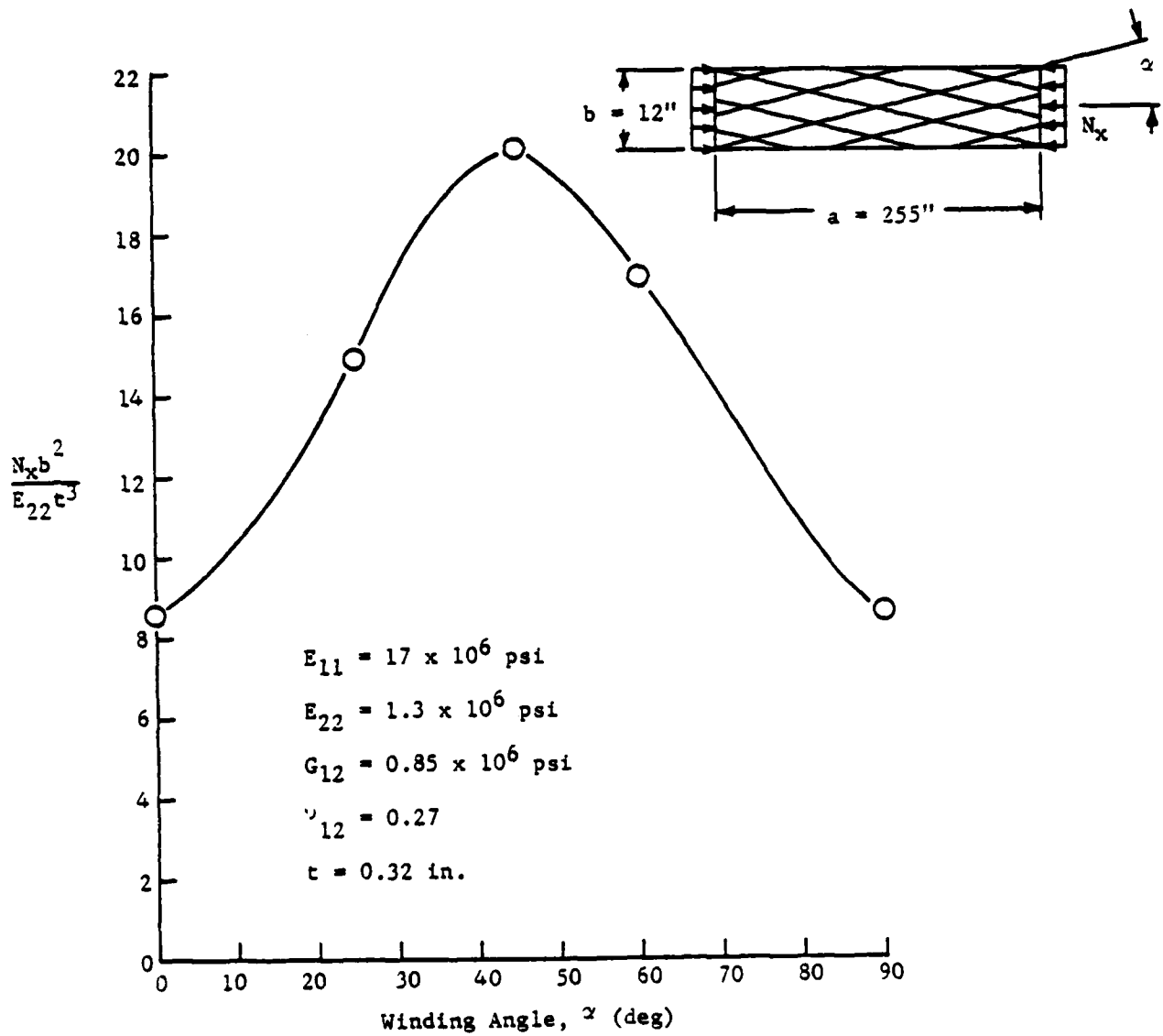
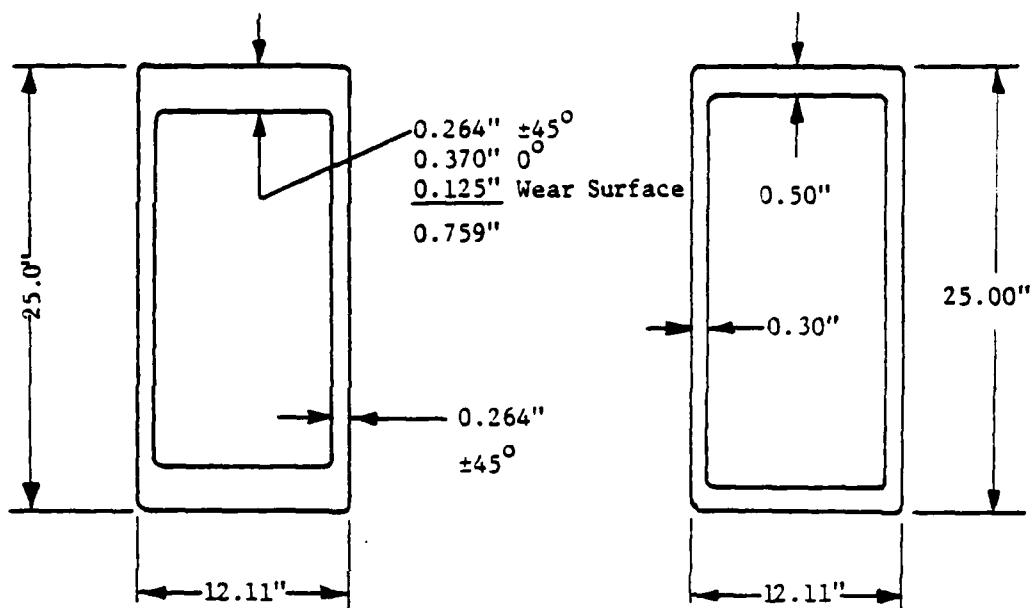


Figure 1. Buckling Load<sup>(1)</sup> V.S. Winding Angle

(1) Reference 1

TABLE 3

COMPARISON OF ABL COMPOSITE AND BASELINE ALUMINUM BEAMS



ABL GRAPHITE DESIGN

BASELINE ALUMINUM DESIGN

Item	Program Requirement	ABL Graphite Beam	Baseline Aluminum Beam
Envelope	12.11 ± 1/16 x 25.00 ± 1/16 x 22.9'	Satisfies requirement	Satisfies requirement
Beam Unit Weight	20 lb/ft	19.1 lb/ft <sup>(1)</sup>	31 lb/ft
Bending Resistance Margin of Safety <sup>(2)</sup>	0.33	+1.1 <sup>(3)</sup>	+0.1 <sup>(4)</sup>
Beam Shear Load Margin of Safety <sup>(5)</sup>	0.33	+1.0 <sup>(6)</sup>	---
Flexural Rigidity, EI	Aluminum Beam	2.89 x 10 <sup>10</sup> lb-in. <sup>2</sup>	2.5 x 10 <sup>10</sup> lb/in. <sup>2</sup>

- (1) Includes 1.0 lb/ft for 1/8" thick hard rubber or polypropylene wear surface.
- (2) Program design ultimate moment is 5.52 x 10<sup>6</sup> in.-lbs.
- (3) Minimum margin anywhere in beam, shear stress in web in this instance.
- (4) Based on a bending stress of 38 ksi and 6061-T6 aluminum.
- (5) Program design ultimate shear is 20,000 lb.
- (6) Minimum margin anywhere in the beam due to the shear load, shear buckling of the web in this case.

allowance for a wear surface, is 19.1 lb/ft. The 20.0 lb/ft limit was not pushed to allow for the possibility of higher resin content in manufacture and for potential changes in wearing surface.

#### B. Analysis

The design was analyzed to assess margins of safety under the design loads. Several potential failure modes were considered. The design bending moment of  $5.52 \times 10^6$  in.-lb creates significant normal and shear stresses in both the  $\pm 45^\circ$  and  $0^\circ$  plies of the flange, as well as in the  $\pm 45^\circ$  web material. Possible compressive buckling of both the web and flange due to in-plane flexurally induced stresses was checked.

The shear force of 20,000 lbs creates a potential for web shear buckling which also was checked. A typical analysis for the box beam is presented in Appendix A and the results are summarized in Table 4.

## II. MATERIALS CHARACTERIZATION

Several composite materials were considered for use in the full scale design optimization phase of the program. These materials included Type AS-2 graphite, Type HM-S graphite, and Kevlar-49 fibers, and epoxy resins. The nominal static composite properties for these materials are shown in Table 5.

In order to determine the design allowables, certain degradation factors were used. The material degradation factor accounts for variations in material handling, fabrication and test data. The fatigue degradation factors for graphite are based on data, collected in Reference 2, on the effects of various environments on the physical and mechanical properties of graphite/epoxy composites. These environments included steady state

TABLE 4

BOX BEAM MARGINS OF SAFETY

## (a) Flange in Bending

Flange - Loaded @ 16,200 lb/in. due to $M = 5.52 \times 10^6$ in.-lbs					
$\pm 45^\circ$ Plies			$0^\circ$ Plies		
Predicted Stress, psi	Allowable, psi	M.S.	Predicted Stress, psi	Allowable, psi	M.S.
$\sigma_{11} = 7842$	122,000	>14	$\sigma_{11} = 38,480$	122,000	+2.2
$\sigma_{22} = 705$	4,500	+5.4	$\sigma_{22} = 975$	4,500	+3.6
$\tau_{12} = 2940$	6,800	+1.3	$\tau_{12} = 0$	6,800	OK

Critical Plate Buckling Load = 42,700 lbs/in. (R. M. Jones' method).

$$\text{M.S.} = \frac{\text{allowable}}{\text{actual}} - 1 = \frac{42,700}{16,200} - 1 = +1.6$$

## (b) Web in Bending

Web - Loaded @ 1750 lb/in. (6615 psi) due to $M = 5.52 \times 10^6$ in.-lbs		
Predicted Stress, psi	Allowable, psi	M.S.
$\sigma_{11} = 6076$	122,000	+19
$\sigma_{22} = 545$	4,500	+7.3
$\tau_{12} = 3300$	6,800	+1.1

Critical Web Buckling Stress = 17,300 psi (S. G. Leknitskii method).

$$\text{M.S.} = \frac{\text{allowable}}{\text{actual}} - 1 = \frac{17,300}{6,615} - 1 = +1.6$$

## (c) Web in Shear

Web - Loaded by 20,000 Shear Force	
Predicted Shear Stress = 1476 psi	
M.S. = $\frac{6800}{1476} - 1 = 3.6$	
Critical Shear Buckling Stress = 2972 (S. G. Leknitskii method)	
M.S. = $\frac{\text{allowable}}{\text{actual}} - 1 = \frac{2972}{1476} - 1 = +1.0$	

TABLE 5

NOMINAL STATIC COMPOSITE PROPERTIES ( $V_F = 55\%$ )

<u>Property</u>	<u>Type AS-2 Graphite</u>	<u>Type HM-S Graphite</u>	<u>Kevlar-49 Aramid</u>
Longitudinal Tensile Modulus, $E_{11}(10)^6$ psi	18.0	30.0	10.5
Transverse Tensile Modulus, $E_{22}(10)^6$ psi	1.3	1.0	0.5
Major Poisson's Ratio, $\nu_{12}$	0.27	0.28	0.34
In-Plane Shear Modulus, $G_{12}(10)^6$ psi	0.85	1.0	0.3
Longitudinal Tensile Strength, $F_{11T}$ (ksi)	200.0	130.0	210.0
Longitudinal Compressive Strength, $F_{11C}$ (ksi)	160.0	120.0	30.0
Transverse Tensile Strength, $F_{22T}$ (ksi)	5.6	5.6	1.7
Transverse Compressive Strength, $F_{22C}$ (ksi)	25.0	25.0	12.0
In-Plane Shear Strength, $F_{12}$ (ksi)	9.0	9.0	2.5
Short Beam Shear Strength, (ksi)	12.5	10.5	5.5
Longitudinal Linear Coefficient of Thermal Expansion, $\alpha_{11}(10)^{-6}$ (in./in./°F)	-0.1	-0.5	-2.0
Transverse Linear Coefficient of Thermal Expansion, $\alpha_{22}(10)^{-6}$ (in./in./°F)	14.5	14.5	14.5

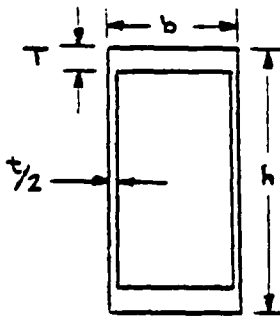
humidity conditioning for two exposure durations, cyclic humidity conditioning which in turn included the effects of thermal shocks and the effect of photodegradative exposures, and steady and cyclic thermal exposures. This report shows a reduction in strength from 10% to 20% for graphite/epoxy composites due to environmental and cyclic fatigue conditions.

The degradation factors for the Kevlar-49/HBRF-55A composite system are based on Reference 3; the DuPont Kevlar Handbook. These degradation factors, along with the design allowables, are presented in Table 6.

### III. HALF-SCALE PROTOTYPE BEAM

#### A. Design and Analysis

The half-scale design consisted of dimensionally halving the full-scale design. Table 7 shows a summary of the full and half scale designs. Based on nominal material normal shear strengths, the predicted half scale beam operating and collapse moments and shears are 1/8 and 1/4 of the full scale values, respectively, as shown by the following:



Moment:

$$\sigma = \frac{Mc}{I} \Rightarrow M = \frac{\sigma I}{c}$$

$$I = \frac{bTh^2}{2}; \quad c = h/2$$

$$M = \sigma bTh$$

For the half scale, where all dimensions are halved:

$$M_{HS} = \sigma \frac{b}{2} \frac{T}{2} \frac{h}{2} = \frac{\sigma bTh}{8} = \frac{M_{FS}}{8}$$

#### Shear:

$$\tau = \frac{VQ}{It} = \frac{V}{A_f} \Rightarrow V = A_f \tau$$

TABLE 6

DEGRADATION FACTORS AND DESIGN ALLOWABLES

(a) MATERIAL DEGRADATION FACTORS

MATERIAL	Material Variation (1) (-3σ) (%)			Degradation Due To Cyclic Fatigue (% of Ultimate)		
	Long.	Trans.	Shear	Long.	Trans.	Shear
Graphite/HBRF-55A	15	10	10	10 (2)	20 (2)	15 (2)
Kevlar-49/HBRF-55A	7.5	15	10	16 (3)	20 (4)	15 (4)

- (1) (-3σ) Variation includes material handling, fabrication, test data
- (2) Based on data obtained in AFML-TR-74-266, "Development of Engineering Data on Mechanical and Physical Properties of Advanced Composite Materials"
- (3) Based on DuPont data
- (4) Estimated

(b) DESIGN ALLOWABLES

Property	Type AS-2/HBRF-55A	HMS/HBRF-55A	Kevlar-49/HBRF-55A
Longitudinal Tensile Strength, F <sub>11T</sub> (ksi)	155.0	100.0	165.0
Longitudinal Compressive Strength, F <sub>11c</sub> (ksi)	122.0	92.0	23.0
Transverse Tensile Strength, F <sub>22T</sub> (ksi)	4.5	4.5	1.4
Transverse Compressive Strength, F <sub>27c</sub> (ksi)	18.0	18.0	8.2
In-Plane Shear Strength, F <sub>12</sub> (ksi)	6.8	6.8	2.0

$$A_f = \text{area of flange} = hT$$

$$V_{fs} = \tau hT$$

For half scale, where all dimensions are halved:

$$V_{HS} = \tau \frac{h}{2} \frac{T}{2} = \frac{\tau hT}{4} = \frac{V_{fs}}{4}$$

Therefore, without considering buckling implications, the shear and flexural strengths of a geometric half-scale beam do not scale linearly with the full scale beam.

TABLE 7

DESIGN SUMMARY OF FULL AND HALF SCALE DESIGN

<u>Parameter</u>	<u>Full Scale</u>	<u>Half Scale</u>
EI, 10 <sup>10</sup> lb-in.	2.89	0.18
Weight, lb/ft	18.1	4.5
Flange Thickness (total), in.	0.636	0.318
0° Thickness, in.	0.372	0.186
±45° Thickness, in.	0.264	0.132
Web Thickness (±45°), in.	0.264	0.132

The scaled predicted design moment and shear were then used in an analysis similar to that shown in Appendix A to predict margins of safety in the half scale design, considering buckling as well as material strengths.

This analysis shows, by comparing the margins of safety for each failure mode, that the most critical failure is that of shear buckling in the webs due to the applied shear. In order to prevent this second order buckling type of failure from occurring in the test load configuration used

for the half-scale box beam, it was necessary to brace the webs during testing. The bracing plan used during the test of the half-scale box beam is explained more thoroughly in Section IV.A.

The second most critical failure mode is that of web shear. This failure mode develops from the loading configuration (four-point-bending) and the high moment necessary to fail the flange material. As was shown in Table 4, shear in the web may be created from the two sources of applied moment (flexure) and applied shear. In the actual launch beam these sources are unlikely to occur at the same location; therefore, these loadings can be examined separately to determine which is more critical. The analysis of Appendix A is performed in reverse order by initially setting the margins of safety equal to zero and calculating the stress necessary for this condition. This yields the critical shear failure mode in the webs due to flexure. At this critical flexural load (moment), the stresses may be calculated, along with the respective margins of safety, for each of the other failure modes. Table 8 shows the results of these calculations. Note that the margin of safety of the shear in the web due to bending is zero, which is the initial failure mode at a load of 21,628 lbs.

#### B. Fabrication

Although the full size beam in a production environment would probably be wet filament wound, prepregged tape was selected for use in fabricating the  $0^{\circ}$  portion of the half scale beams to allow the use of simple and inexpensive fabrication techniques (Figure 2).

The fabrication technique features a winding mandrel and a mold. The desired beam cross sectional thicknesses and plying sequences are built up by alternately wrapping the mandrel with  $\pm 45^{\circ}$  layers and laying

TABLE 8

HALF SCALE BOX BEAM MARGINS OF SAFETY AT FAILURE

## (a) Flange in Bending

Flange - Loaded @ 11,621 lb/in. due to $M = 0.91 \times 10^6$ in.-lbs					
$\pm 45^\circ$ Plies			$0^\circ$ Plies		
Predicted Stress, psi	Allowable, psi	M.S.	Predicted Stress, psi	Allowable, psi	M.S.
$\sigma_{11} = 11,272$	160,000	13	$\sigma_{11} = 54,619$	160,000	1.93
$\sigma_{22} = 1,046$	160,000	>20	$\sigma_{22} = 1,395$	160,000	>20
$\tau_{12} = 4,184$	160,000	1.15	$\tau_{12} = 9,000$	9,000	OK

Critical Plate Buckling Load = 25,521 lb/in. (R. M. Jones' method).  

$$\text{M.S.} = \frac{\text{allowable}}{\text{actual}} - 1 = \frac{25,521}{11,621} - 1 = 1.20$$

## (b) Web in Bending

Web - Loaded @ 2374 lb/in. (8991 psi) due to $M = 0.91 \times 10^6$ in.-lbs		
Predicted Stress, psi	Allowable, psi	M.S.
$\sigma_{11} = 16,497$	160,000	8.70
$\sigma_{22} = 1,495$	160,000	>20
$\tau_{12} = 8,996$	9,000	0.0

Critical Web Buckling Stress = 17,300 psi (S. G. Leknitskii method).  

$$\text{M.S.} = \frac{\text{allowable}}{\text{actual}} - 1 = \frac{17,300}{8,991} - 1 = 0.92$$

## (c) Web in Shear

Web - Loaded by 21,628 lbs Shear Force	
Predicted Shear Stress = 6911 psi;	$\text{M.S.} = \frac{9000}{6911} - 1 = 0.30$
Critical Shear Buckling Stress = 467,000 psi (with external support)	
$\text{M.S.} = \frac{467,000}{6,911} - 1 = 66$	

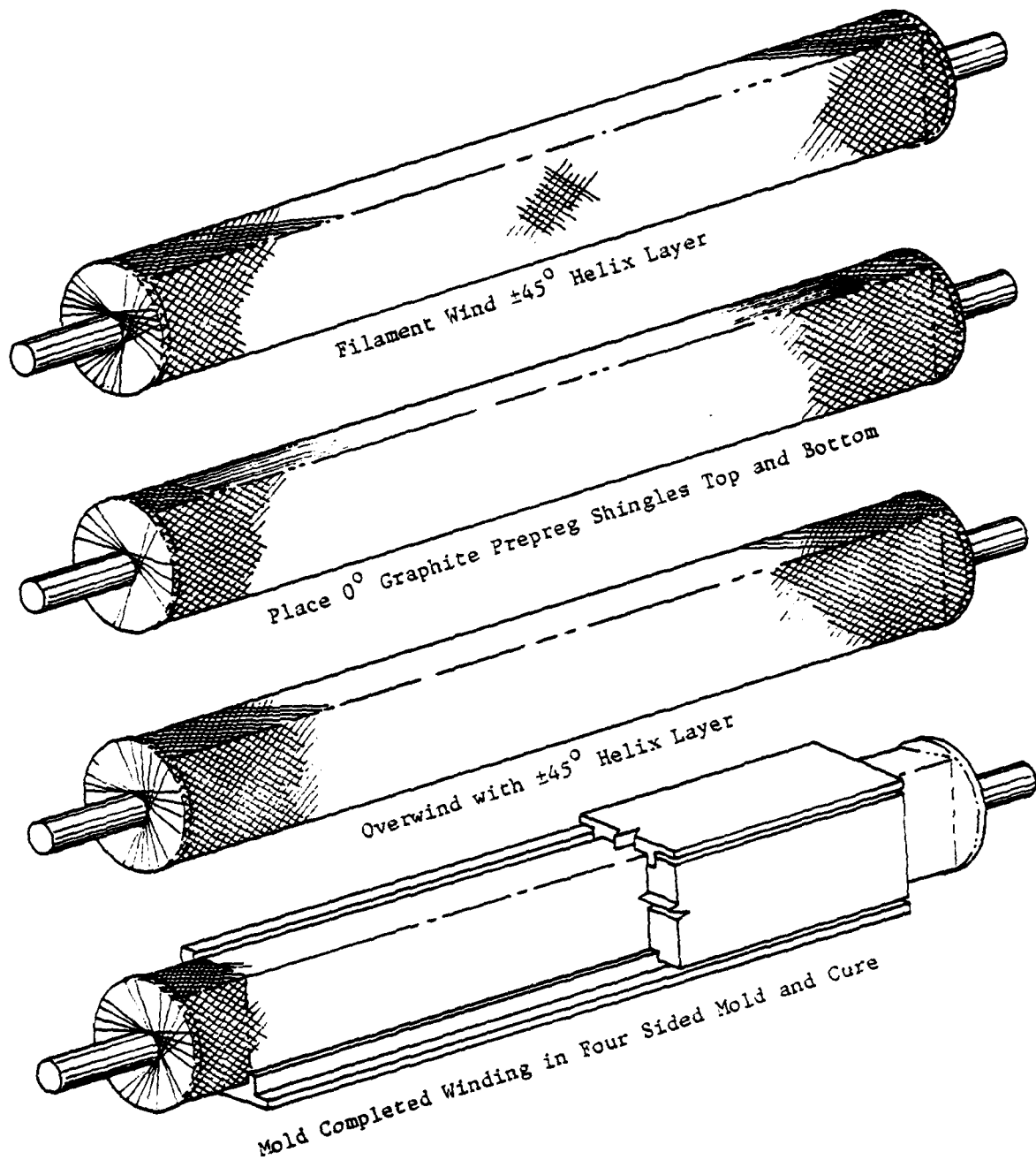


Figure 2. Box Beam Fabrication Sequence

continuous prepreg 0° tape along the flanges. The assembly is then placed inside a simple four sided mold and cured. The mold assures conformity to the desired external dimensions.

A key element allowing the use of the suggested fabrication technique is the availability of a prepreg resin system which is compatible with a usable wet filament winding resin. A suitable combination exists in Hercules 1904 graphite prepreg and HBRF-55A winding resin, for use with the Hercules AS-4 graphite filament winding roving. The winding resin decreases in viscosity and flows freely during the early stages of cure, causing resin bleed out and allowing mold closure. Resin cure in the prepreg was prevented by freezer storage. The material was thawed immediately prior to use and was soft, flexible, and easy to apply. Therefore, it conforms to the mandrel surface under mold pressure. The prepreg resin does not flow to any extent but does bond well to HBRF-55A. The result is a well compacted strong combination without undue criticality regarding resin staging.

The desired thickness of ±45° and 0° material for the half-scale design can be achieved by the combination shown in Figure 3. Each ply of 1904 0° prepreg is nominally 0.0052-in. thick at a 55% fiber volume, so 36 total plies are needed to meet the 0.185-in. requirement. For the ±45° material, six layers of windings at a band width of 0.75-in./six tows gives:

$$\epsilon_{\pm 45} = \frac{2n A_R}{(BW) V_f} = 0.135$$

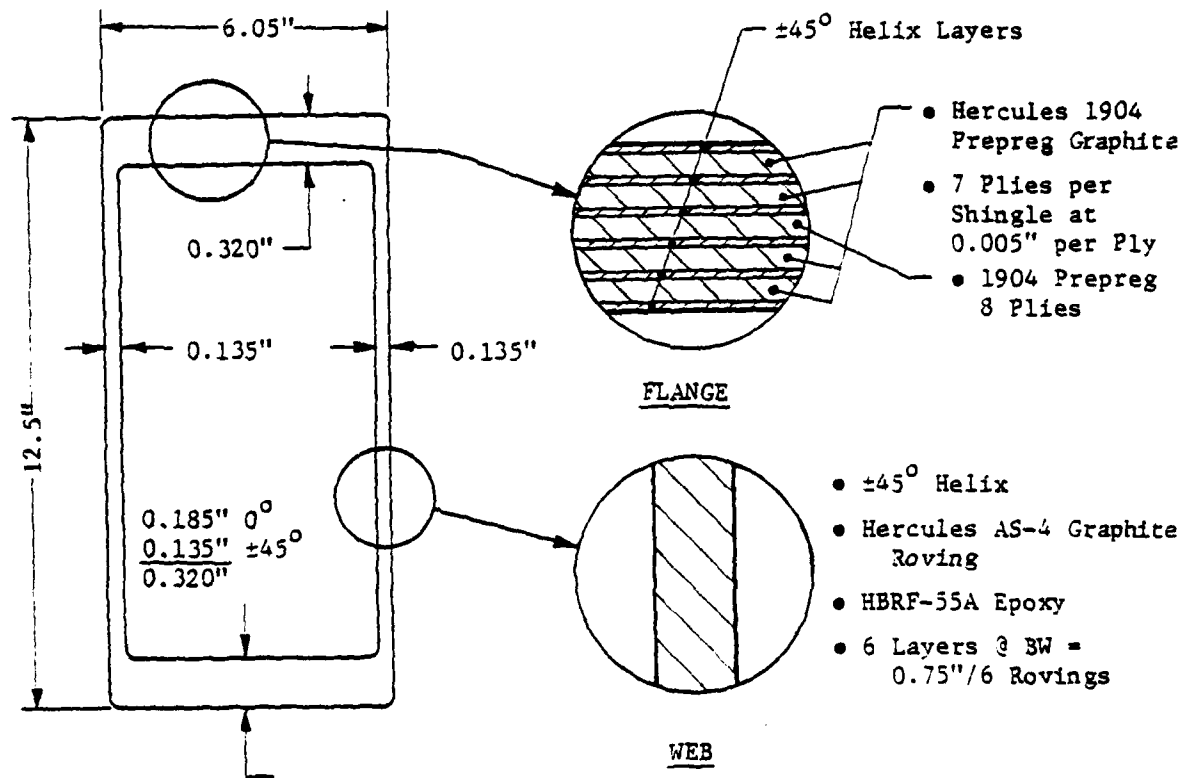


Figure 3. Half Scale Beam

where:  $n$  = number of layers = 6

$A_R$  = effective fiber area per roving =  $0.00077 \text{ in.}^2 /$   
roving

BW = bandwidth/roving =  $0.75/6 = 0.125 \text{ in.}$

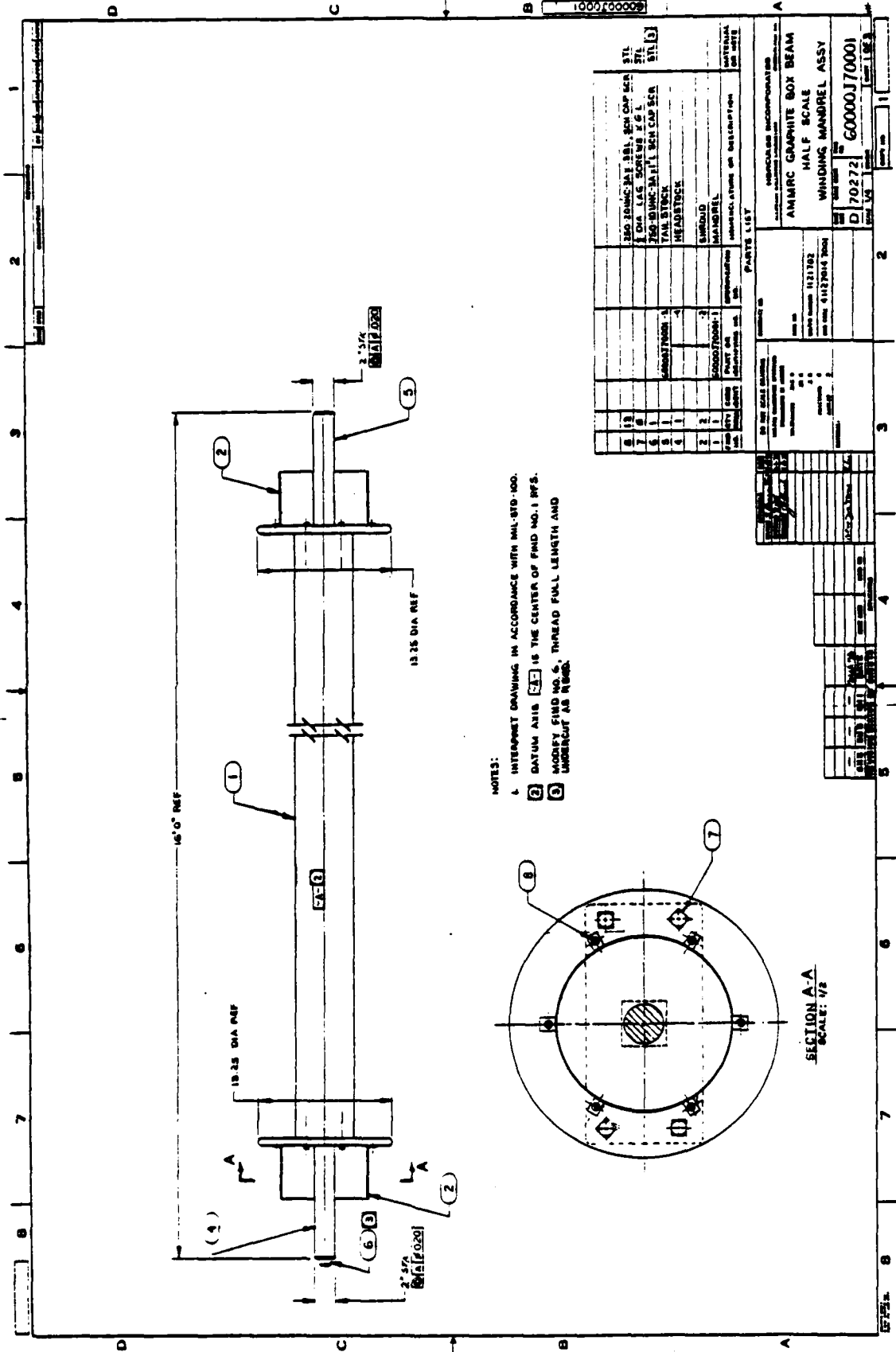
$V_f$  = fiber volume fraction = 0.55

The 36 plies of prepregged  $0^\circ$  material were interspaced between the six layers of helix as four shingles of seven plies each and one shingle of eight plies.

The first half-scale beam was fabricated by the technique previously described. The winding mandrel (Figures 4a and 4b) was a glue laminated wooden rectangle with radiused corners over which a section of aluminum sheet metal was placed to provide sliding surfaces for mandrel extraction. A longitudinal hole through the wood provided a location for an extraction rod.

The winding sequence consisted of alternating  $\pm 45^\circ$  helix layers covering the entire mandrel periphery and  $0^\circ$  prepreg tape shingles along the narrow or flange surfaces. Six layers of helix and five shingles top and bottom completed the winding phase. The helix layers were wet wound using a band comprised of six rovings of Hercules AS-4 graphite fed through an epoxy resin cup. At the completion of each helix layer, shingles of seven or eight plies of  $0^\circ$  Hercules 1904 graphite prepreg were positioned top and bottom, held in place with hand ties and overwound with the next helix layer.

At winding completion, the assembly was placed in a four sided mold (Figure 5) and the mold plates pulled together with tie rods and cross bars. The assembly was then placed in an oven and cured at  $120^\circ\text{F}$  for 6 hours and then  $250^\circ\text{F}$  for 4 hours.



NOTES:

- INTERPRET DRAWING IN ACCORDANCE WITH MIL-STD-100.
- DATUM AXIS (A) IS THE CENTER OF FIND NO. 1 RFS.
- MODIFY FIND NO. 6, THREAD FULL LENGTH AND UNDERCUT AS SHOWN.

Figure 4a. Half-Scale Box Beam Winding Mandrel Assembly



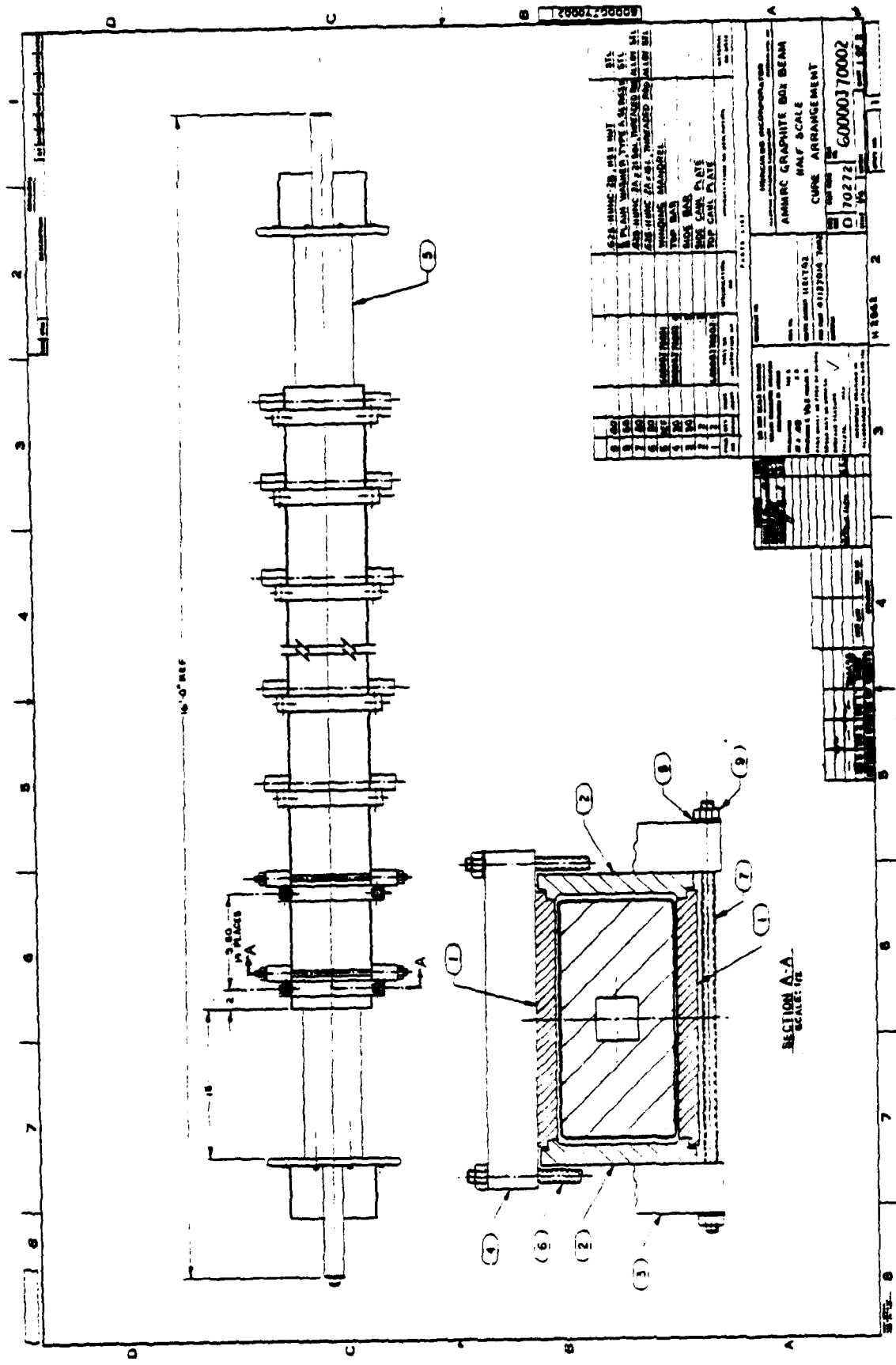


Figure 5. Half-Scale Box Beam Cure Arrangement

On the first beam, mold closure was poor for reasons discussed below. The mold plates could not be closed to their bearing plates. The resulting beam cross section geometry is shown in Figure 6.

On the second half-scale beam, several corrective steps were implemented to enhance mold closure, including:

- Increased winding tension during helix winding, from 3 lb/tow to ~10 lb/tow.
- Wiped off excess resin after each helix layer.
- Lumped all of the 0° prepreg mat into a single, thicker shingle to minimize resin build-up during the helix overwinds.
- Modified mold closing technique to nearly close side plates before the top plates are brought in.
- Held the assembly in the cure oven at 120°F for 30 minutes, removed and tightened the mold closure bolts while the resin was very fluid and mobile, to promote resin bleedout.

As may be seen in Figure 6, the second beam was much more satisfactory, although both webs and flanges were still a little thick, reflecting a higher than desired resin volume. The finished beam weight was 4.92 lb/ft versus a target of about 4.80 lb/ft.

#### IV. HALF-SCALE BEAM TESTING

Near the completion of the program phase involving the fabrication of the half-scale beams, the program scope was expanded beyond beam design and fabrication feasibility to encompass flexural testing of the fabricated half-scale units.

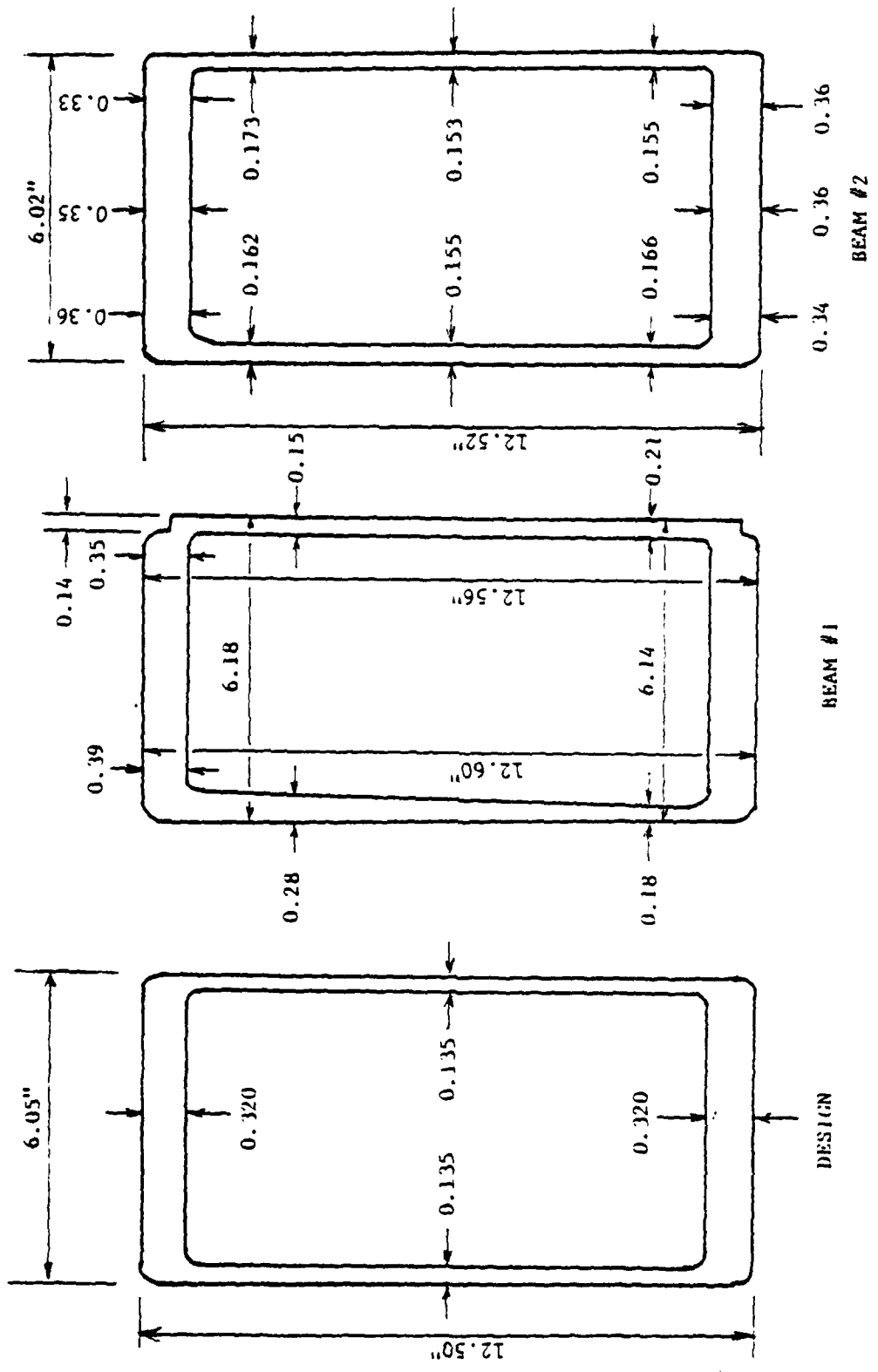


Figure 6. Graphite Box Beam Cross Sections

A problem related to the ratio of the bending moment to shear force is encountered in trying to test one segment of a multi-segment traversing beam in flexure, as shown in Figure 7. In use, a traversing beam will consist of at least three of the nominal 7 meter segments pin joined for moment continuity at the top and bottom flanges. If the traversing beam is loaded at mid-span with a concentrated load and supported on end rollers (an over simplified loading), a moment to shear ratio  $M_T/V_T$ , of 413 in. results. (The fact that the M/V design requirement is 276 in. indicates that the actual traversing beam is not loaded in the simplified manner shown in Figure 7.) To develop the same moment in a single 7 meter segment loaded in a similar fashion requires a factor of three increase in the shear to moment ratio compared to a 21 meter span. Thus, the 7 meter test span will probably be shear critical rather than bending critical. This situation is exacerbated in the half-scale segment because shear and moment capacity resulting from a geometric half-scaling do not scale in the same ratio. As noted in Figure 7, the section moment capacity scales by a factor of 1/8 while the shear capacity scales by a factor of 1/4, when buckling is ignored and material normal and shear strengths are presumed to control behavior. When the three-point-bending configuration is used to model the load application, the concentrated load to achieve the allowable normal stress,  $\sigma$ , and the allowable shear stress,  $\tau$ , both scale to 1/4 of those required to produce similar effects in the full 7 meter segment. In both instances (7 meter segment and its geometric half scale), the maximum allowable shear is reached at about 1/3 of the load at which maximum allowable flexural loads are reached.

	TOTAL TRAVERSING BEAM	TRAVERSING BEAM SEGMENT	HALF SCALE SEGMENT
RELATIONSHIPS BETWEEN TRAVERSING BEAM (MULTIPLE 7 METER SEGMENTS) AND A SINGLE 7 METER SEGMENT	$M_{TMAX}$	$M_T = \frac{3P\ell}{4}$	$M_{HS} = \frac{P\ell}{8}$
	$V_{TMAX}$	$V_T = \frac{P}{2}$	$V_{HS} = \frac{P}{2}$
	$M_{TMAX} / V_{TMAX}$	$M_T / V_T = 3\ell / 2 = (\text{@ } \ell \text{ OF } 7M) = 413 \text{ IN.}$	$\frac{M_{HS}}{V_{HS}} = \ell - (\text{@ } \ell = 7M) = 138 \text{ IN.}$
	$M_T - M_S$	$\frac{3P\ell}{4} - \frac{P\ell}{4} = P\ell - 3 \therefore \frac{V_S}{V_T} = 3$	$\frac{M_{HS}}{V_{HS}} = 68 \text{ IN.}$
	$M_{DESIGN}$	$M_D = 5.52 \times 10^6 \text{ IN.-LB}$	
$V_{DESIGN}$	$V_D = 20,000 \text{ LBS}$		
$M_{DESIGN} / V_{DESIGN}$	$M_D / V_D = 276 \text{ IN.}$		
LOAD / FAILURE RELATIONSHIPS FOR THE THREE CONFIGURATIONS	$M_{CAPACITY}$	$M_T = \frac{\sigma I}{C} = \sigma bth$	$M_{HS} = \sigma \frac{b}{2} \frac{\ell}{2} \frac{h}{2} = \sigma \frac{bth}{8} = \frac{M_S}{8}$
	$V_{CAPACITY}$	$V_T = \frac{ht}{2} \approx \frac{Tht}{2}$	$V_{HS} = T \frac{h}{2} \frac{t}{2} = \frac{Tht}{4} = \frac{V_S}{4}$
	LOAD TO COLLAPSE BASED ON NORMAL STRESS	$M = M_T = \frac{3P\ell}{4} = \sigma bth; P = \frac{4}{3} \frac{\sigma bth}{\ell} = 87K (1)$	$M = M_{HS} = \frac{P\ell}{8} = \sigma bth; P = 4 \frac{\sigma bth}{\ell} = 260 (1)$
	LOAD TO COLLAPSE BASED ON SHEAR STRESS	$V = V_T = \frac{P}{2} = ht; P = 2ht = 238K (1)$	$V = V_{HS} = \frac{P}{2} = \frac{ht}{2}; P = ht = 59K (1)$
(1) BASED ON $bT = \text{AREA OF FLANGE } 0^\circ = 12.11'' \times 0.370''$ ; $ht = \text{AREA OF WEB } = 26.00 \times 2 \times .264$ ; $h = 26.00''$ ; $\ell = 7 \times 39.37''$ ; $\sigma = 160 \text{ KSI}$ ; $T = 9.0 \text{ KSI}$			

9226

Figure 7. Relative Moment / Shear Relationships Between a Traversing Beam, a Traversing Beam Segment & a Half Scale Segment

It should be noted that the analyses outlined in Figure 7 do not consider either buckling characteristics or laminate stresses but are a simplified qualitative assessment of scaling phenomenon using nominal material normal and shear strengths in the homogeneous sense. The detailed analyses presented in preceding sections, on the other hand, have taken these complexities into consideration.

A. Test Configuration and Procedure

One half-scale prototype box beam was subjected to a structural test in four-point-bending as shown schematically in Figure 8. This box beam was instrumented with twenty (20) electrical resistance strain gages. The gage types and positions are listed in Table 9 and their locations on the box beam are shown in Figure 9. Also, five displacement gages were used during the test. These gages monitored centerline beam deflection both in the plane of loading and transverse to that plane, beam deflection in the plane of loading at one interior load point, and web deflection in the shear region.

The structural tests were conducted as follows:

(1) The box beam was proof tested to 17,000 lbs (total load) four times at a rate of 100 lb/sec. Continuous recording of strains and displacements were made to permit determination of average elastic properties and flexural rigidity of the beam.

(2) The beam was subsequently provided with wooden inserts and exterior web bracing which was strapped to the beam using metal bands (shown schematically in Figure 10). These supports were necessary to prevent web shear buckling at loads below those required for flange failure. The beam

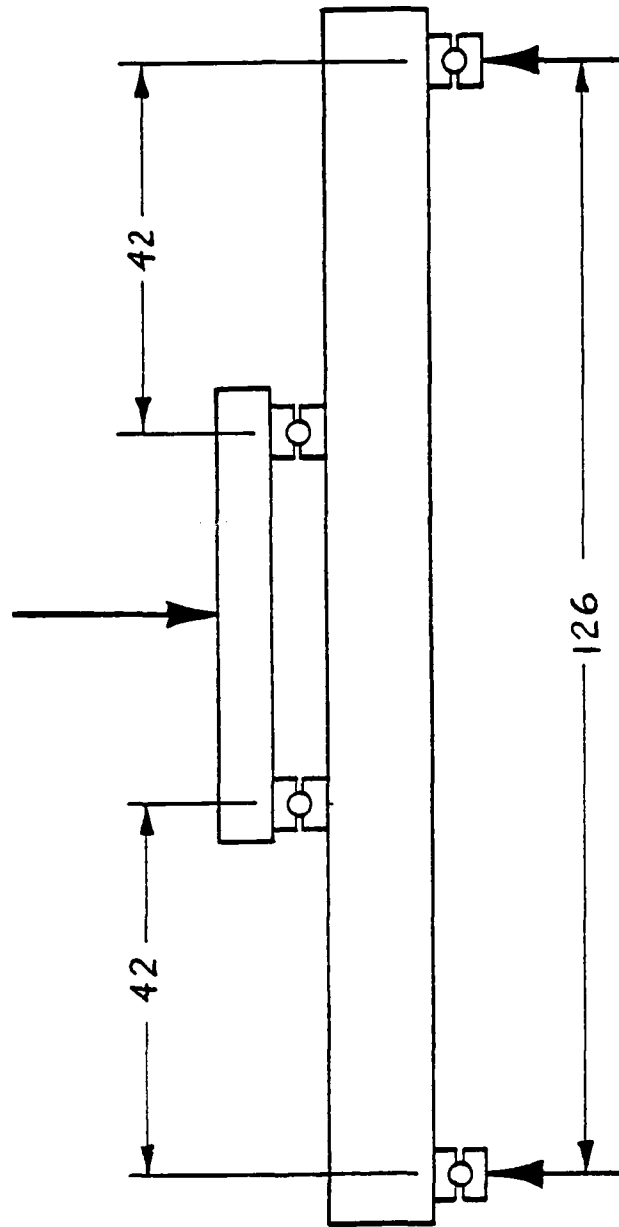


Figure 8. Schematic of Four-Point-Bending Beam Test

TABLE 9

STRAIN GAGE TYPES AND POSITIONS

Gage No.	Location
S1	Front Web, Transverse
S2	Front Web, Axial
S3	Front Web, +45°
S4	Front Web, -45°
S5	Front Web, +45°
S6	Front Web, -45°
S7	Top Flange, Transverse
S8	Top Flange, Axial
S9	Front Web, Transverse
S10	Front Web, Axial
S11	Bottom Flange, Transverse
S12	Bottom Flange, Axial
S13	Back Web, Transverse
S14	Back Web, Axial
S15	Back Web, +45°
S16	Back Web, -45°
S17	Back Web, +45°
S18	Back Web, -45°
S19	Back Web, Transverse
S20	Back Web, Axial
L1	Mid Span, Bottom Flange
L2	Mid Span, Front Web
L3	Load Point, Bottom Flange
L4	Between Load Points, Front Web
L5	Between Load Points, Back Web

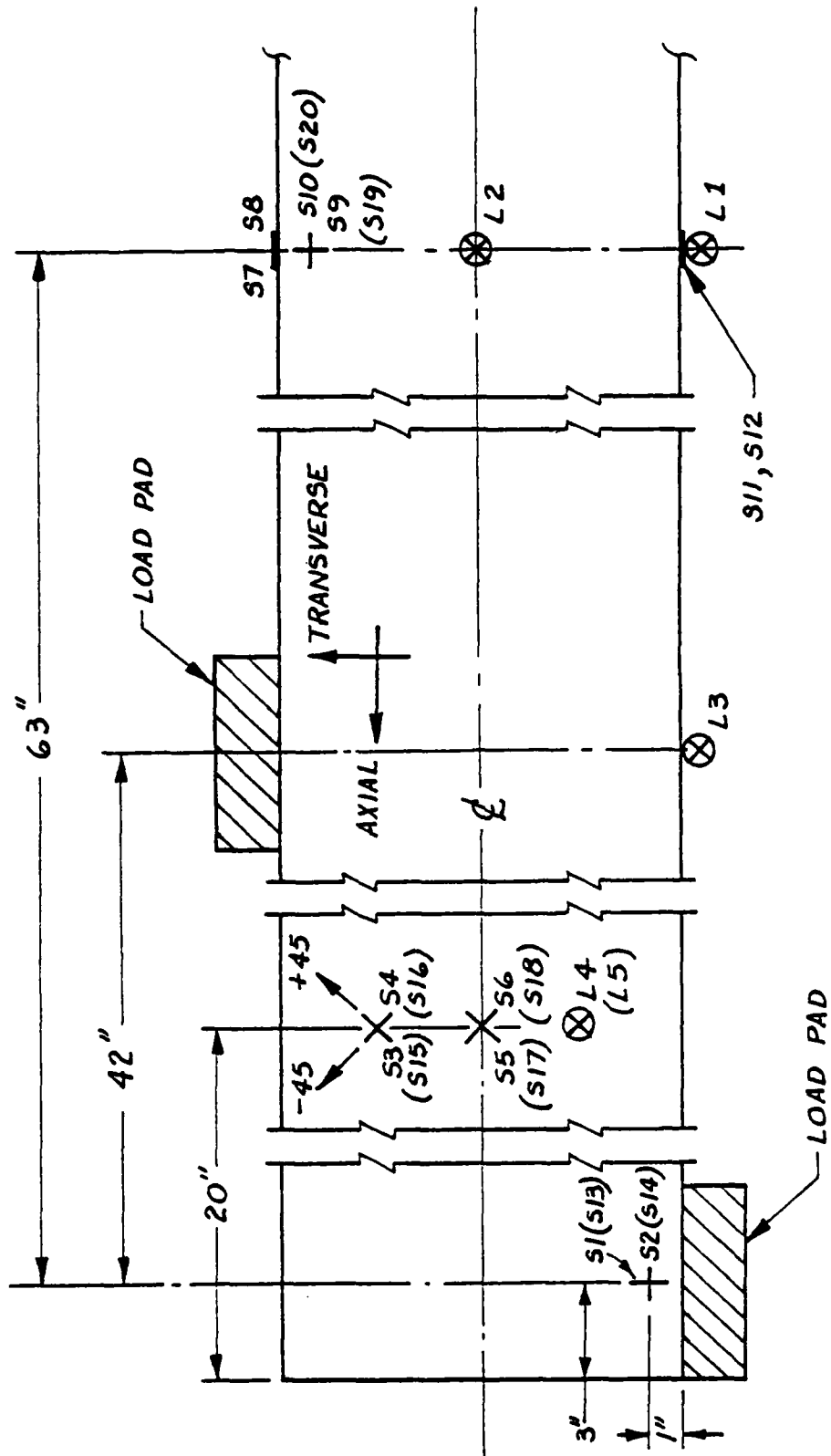


Figure 9. Strain Gage Locations

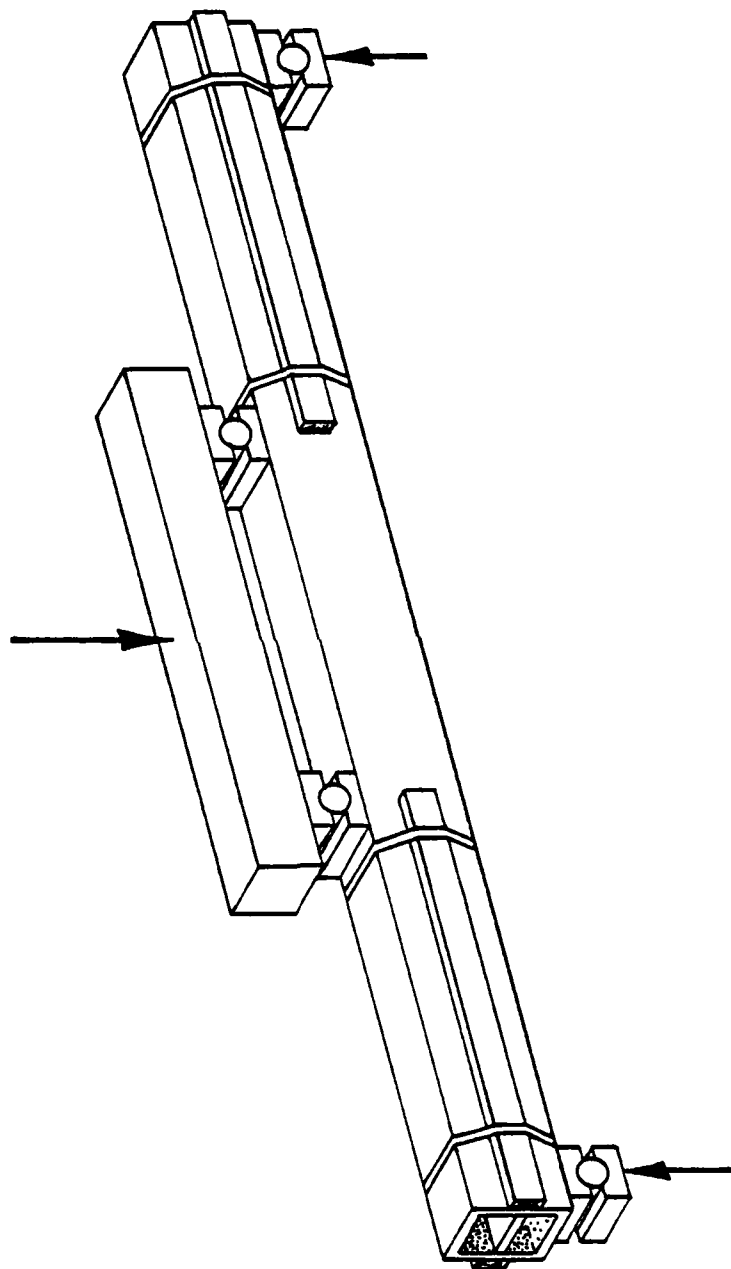


Figure 10. Schematic of Interior and Exterior Web Bracing

was then loaded at a rate of 100 lb/sec until failure. Continuous recording of strains and deflections was made during the load cycle.

(3) The web bracing was removed and an undamaged length of the beam was cut from the total length. This short beam was loaded in three-point-bending, with wooden bulkheads placed inside the beam directly below (above) the load points, until failure occurred.

## B. Results

### 1. Full Half-Scale Beam

#### a. Visual Inspection

The beam passed the four proof tests to 17,000 lb, but failed at -25,000 lb when loaded to ultimate; only 58% of the predicted collapse load of 43,000 lbs. This early failure was due to a load pad crushing through the beam upper flange with subsequent total collapse of the beam. Photographs of the test set-up before and after failure are shown in Figures 11 through 14. Figure 11 shows the four-point-bending test set-up. Figure 12 shows the internal and external web bracing. Figures 13 and 14 show the region of crushing failure in the upper flange under the loading pad.

A computer graph of load vs. time is shown in Figure 15. Notice that the load is F1F2AVE which is the average of the two loading cylinders in the test set-up. Therefore, the total load is twice this value. Also notice that the load was held constant for approximately 45 seconds at -19,000 lb. This was done to visually inspect the beam after some cracking had been heard during the test. Subsequently, the load was raised continuously until failure occurred at -25,000 lb.

The load vs. strain curves for each of the twenty (20) strain gages and load vs. displacement for the five (5) displacement gages

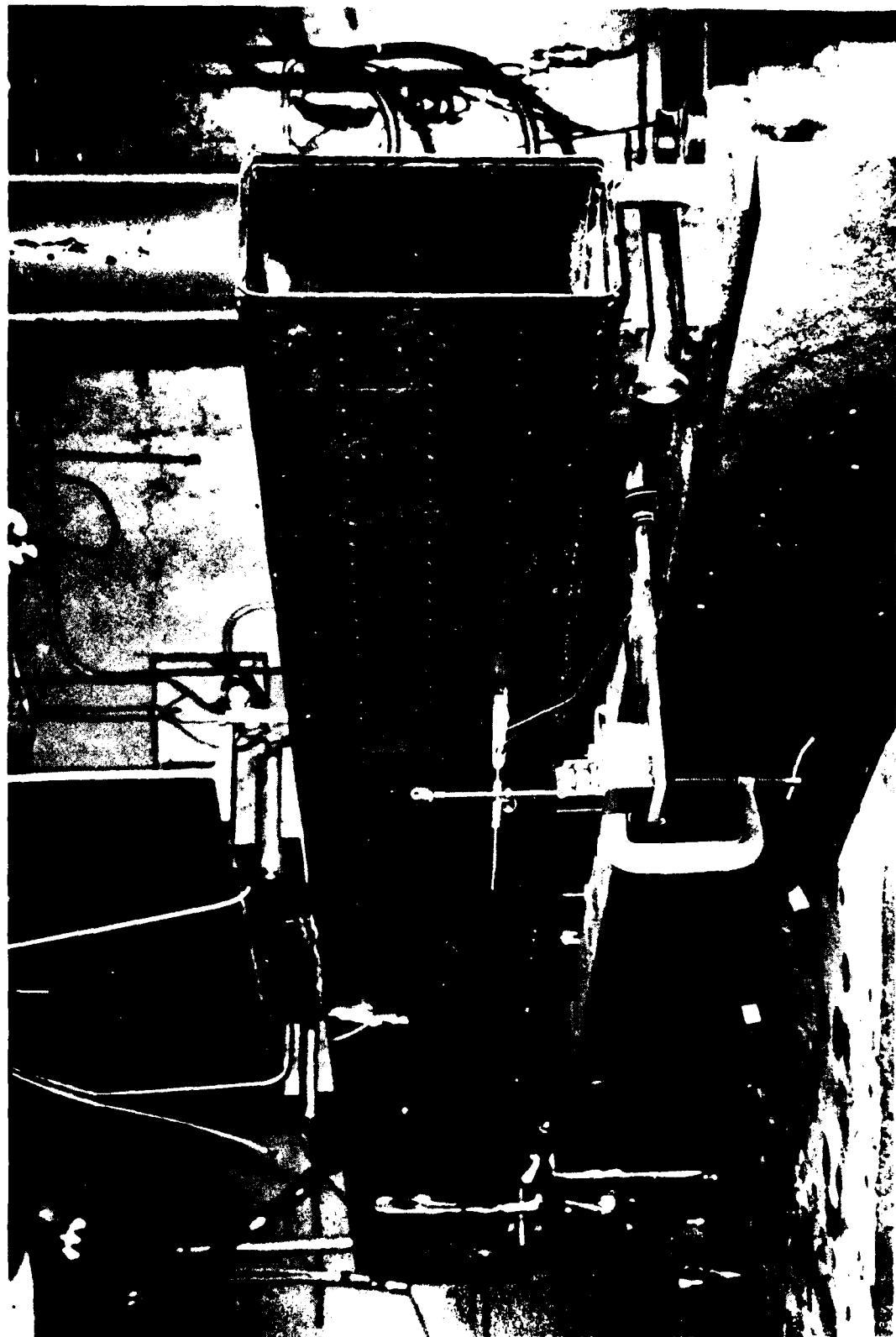


Figure 11. Test Configuration

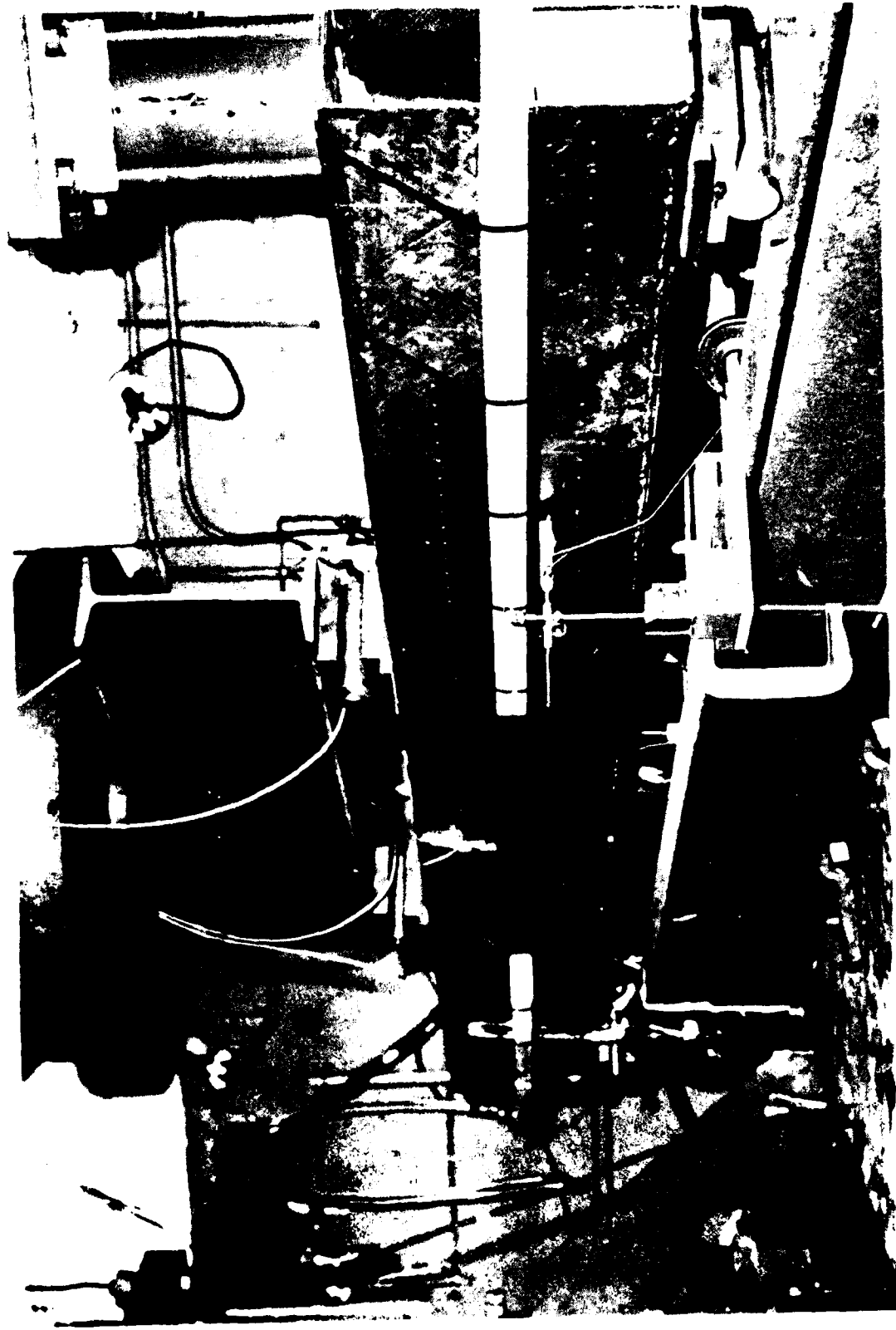


Figure 12. Test Set-up with the Inclusion of Web Bracing

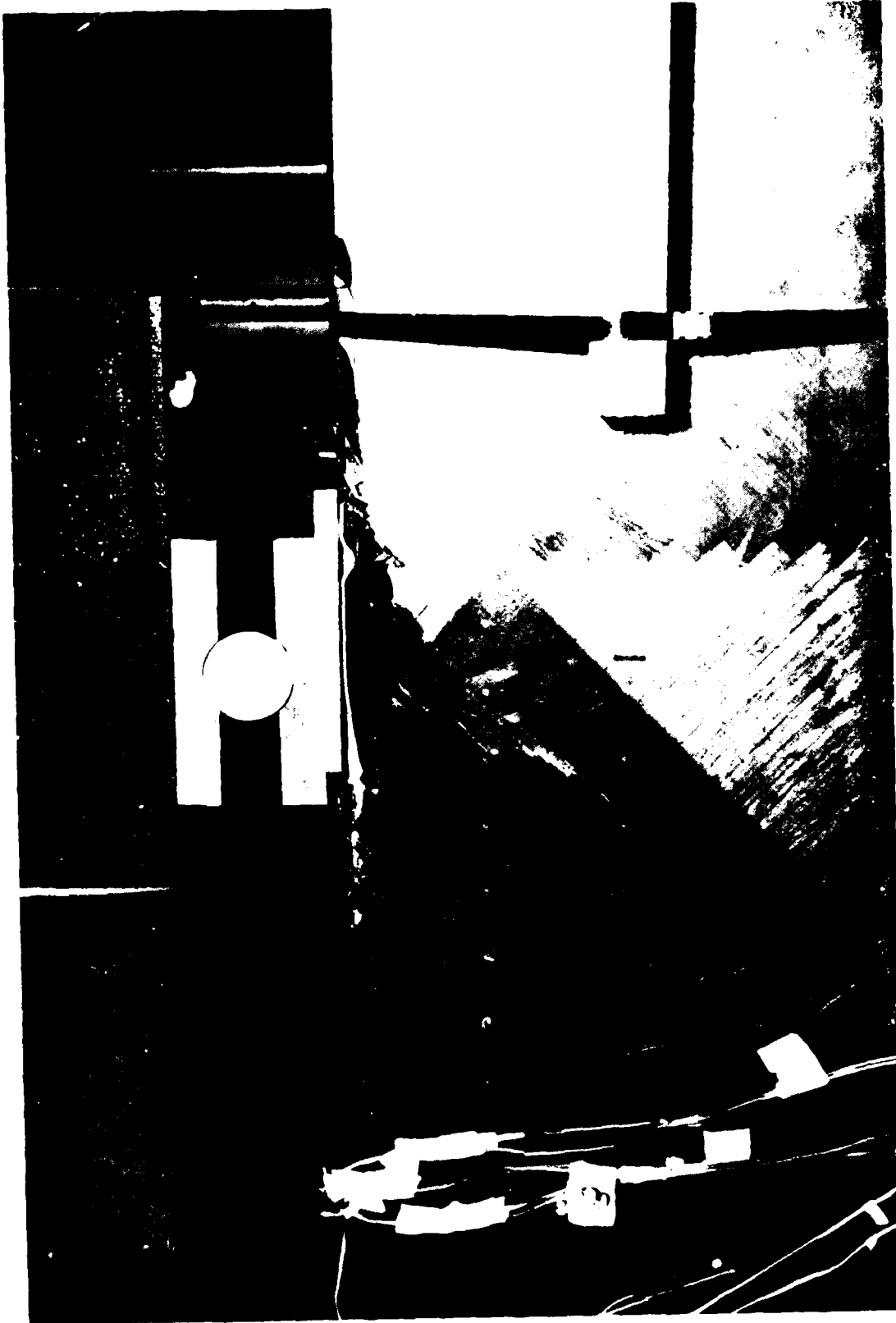


Figure 13. Upper Hesperia Crater Hill.

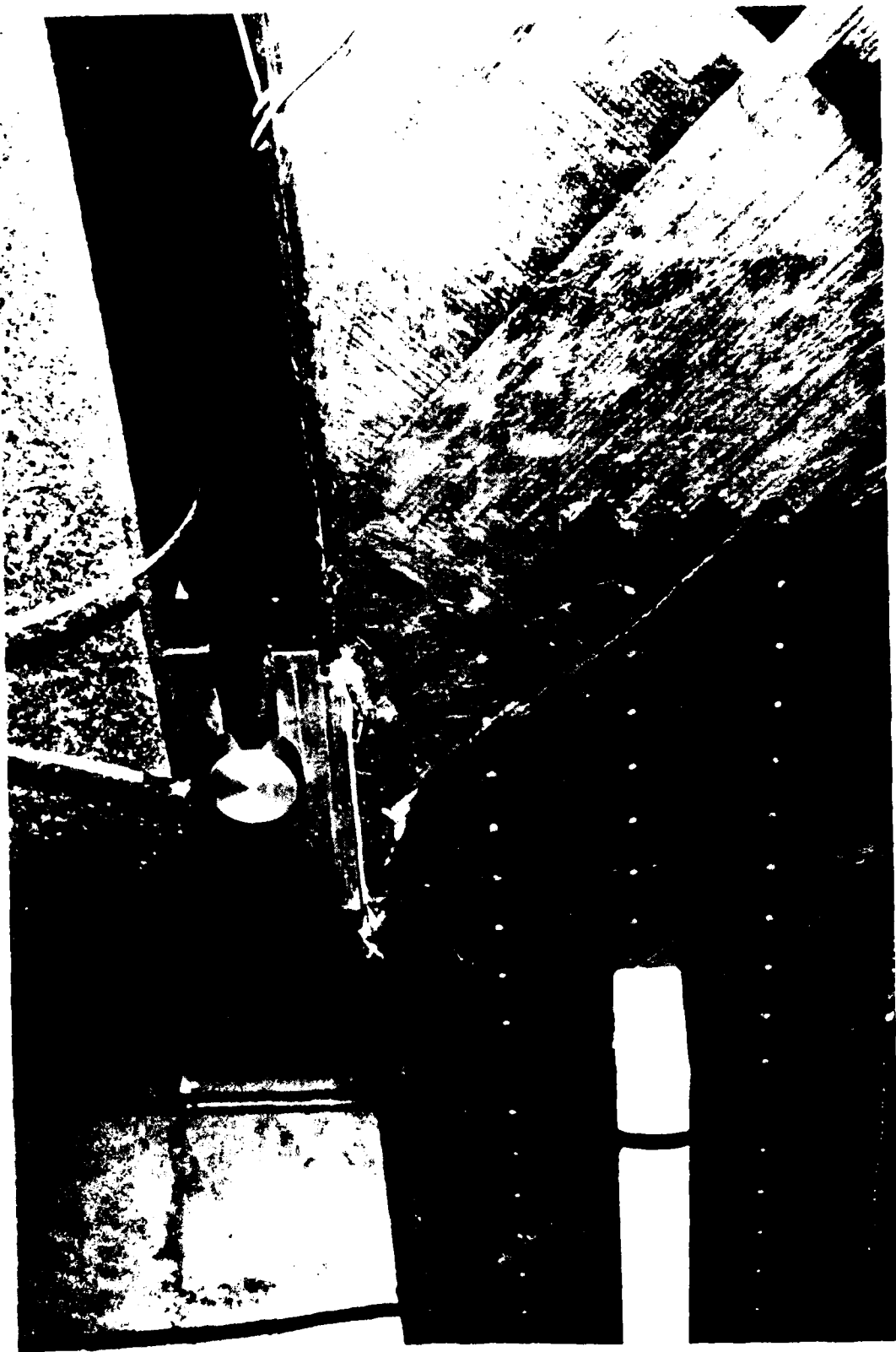
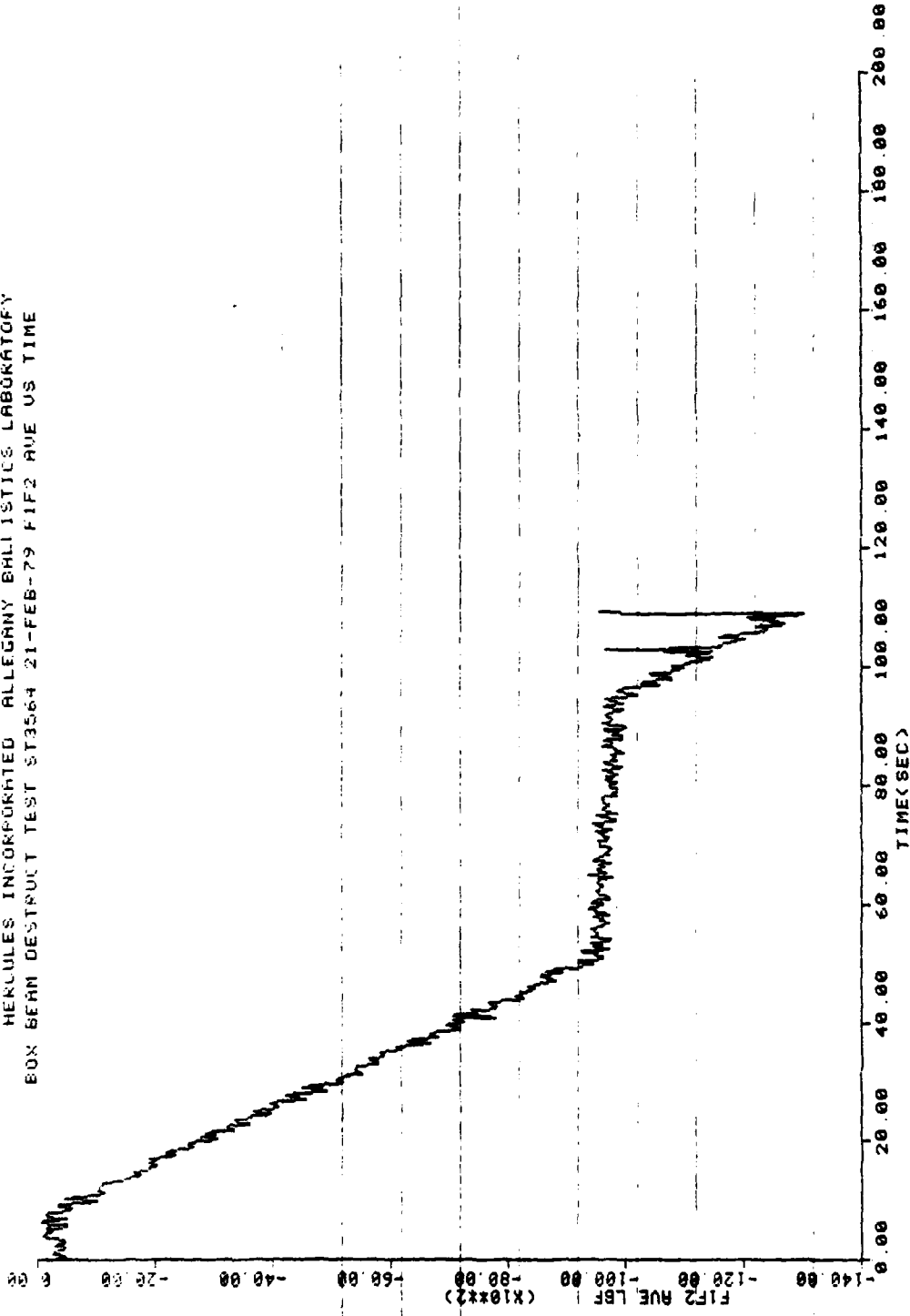


Figure 14. Upper Flange Point Load Crush Failure

HERCULES INCORPORATED ALLEGANY BALLISTICS LABORATORY  
BOX BEAM DESTRUCT TEST ST3564 21-FEB-79 FIF2 AVE US TIME



-47-

Figure 15

are given in Appendix B. NOTE: In each of these graphs the load shown is the average or half of the actual load.

Post test visual inspection of the beam indicated that the initial mode of failure was bearing crushing of the corner radius material which transitions from the  $\pm 45^\circ$  web to the flange.

b. Analytical Assessment and Analysis

The experimental determinations of the flexural rigidity (EI) of the beam agree well with the predicted value of  $1.79 \times 10^9$  lb-in.<sup>2</sup> (Table 7). The experimental value for EI can be determined from both the strain and deflection measurements.

Figure 16 shows the load vs. strain curve for strain gage S8; the gage on the top flange in the axial direction. Figure 17 shows the graph of load vs. strain for strain gage S12 (bottom flange, axial direction). At time 108.116 sec, the load F1F2AVE was 12,616 lb. The respective strains in the gages were  $\epsilon_8 = .192\%$  and  $\epsilon_{12} = .196\%$ . Then from the equation:

$$\epsilon = \frac{M y}{EI}$$

where:  $M = (F1F2AVE)(L/3) = (12,616)(42) = 529,000$  in.-lb

$y = 6.25$  in. (beam depth = 12.50 in.)

the value(s) for EI can be calculated. These calculated values yield:

$$EI_8 = 1.72 \times 10^9 \text{ lb-in.}^2$$

$$EI_{12} = 1.69 \times 10^9 \text{ lb-in.}^2$$

HERCULES INCORPORATED ALLEGANY BALLISTICS LABORATORY  
BOX BEAM DESTRUCT TEST ST3564 21-FEB-79 FIF2 AVE US S8

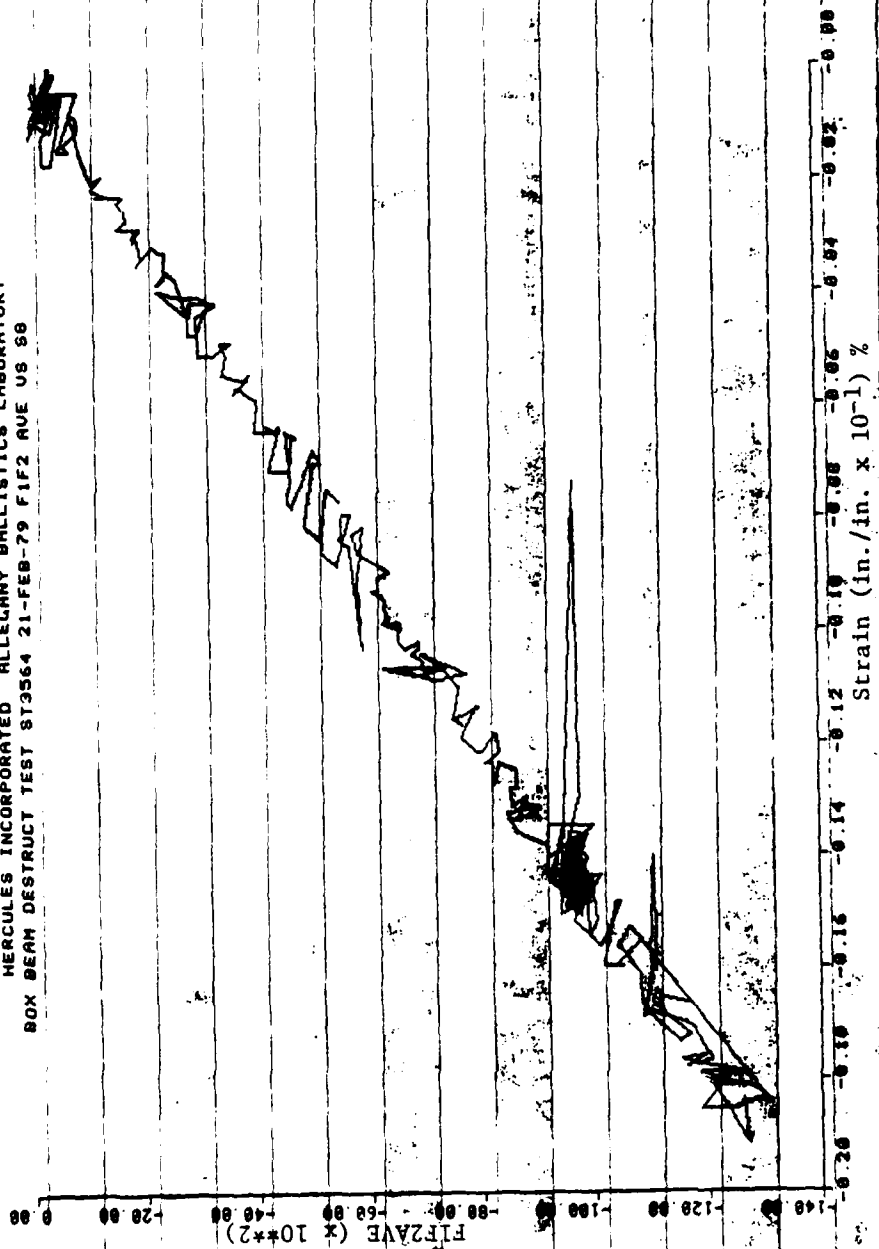


Figure 16. Load vs. Strain for Gage S8 (Top Flange)

HERCULES INCORPORATED ALLEGANY BALLISTICS LABORATORY  
BOX BEAM DESTRUCT TEST ST3564 21-FEB-79 FIF2 AVE US 512

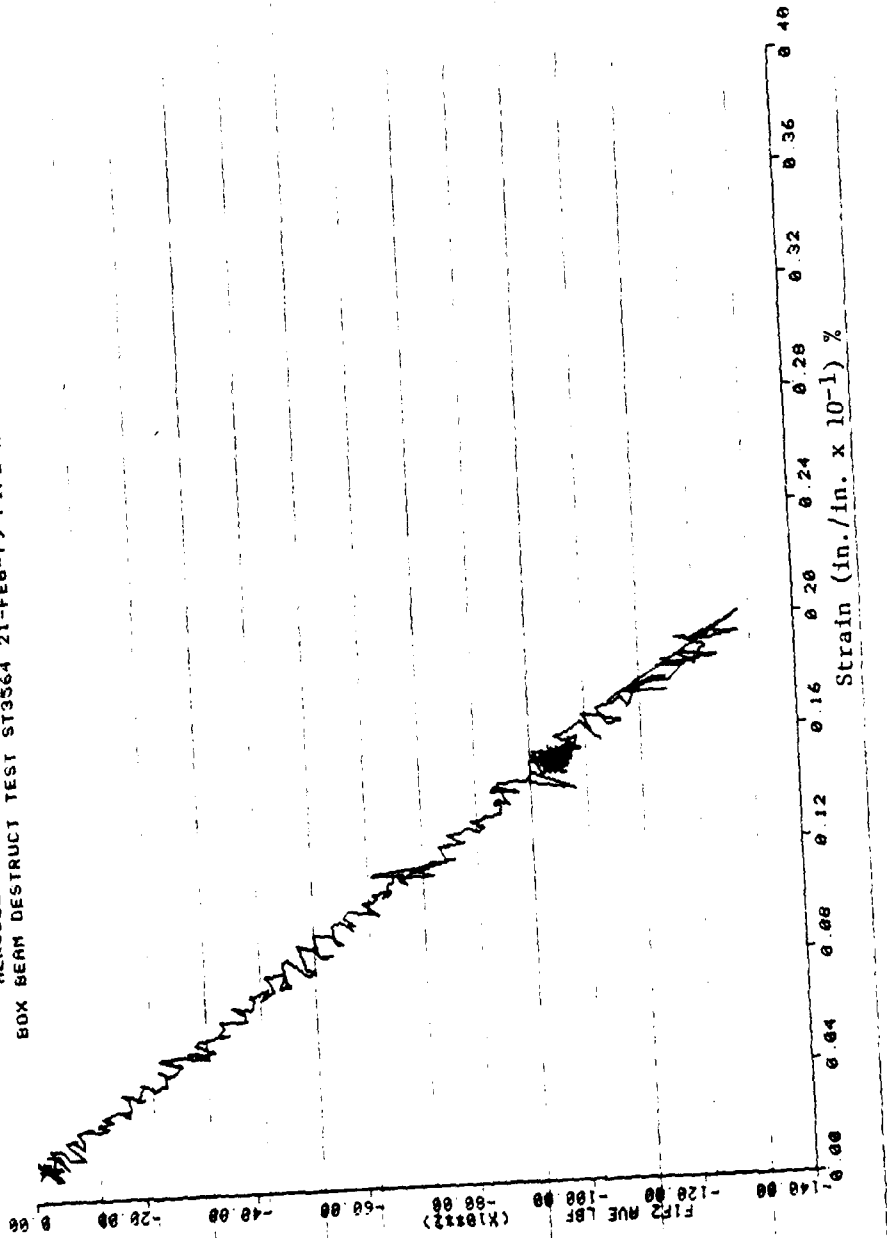


Figure 17. Load vs. Strain for Gage S12 (Bottom Flange)

Alternatively, the flexural rigidity of the box beam is calculated from the deflection of the beam under load. The equation for the mid-span deflection of a beam under four-point-bending is:

$$Y_m = \frac{Fa}{24 EI} [3L^2 - 4a^2] \quad (\text{Ref. 4})$$

Under a load point the deflection is:

$$Y_L = \frac{Fa^2}{6 EI} [3L - 4a] \quad (\text{Ref. 4})$$

Figures 18 and 19 show the graphs of load vs. deflection for the mid-span and load point locations, respectively.

In order to eliminate any problems with the deflections of the end supports during the test, the EI is calculated according to the deflections between the mid-span and load point locations. Therefore:

$$(Y_m - Y_L) = \frac{1}{EI} \left( \frac{Fa}{24} [3L^2 - 4a^2] - \frac{Fa^2}{6} [3L - 4a] \right)$$
$$\Rightarrow EI = \frac{1}{(Y_m - Y_L)} \left( \frac{Fa}{24} [3L^2 - 4a^2] - \frac{Fa^2}{6} [3L - 4a] \right)$$

where:  $F = 12,616 \text{ lb}$  (same load as strain calculations)

$Y_m = .729 \text{ in.}$  (displacement gage L1 - mid-span)

$Y_L = .664 \text{ in.}$  (displacement gage L3 - load point)

$a = L/3 = 42 \text{ in.}$

Using these values yields:

$$EI = 1.80 \times 10^9 \text{ lb-in.}^2$$

HERCULES INCORPORATED ALLEGANY BALLISTICS LABORATORY  
BOX BEAM DESTRUCT TEST ST3564 21-FEB-79 FIF2 AVE US LP1

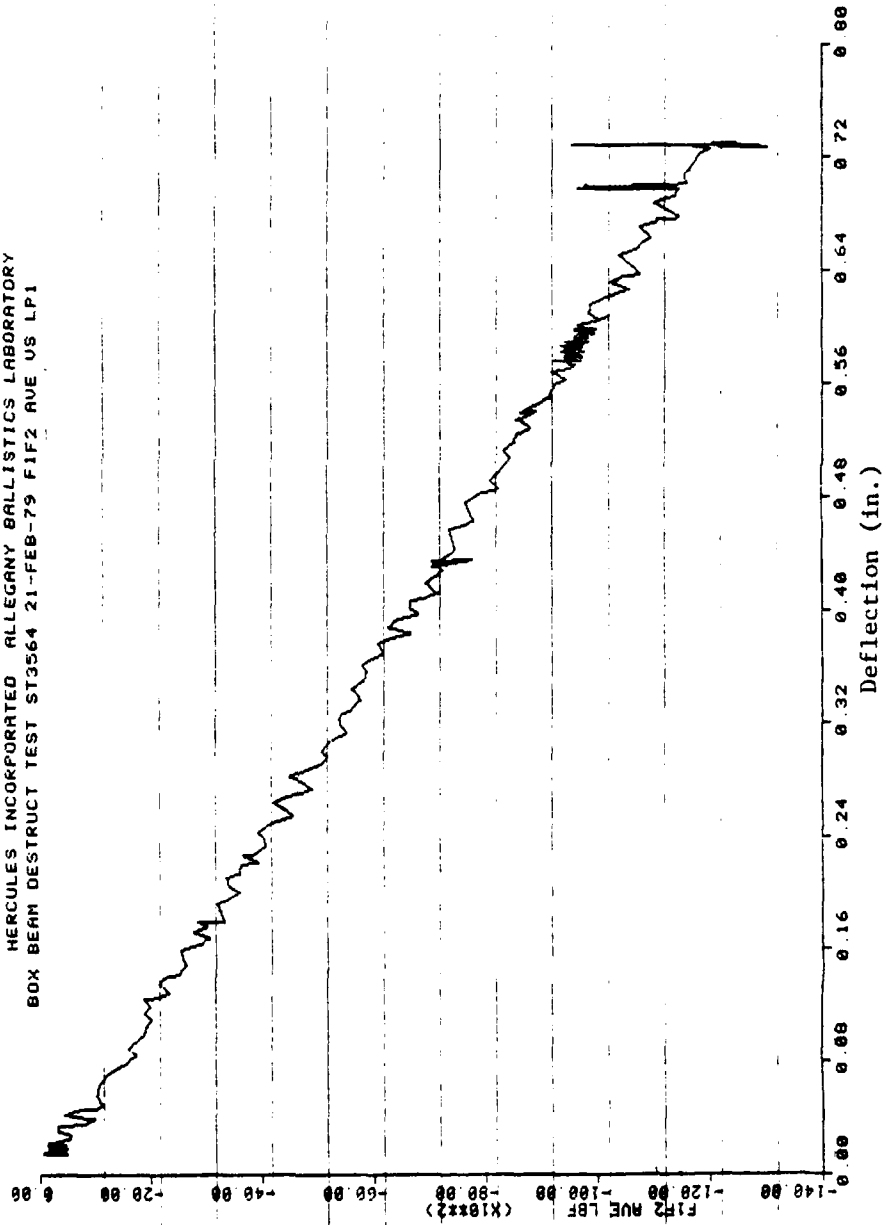


Figure 18. Load vs. Deflection at Mid-Span (Gage L1)

HERCULES INCORPORATED ALLEGANY BALLISTICS LABORATORY  
BOX BEAM DESTRUCT TEST ST3564 21-FEB-79 FIF2 AVE US LP3

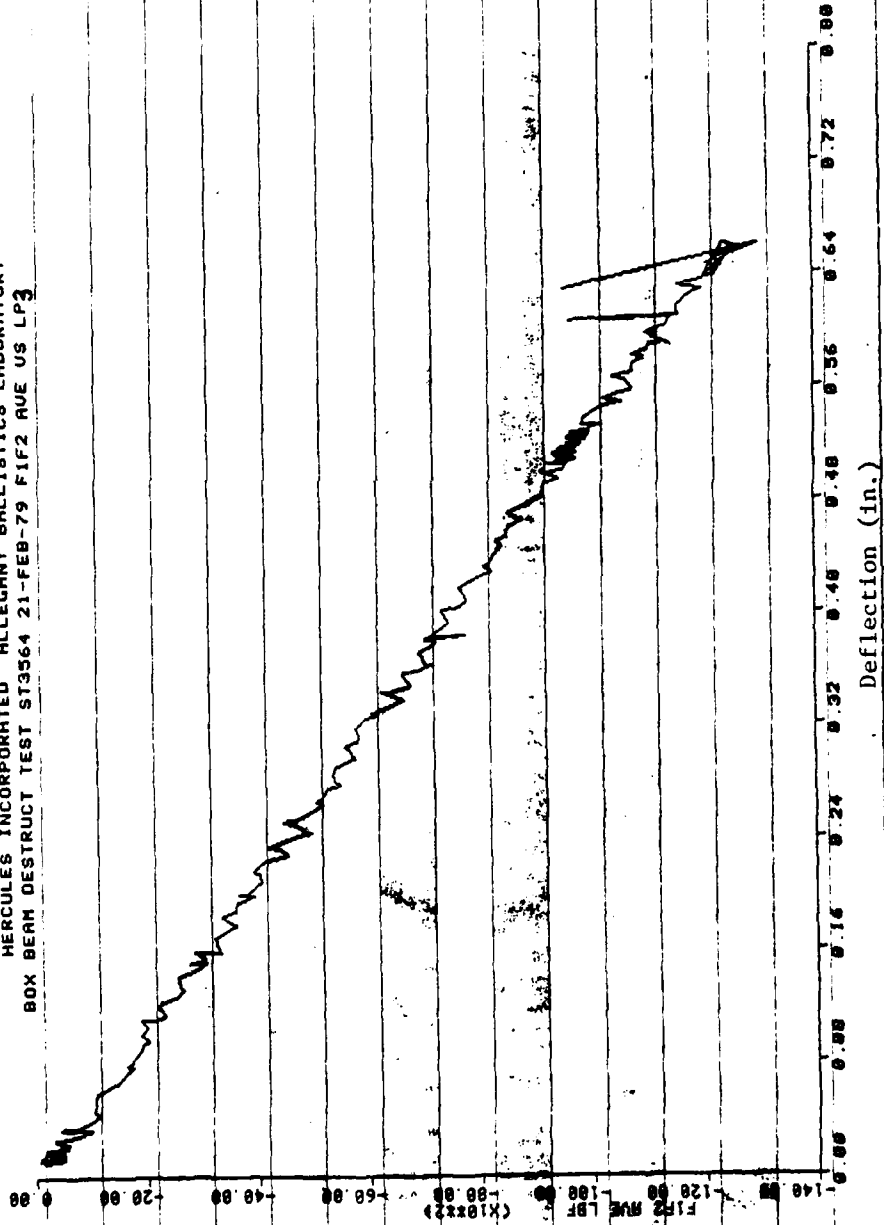


Figure 19. Load vs. Deflection at Load Point (Gage L3)

The surface strain in the outer  $\pm 45^\circ$  ply of the flange was also compared to predicted values. As shown before, at a load of 25,232 lb the maximum strain in the flanges occurred at mid-span and was:

$$\epsilon_8 = 0.00192 \text{ in./in.}$$

$$\text{or } \epsilon_{12} = 0.00196 \text{ in./in.}$$

The predicted strain determined from laminate analysis is  $\epsilon_{pre} = 0.00196$  in./in. which agrees quite well with the experimental results.

The test beam showed no indication of web lateral deflection during proof tests. This is seen in Figures 20 through 23 in which the strain measured by S5, S6, S17, S18, are linear with load. These are the  $\pm 45^\circ$  gages which were placed on the two sides of the beam (webs) in the high shear region during loading (Figure 9). Therefore, it appears that the webs did not buckle in shear under the loads attained in these tests.

## 2. Short Half-Scale Beam

This test was performed on an undamaged, unbraced, 34-in. section of the full half-scale beam. To avoid the crushing failure of the  $3\frac{1}{2}$  meter beam, wooden bulkheads were placed inside the box beam in the region of the load points (Figure 24). The short beam was then tested in three-point-bending to failure which occurred at 28,500 lb.

HERCULES INCORPORATED ALLEGANY BALLISTICS LABORATORY  
BOX BEAM PROOF 2 THRU 5 ST3563 21-FEB-79 FIF2 AVE US S5

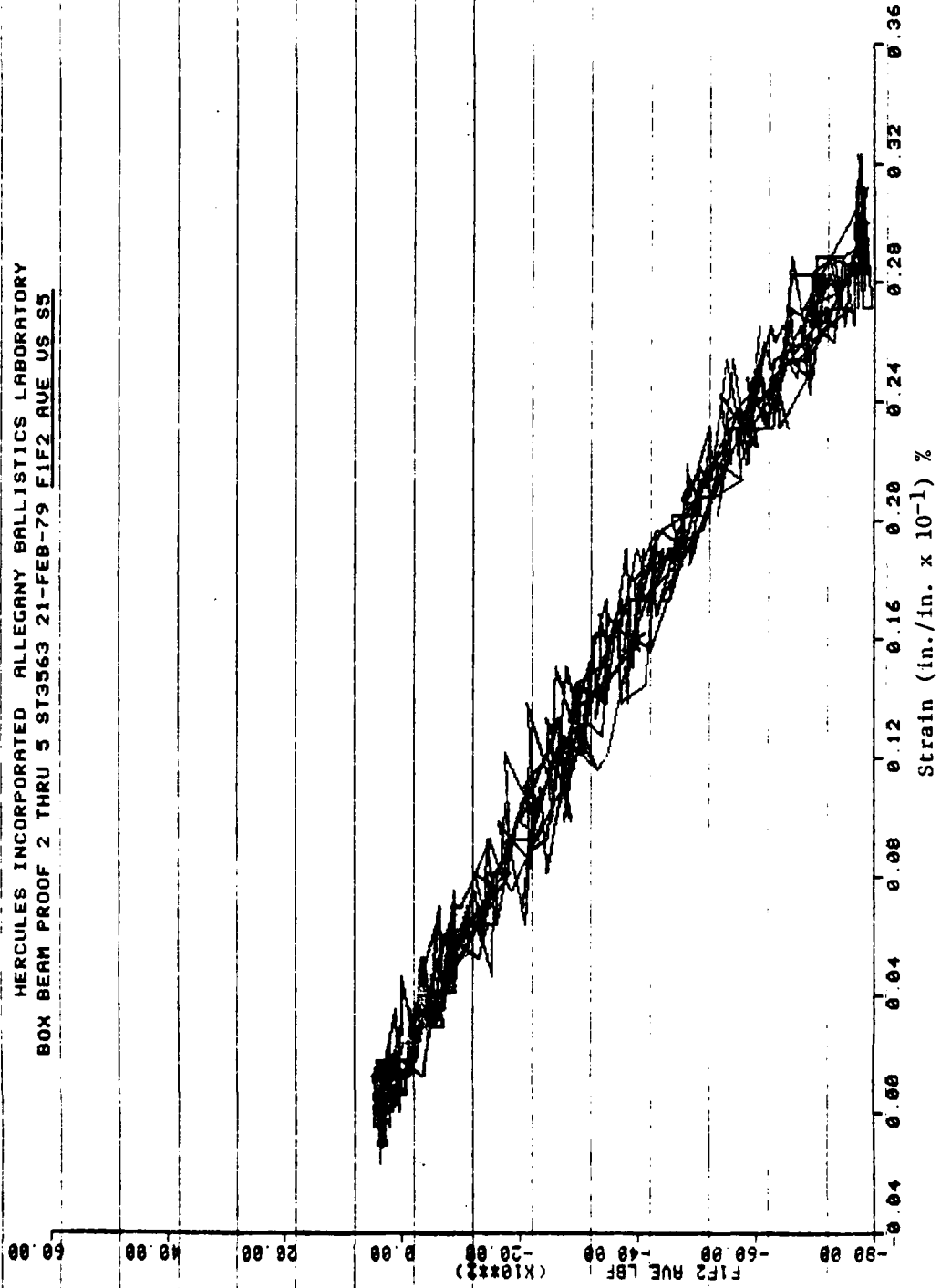


Figure 20. Load vs. Strain - Gage S5

HERCULES INCORPORATED ALLEGANY BALLISTICS LABORATORY  
BOX BEAM PROOF 2 THRU 3 21-FEB-79 PIF2 RUE VS 36

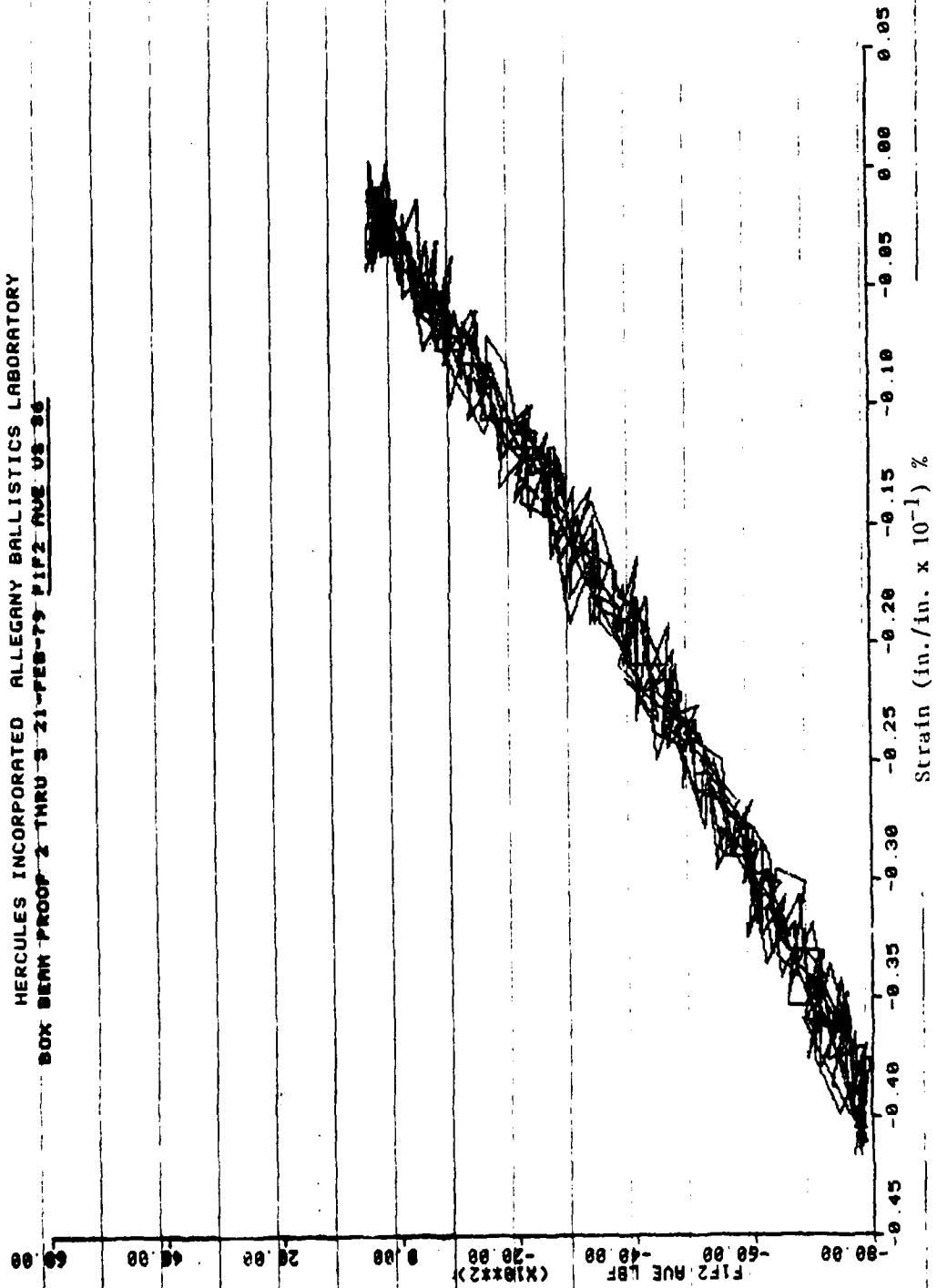


Figure 21. Load vs. Strain - Gage S6

HERCULES INCORPORATED ALLEGANY BALLISTICS LABORATORY  
BOX BEAM PROOF 2 THRU 5 ST3563 21-FEB-79 FIF2 AVE US S17

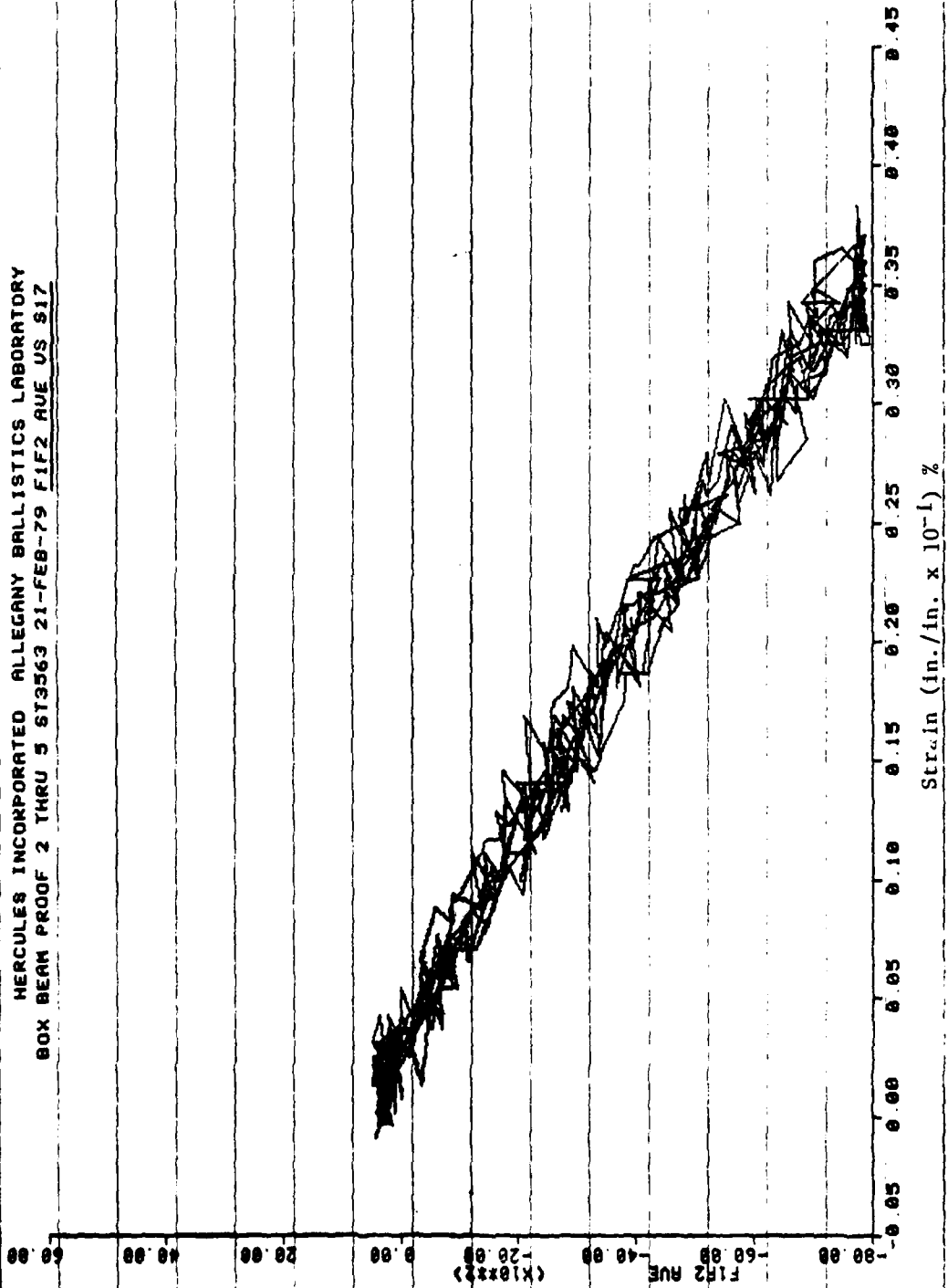


Figure 22. Load vs. Strain - Cage S17

HERCULES INCORPORATED ALLEGANY BALLISTICS LABORATORY  
BOX BEAM PROOF 2 THRU 5 ST3563 21-FEB-79 F1F2 RUE US 810

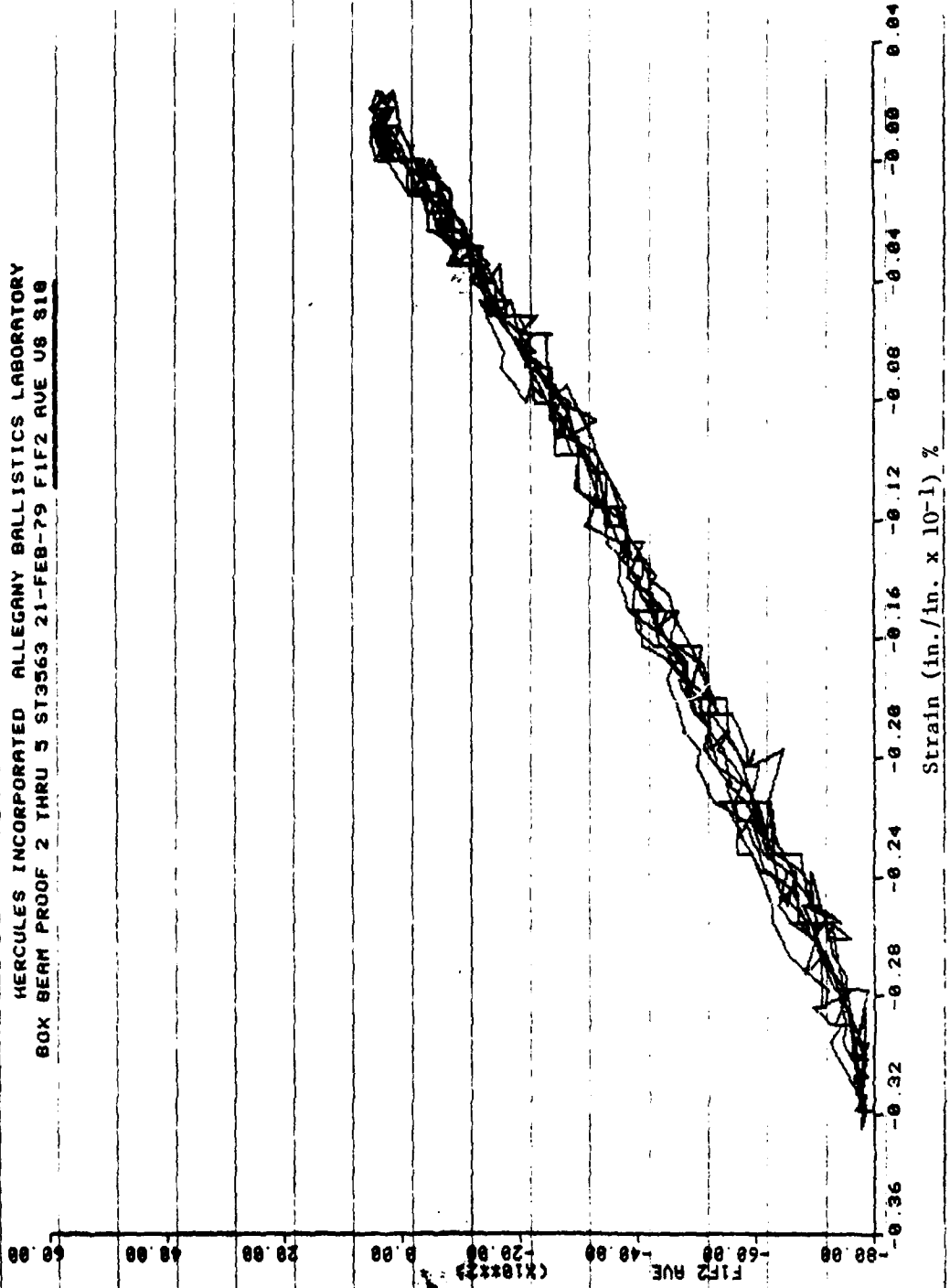


Figure 23. Load vs. Strain - Gage S18

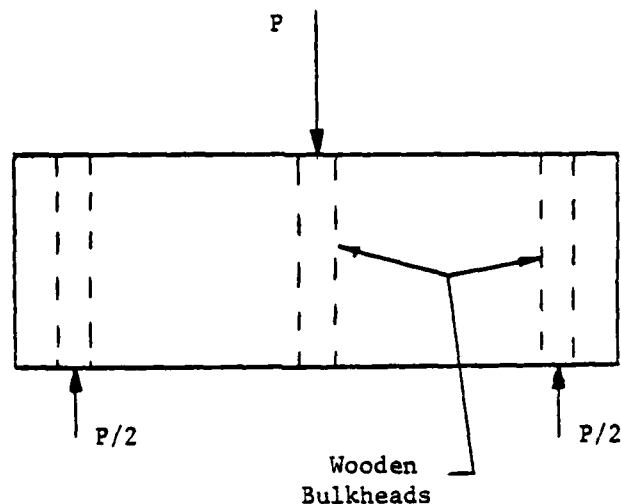


Figure 24. Schematic of the Three-Point-Bending Short Beam Test

a. Visual

As in the previous test, failure was due to the point load crushing of the flange. The failure was at the middle of the section where the middle wooden bulkhead transferred the load to the bottom flange. This resulted in the failure of the corner radius material which transitions from the  $\pm 45^\circ$  web to the flange. Photographs of the test, before and after, are given in Figures 25 through 27. Figure 25 shows the test configuration; Figure 26 shows the wooden bulkhead at the end load point; Figure 27 shows the short beam after failure.

b. Analysis

The calculations (Appendix A) for an unbraced short beam, predict the critical web shear buckling strength to be 3312 psi. Using this critical strength value and the equation:

$$\tau_{cr} = \frac{V EQ}{2b EI}$$

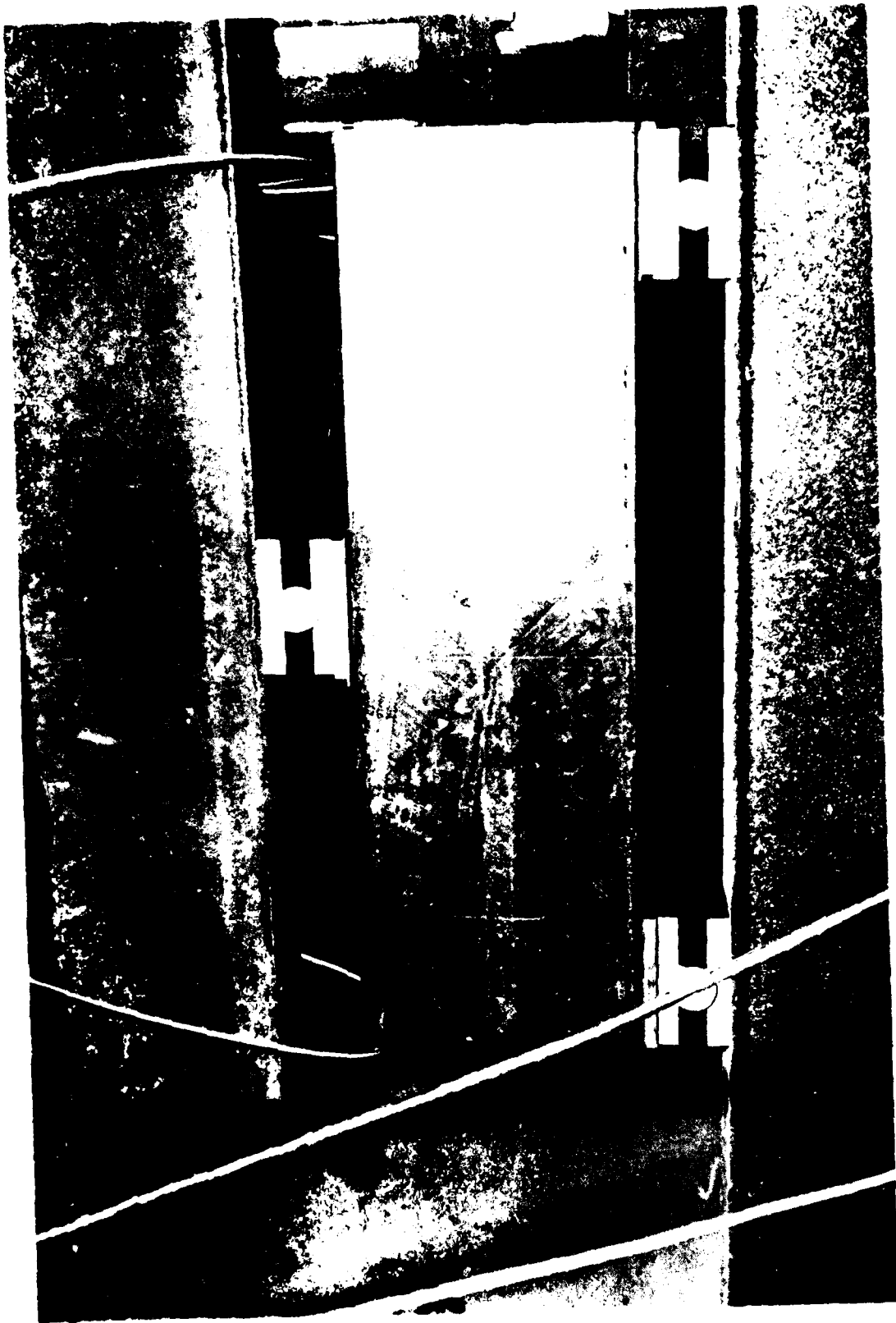


Figure 25. Three-Point Bending Test Configuration

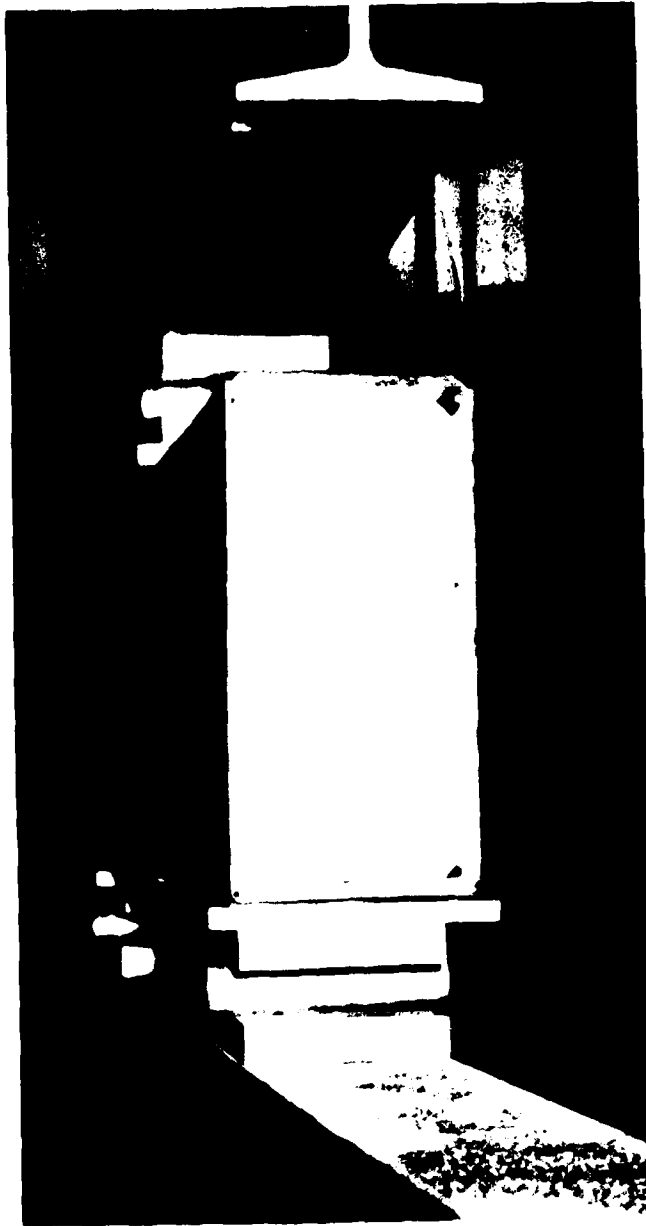


Figure 26. Short Beam with the Inclusion of Wooden Bulkheads

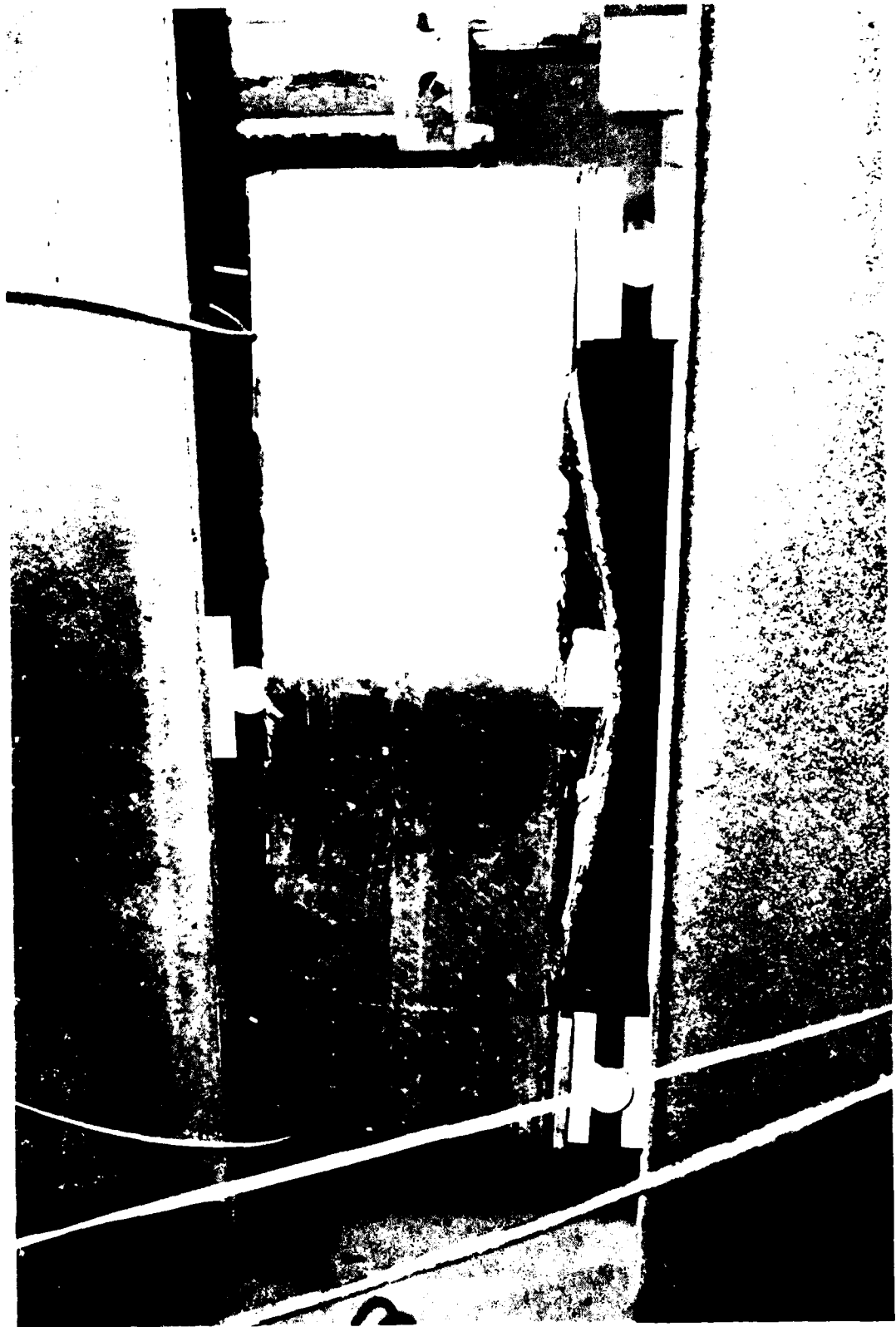


Figure 27. Failure Mode of Short Beam Section

where:  $V = F/2 =$  applied shear

$$EQ = 1.51 \times 10^8 \text{ lb-in.}$$

$$EI = 1.79 \times 10^9 \text{ lb-in.}^2$$

$$b = 0.132 \text{ in.}$$

yields a predicted failure load of:

$$F = 2V = 20,700 \text{ lb.}$$

This value is lower than the actual failure load of -28,500 lb. As noted previously, web shear buckling was not detected prior to failure. The laminated plate equation used to predict shear buckling failure in Appendix A is apparently conservative for this beam configuration.

## V. PIN-BEARING END CONNECTORS

### A. Full Scale Design

The design requirements of the pin-bearing end connectors were:

(1) that they be of integral construction with the flanges (not attached by bolts, rivets, etc.), (2) they must be capable of transmitting full box beam design loads with a 33% margin of safety, (3) they must be mating so that box beam modules can be attached end-to-end interchangeably to form a beam of an arbitrary number of modules, and (4) there must be no projection above the outer surface of the top flange or below the outer surface of the bottom flange.

The design for the end connectors is shown in Figure 28. It consists of a composite overwrapped fitting which transfers the load from the pin to the composite. This design is nearly the same as that used in production of helicopter main rotor blades at Hercules. The technology is

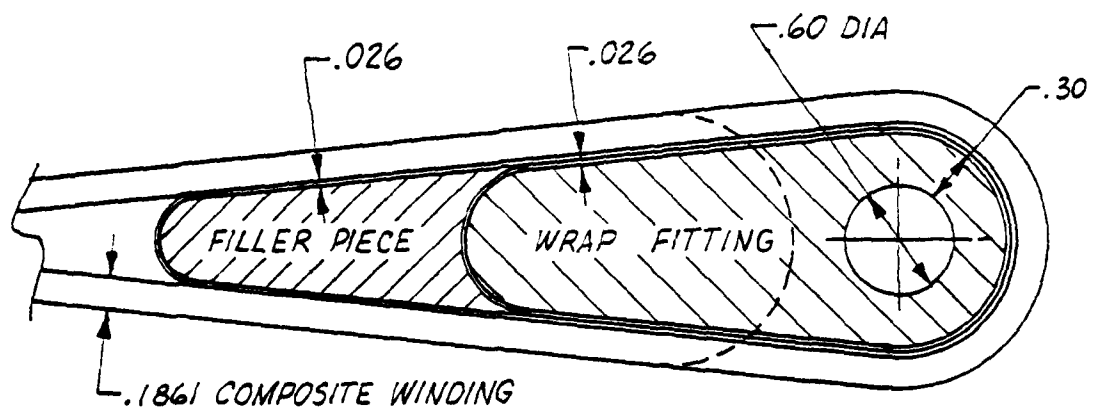
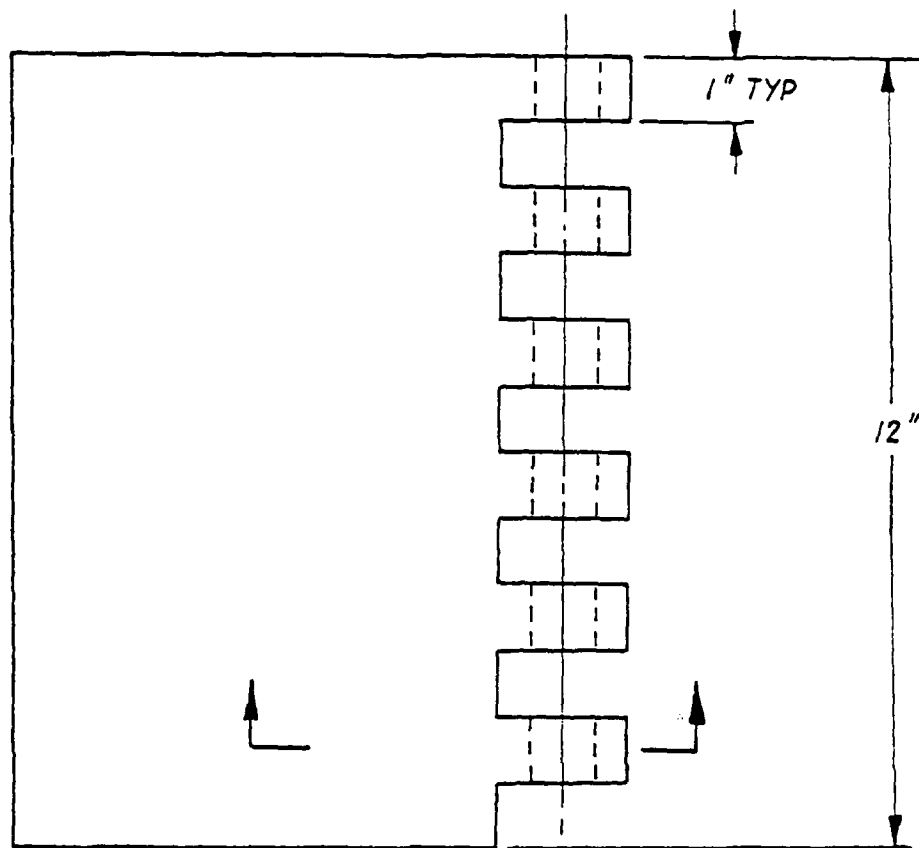


Figure 28. End Connector Configuration

based on a completely mechanized filament winding fabrication process and has been proven in the rotor blade connector program. The determination of composite thickness, pin diameter and wrap fitting dimensions of the connector were performed for full scale box beam loads.

To size the composite thickness around the wrap fitting, the force in the flange due to the box beam maximum moment must be determined. This is found from:

$$F = \frac{M}{h} = \frac{5.52 \times 10^6}{23.7} = 233,000 \text{ lbs}$$

where: M = design moment

h = distance from centerline of top flange to centerline of bottom flange

so 1.33 F = 310,000 lbs (includes MS).

Results of experiments performed by Kaman on similar joint specimens indicate that the delivered fiber stress for this configuration is  $\sim \sigma_f/2$ . Therefore, for AS graphite,  $\sigma_f = 400,000$  psi, so the delivered fiber stress,  $\sigma_{f_{del}}$ , is:

$$\sigma_{f_{del}} = 200,000 \text{ psi.}$$

From this value, the thickness of composite around the wrap fitting necessary to withstand the load can be calculated as:

$$\sigma_{f_{del}} = \frac{F}{wt_f} \quad w = \left( \frac{12.11 - 0.364}{2} \right) = 5.92 \text{ in.}$$

$$t_f = \frac{310,000}{(5.92)(200,000)} = 0.262 \text{ in. (fiber thickness)}$$

$$t_c = 0.476 \text{ in. (composite thickness } \approx 0.55 V_f)$$

Therefore, more unidirectional composite material is necessary in the joint than in the flanges (0.3722 in.). This additional material can

be provided by the following procedure. Initially, the wrap fitting is overwound with 0.026 in. of composite material (shown in Figure 28). A filler piece is placed behind the composite and a second layer of 0.026 in. of composite is wound over the wrap fitting and filler piece combination. This provides the build-up of additional material around the wrap fitting. Finally, another filler piece is placed in position and the final 0.1861 in. of composite is wound, yielding a gage length thickness of 0.3722 in., the required thickness in the flange.

The pin size must also be determined. This sizing is performed according to shear calculations. First, a configuration such as Figure 28 is assumed so that the number of shear surfaces is known, eleven in this case. The pin is also assumed to be steel, having an ultimate shear strength of 100,000 psi. Then:

$$F = (11)(\tau_{ult})\left(\frac{\pi D^2}{4}\right)$$

$$D^2 = \frac{(4)(310,000)}{(11)(100,000)\pi} = 0.359 \text{ in.}^2$$

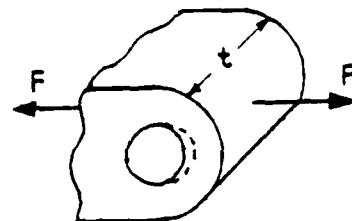
$$D = 0.599 \text{ in.} \Rightarrow \text{Select } D \geq 0.600$$

Next, the metal wrap fitting must be sized. It also is assumed to be steel with an ultimate bearing strength of 120,000 psi. In bearing:

$$F = Dt \sigma_{BR_u}$$

$$t = \frac{310,000}{(0.600)(120,000)} = 4.30 \text{ in.}$$

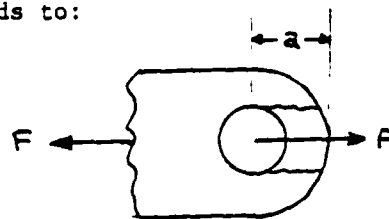
so 6 fittings, 1-in. thick are OK.



Checking the possibility of tear-out leads to:

$$F = 2a \tau_{ult}$$

$$a = \frac{310,000}{(2)(100,000)} = 1.55 \text{ in.}$$



Now, assume the steel carries all of the load. With six fittings, each must carry:

$$\frac{310,000}{6} = 51,677 \text{ lb}$$

∴  $a = 0.26 \text{ in.}$  on each fitting.

#### B. Full Scale Fabrication Including End Connectors

The fabrication scheme which includes the end connectors is shown in Figure 29. It is a variation of the process used to fabricate the half-scale prototype beams. Initially, the end connection inserts are wound and the unidirectional flange material is wound around the inserts. Meanwhile, the beam mandrel and generating discs have been assembled and the interior  $\pm 45^\circ$  layers have been wound. The unidirectional windings with the end connectors are placed on the top and bottom of the beam and the final layers of  $\pm 45^\circ$  composite are wound in place. Finally, the entire configuration is placed in a mold and cured.

#### C. Test Specimens

##### 1. Design

The specimen configuration, seen in Figure 30, was selected so that existing tooling could be used to produce the specimens. This specimen is 48 in. long from pin-center to pin-center and 2.245 in. wide.

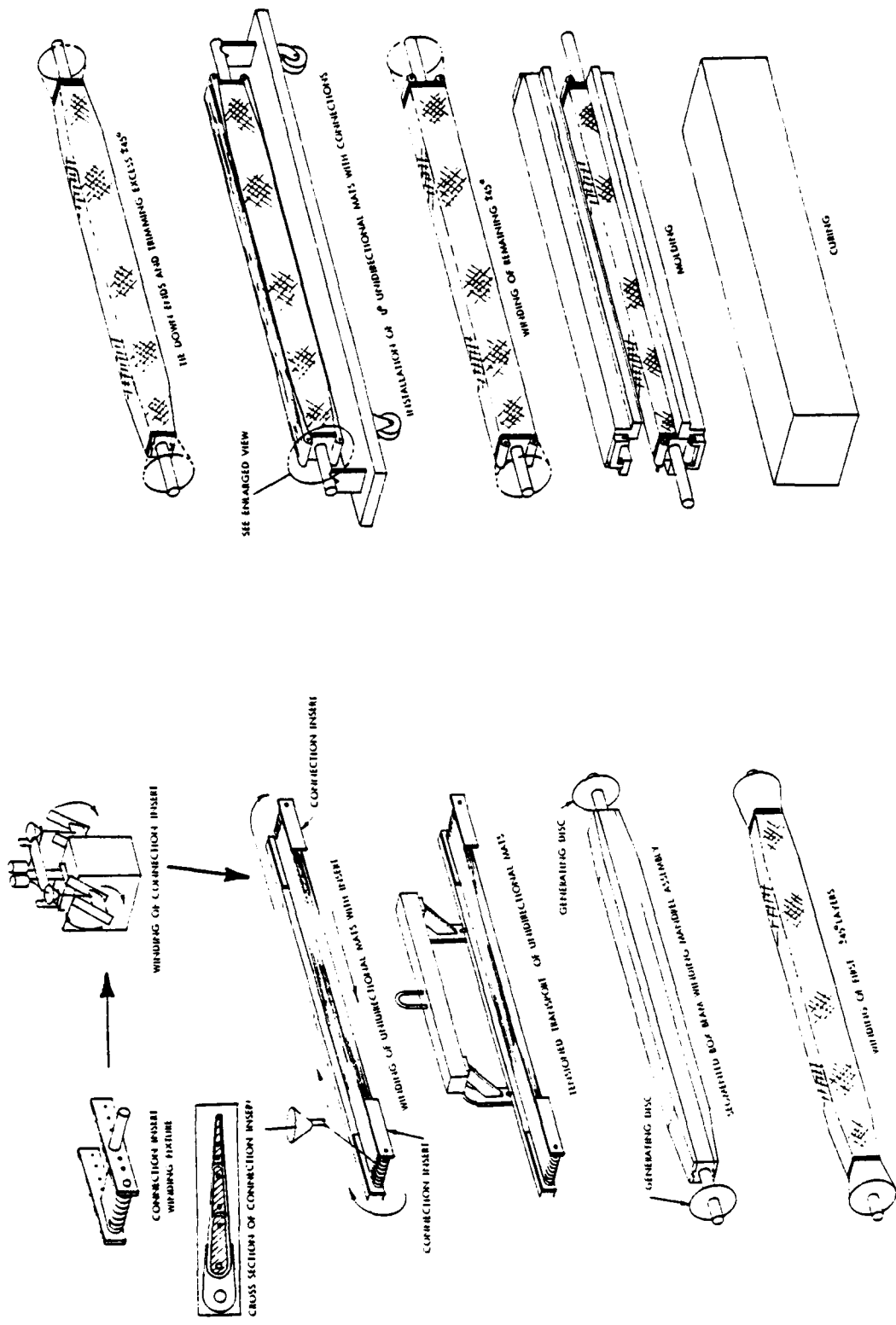


Figure 29. Fabrication Scheme Including End Connectors

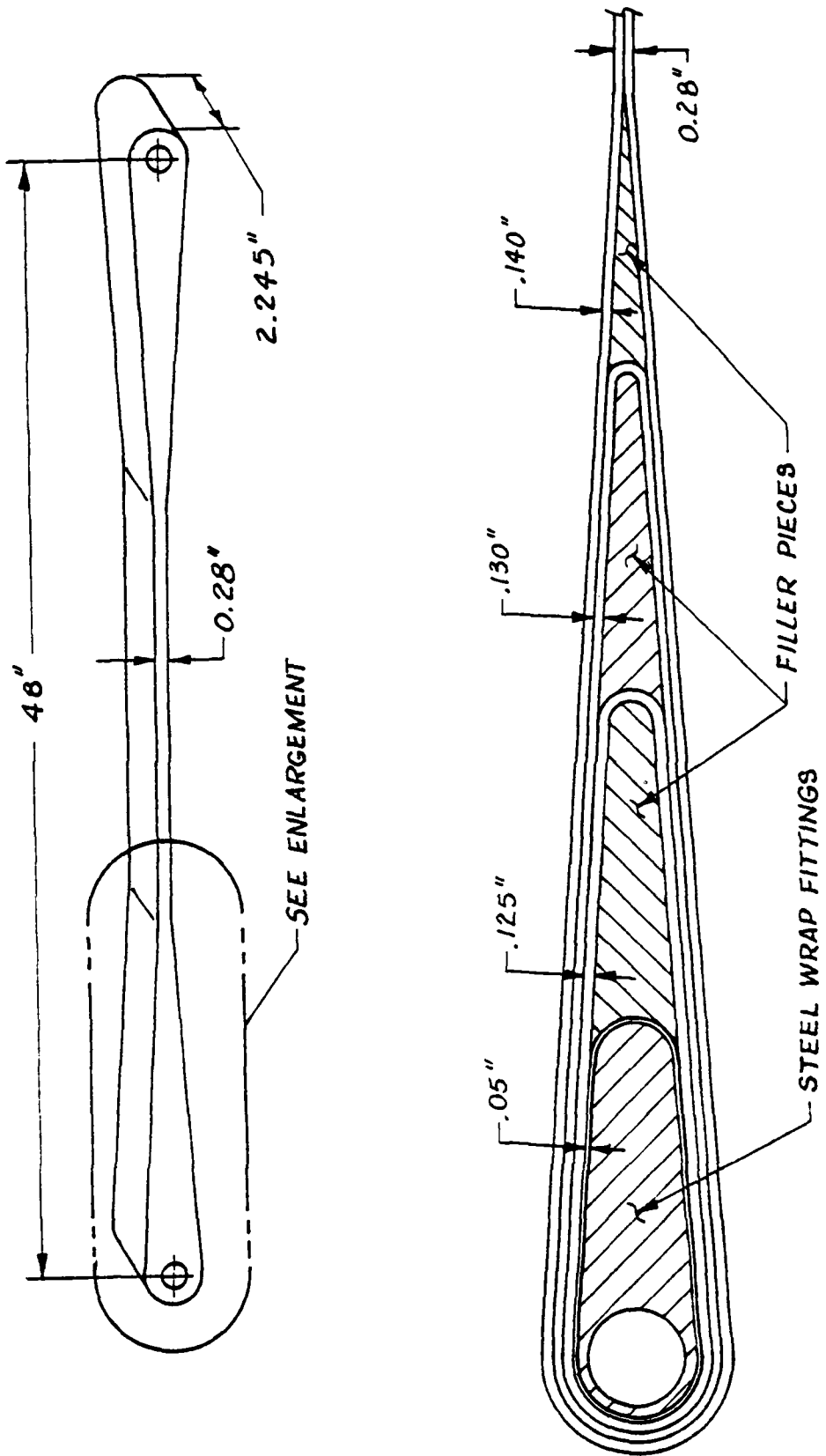


Figure 30. End Connector Test Specimen

The thickness in the gage length is 0.280 in. The winding thicknesses around the wrap fitting and subsequent filler pieces are: 0.050 in., 0.125 in., and 0.130 in., respectively. The final exterior winding is 0.140 in. which provides the 0.280 in. in gage length thickness.

One problem with this existing design, however, is that the thickness build-up ratio around the pin is approximately 3:1. This is much greater than is desired in the full scale design. Therefore, a change in the design was made by replacing the composite material in the first two windings (0.050 in., 0.125 in.) with aluminum "shims". This leaves an interior composite winding of 0.130 in. along with the exterior winding of 0.140 in., resulting in the desired build-up ratio of approximately 2:1.

## 2. Fabrication

Each specimen was fabricated identically with the same amount of graphite windings. However, during the cure cycle, the mold closure on each specimen varied, yielding different gage length thicknesses. The thicknesses obtained were 0.32 in., 0.34 in., and 0.40 in., respectively, for the three specimens fabricated. Only three specimens were necessary in the program because in the compression test one of the "as fabricated" specimens was cut in half to yield two compression specimens.

## 3. Tension Tests

In order for the joint to be effective it must be able to carry the same load as the flange of the box beam. Therefore, the joint must carry the equivalent of 310,000 lbs or a stress of:

$$\sigma = F/wt = \frac{310,000}{(6)(0.3722)} = 138,800 \text{ psi}$$

a. Unit #1

The test configuration is shown in Figure 31. The test was performed in a Baldwin Universal Testing Machine capable of applying 200,000 lbs of force in tension and compression. The load was applied at a rate of 12,000 lb/min. The results of the first test are shown in Table 10.

TABLE 10

TENSILE TEST RESULTS - UNIT #1

Test Rate	12,000 lb/min.
Ultimate Load	92,000 lb
Elongation (ultimate)	0.785 in.
Fiber Area in Gage Length	0.324 in. <sup>2</sup>
Composite Area in Gage Length	0.718 in. <sup>2</sup>
Calculated Fiber Stress	283,950 psi
Calculated Composite Stress	128,150 psi

Catastrophic failure occurred at 92,000 lbs load near the wrap-around area of the joint. Just prior to failure, separation of the gage length material occurred and influenced subsequent behavior. The separation undoubtedly resulted in a premature failure of the specimen. A photograph of the failed specimen is shown in Figure 32.

The composite stress at failure calculated for this specimen is 8% below the required value of 138,800 ( $MS = 0.22 < 0.33$ ).

b. Unit #2

In order to prevent the material separation which caused the early failure of Unit #1, metal clamps were used on Unit #2, as shown

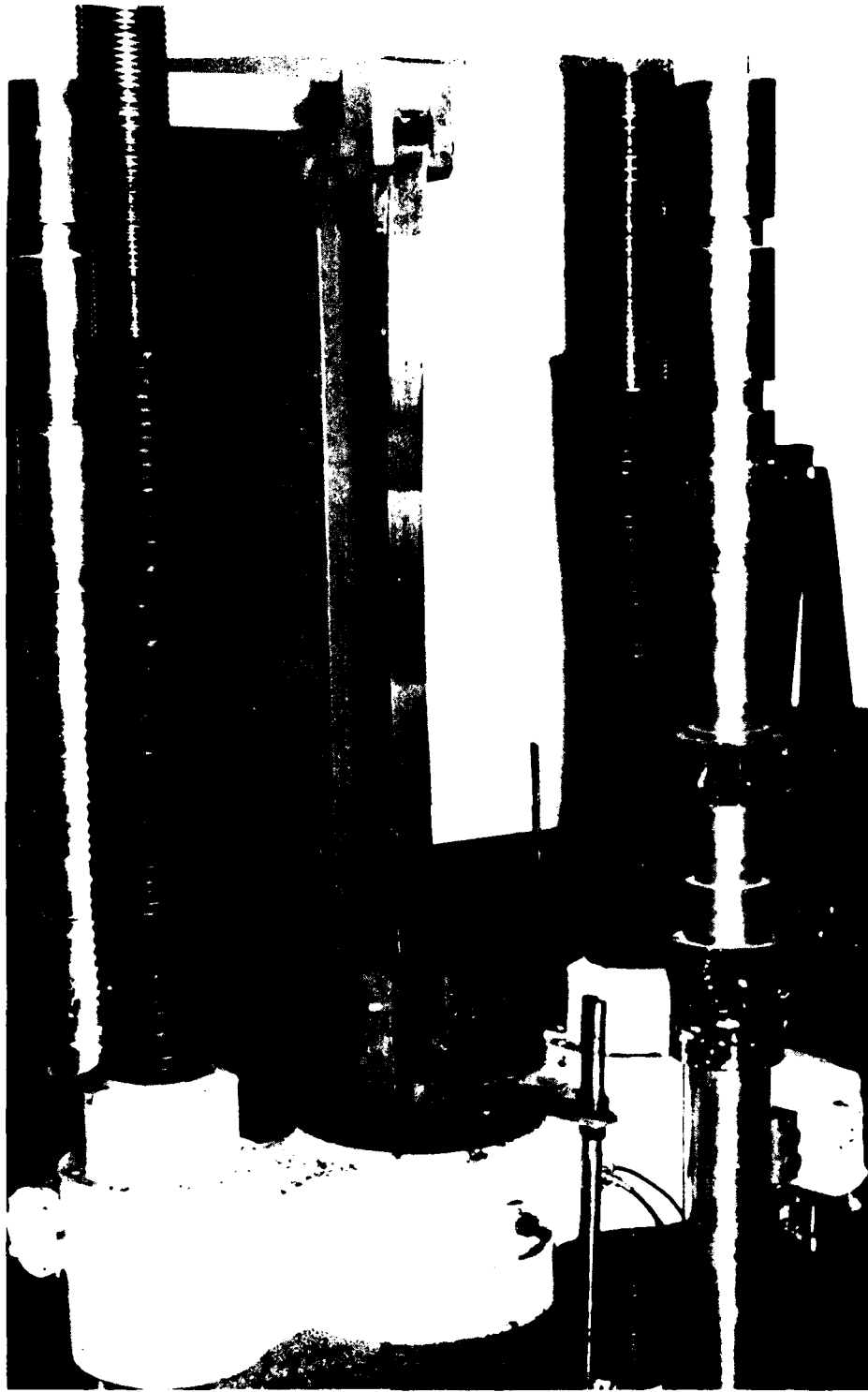


Figure 21 - Torque Test Configuration - Unit No. 1



Fig. 1. (a) Failure of Unit 11, 1

in Figure 33. These clamps are steel plates with rubber pads to prevent composite/steel contact damage, positioned on both sides of the specimen and bolted together. They are located at the point of transition from the joint to the gage section. It should be noted that the constraint to separation afforded by the clamps is a more realistic simulation of conditions in an actual overwrapped joint than the unclamped condition.

Specimen #2 was also instrumented with six electrical resistance strain gages, three axially, three transverse in order to define the stress-strain profile in the specimen. The results of Unit #2 are shown in Table 11. The gage section stress-strain curve, Figure 34, was used to determine the ultimate strain and composite modulus of the specimen shown in Table 11. This stress-strain curve was derived from load versus time and strain versus time test data.

TABLE 11

TENSILE TEST RESULTS - UNIT #2

Test Rate	12,000 lb/min.
Ultimate Load	103,500 lb
Elongation (ultimate)	0.910 in.
Fiber Area in Gage Length	0.324 in. <sup>2</sup>
Composite Area in Gage Length	0.763 in. <sup>2</sup>
Calculated Fiber Stress	319,450 psi
Calculated Composite Stress	135,650 psi
Composite Ultimate Strain	0.010 in./in.
Composite Modulus	15.2 x 10 <sup>6</sup> psi



Figure 1. Test Configuration - Unit No. 2

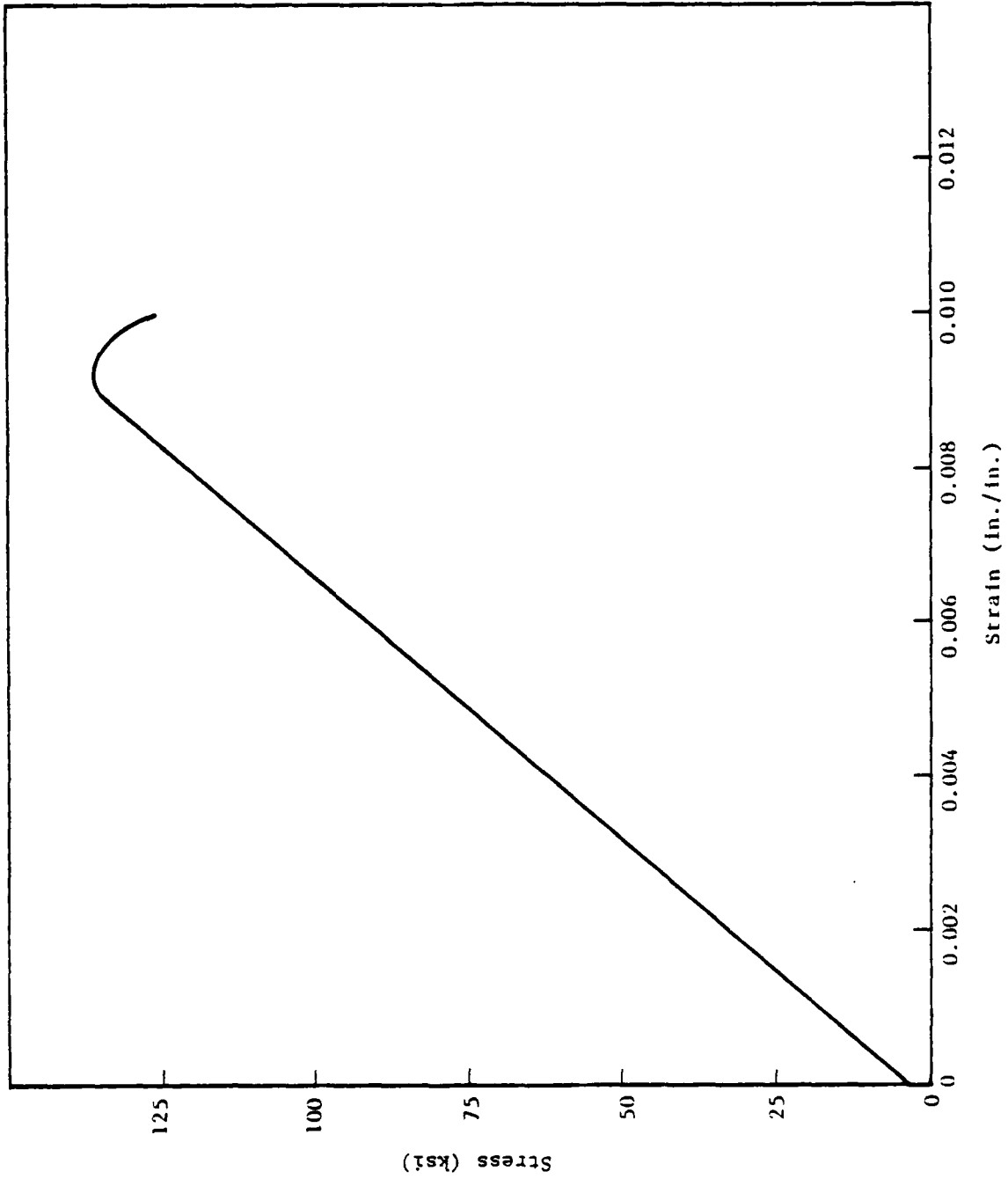


Figure 34. Stress vs. Strain - Tensile Unit #2

The breaking strength of this specimen shows an increase of almost 12,000 lbs over Unit #1 due to the material separation constraint. However, when compared with the desired ultimate stress of 138,800 psi, the joint is still 2% low (or MS = 0.30). A photograph of the failed specimen is shown in Figure 35.

#### 4. Compression Tests

The compression test setup is shown in Figure 36. The two specimens used for these tests were obtained by cutting one complete specimen, in half, through the gage section. The test fixture consists of two large steel blocks at the bottom of the specimen. These blocks are bolted together with a rubber pad to protect the specimen from abrasion. At the top of the specimen is another large steel block with a semi-circular cut-out to fit the curvature of the specimen. A rubber pad is also placed between the compression cap and the specimen for protection. The testing was performed in the Baldwin Universal Testing Machine with a loading rate of ~8000 lb/min. The results of the two compression tests are presented in Table 12.

TABLE 12

#### COMPRESSION TEST RESULTS

	<u>Unit #3</u>	<u>Unit #4</u>
Test Rate	7,500 lb/min.	8,000 lb/min.
Load at End of Test	20,000 lb	21,000 lb
Crosshead Displacement	0.235 in.	0.200 in.
Fiber Area in Gage Length	0.324 in. <sup>2</sup>	0.324 in. <sup>2</sup>
Calculated Fiber Stress	61,730 psi	64,815 psi
Calculated Composite Stress	22,270 psi	23,385 psi

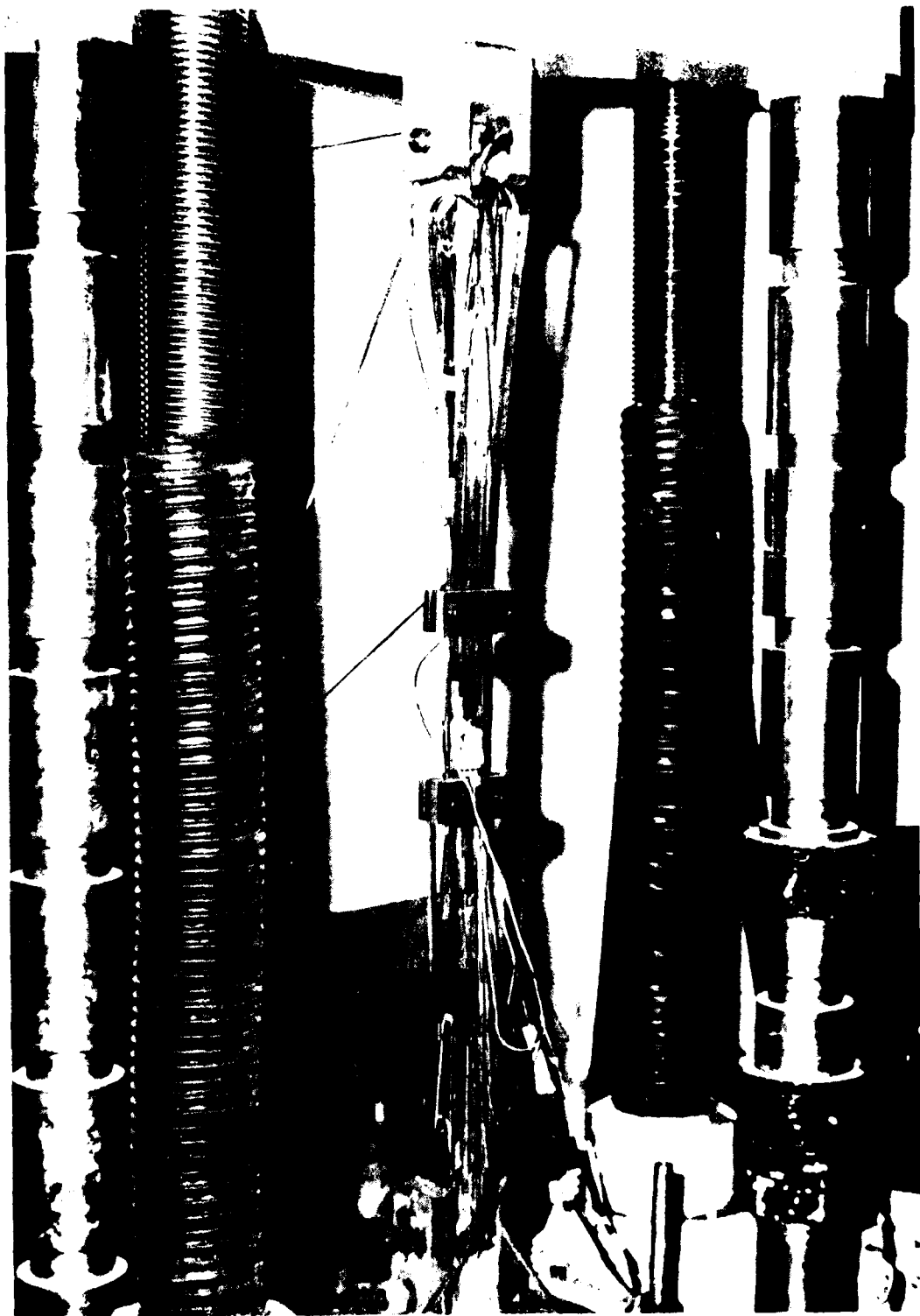


Figure 39. Tail unit, Unit No. 2

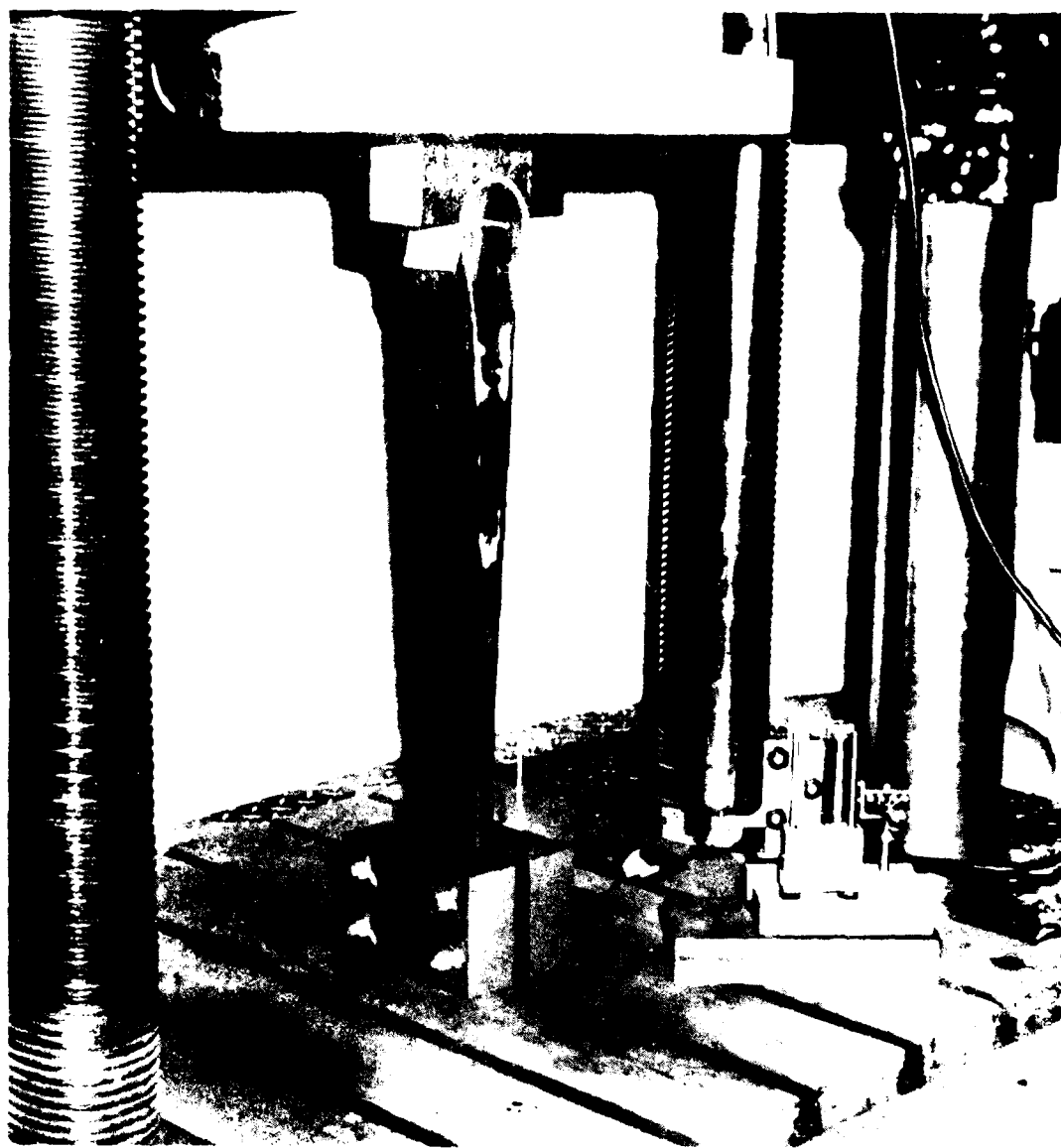


Figure 36. Compression Test Configuration

Both tests were terminated prior to compression failure due to the occurrence of lateral instability in the specimen. This may have occurred because the Euler buckling load for this specimen configuration had been reached. Due to the complexity of the specimen geometry, it is difficult to make an analytical prediction of the Euler buckling load; however, rough calculations lead to an estimated buckling load of approximately 20,000 lb. Another possibility is a fabrication induced prestress in the specimens may have caused a slight initial curvature prior to testing. This initial curvature would tend to increase with continued loading resulting in a lateral instability prior to reaching the ultimate strength in compression. Strain data were collected in both the unidirectional and transverse directions in the compression tests; however, due to instrumentation malfunction the data were meaningless.

## DISCUSSION

The objectives of this program have all been met. A fibrous composite box beam using AS graphite/HBRF-55A epoxy has been designed for use as a bridging launch beam. The beam design achieves a 50% weight reduction and a 16% increase in flexural rigidity over a comparable aluminum design.

Several fiber/resin composite materials were investigated to determine those with the best potential ability to withstand the load, environment, and fatigue life requirements, and stay within the 20 lb/ft weight constraint. The most suitable materials were ascertained to be AS graphite fiber and HBRF-55A epoxy resin.

Fabrication technology applicable to commercial production of such beams was demonstrated via the fabrication of geometric half-scale beams. The fabrication technique employed filament winding, an efficient production oriented low manpower process.

The half-scale constant cross section box beams were fabricated with no end connectors in order to prove the fabrication techniques. However, a later addition to the contract requested that one of these beams be structurally tested to determine the moment and shear carrying capabilities of the design. The problem of accurately introducing loads in the beam to produce the desired moment and shear was encountered in carrying out the test program.

A four-point-bending arrangement was determined to be the most advantageous method of introducing the loads. However, this test arrangement proved

to be inadequate due to the high point loads, necessary to induce the desired moment and shear, which resulted instead in a crushing failure of the web/flange transition region at 58% of the predicted failure strength.

Several changes in the test arrangement might alleviate this problem. First, a more complex load transfer system having a six-point or eight-point-bending configuration might be utilized. This would reduce the point loads proportionately to the extent that bending or shear failure could be induced. Second, bulkheads could be placed in the beam to produce a more even distribution of the point loads throughout the beam. Finally, a test beam could be fabricated complete with end connectors. This would allow the loading of the box beam in a manner more realistically simulating the actual loading conditions of the full scale traversing beam.

Another problem encountered in the testing phase of this program was due to the geometric scaling of the half-scale beam. It was determined that when physical scaling is performed, the load carrying capabilities in flexure and shear do not scale linearly. This scaling produced the half-scale beam which was determined to be failure critical in shear in the webs due to the flexural load. Therefore, flange failure, which was the object in the four-point-bending test, was made all the more difficult to induce.

The experimental data obtained from the half-scale beam test indicate that the beam behaved according to laminate theory in terms of flexural rigidity, surface strain, and deflection. The calculations for flexural

rigidity show a maximum variation from the experimental value of only 6% while the strain values show only a 2% deviation between predicted and experimental results. These results increase confidence in the application of laminate theory to composite structures.

The three-point-bending test of the half-scale beam section to determine web failure characteristics showed that the predicted load for web shear buckling may be conservative for this beam configuration. The short section failed at a load of ~28,500 lb as compared to a predicted critical web shear buckling value of ~20,700 lb. The collapse of the beam at this load was due to the failure of the web/flange region under the load point.

A full scale joint concept was designed. This concept provides a pin-bearing end connector which is of integral construction with the flange of the beam. This joint design concept was tested on a subscale dimension in tension and compression. The tension tests showed that the design is feasible with failures occurring with 2% of the required flange tensile load capability.

On the other hand, the compression tests on joint specimens proved meaningless. The two specimens tested in compression both failed prematurely by lateral instability prior to compressive failure. These failure loads attained were 10,000 lb and 21,000 lb, less than half the target value.

In retrospect, it is felt that a more realistic compression test would result if a specimen configuration were employed in which an exterior

layer of  $\pm 45^\circ$  graphite/epoxy material was wound around the specimen. This would more accurately simulate the configuration and constraint in the full scale design and would tend to prevent premature buckling failure.

## CONCLUSIONS

- A fibrous composite box beam, achieving a 50% weight reduction and a 16% increase in flexural rigidity over a comparable aluminum design, has been designed, using AS graphite/HBRF-55A epoxy, for use as a U. S. Army mobile bridging launch beam.

- Filament winding fabrication technology applicable to commercial production of such beams was demonstrated via the fabrication of two geometric half-scale beams.

- One (1) half-scale box beam was structurally tested in four-point-bending to determine its load carrying capabilities. Geometric scaling and load application problems resulted in the beam being web shear critical rather than flange critical. Failure occurred at 58% of the predicted ultimate due to crushing of the web/flange transition region under the concentrated load points.

- Experimental data from the half-scale test correlate well with predicted values for flexural rigidity, surface strain, and deflection.

- The three-point-bending of the short beam section showed that the web shear buckling load predicted by laminate theory tends to be conservative. The beam failed at 138% of the predicted web shear buckling load and the failure was again due to crushing of the web/flange transition region.

- A full scale joint concept, providing a pin-bearing end connector of integral construction with the beam flanges, was tested on a subscale

dimension in tension and compression. The tensile tests indicate that the design is feasible, failing within 2% of the predicted ultimate. The compression tests were terminated prior to compressive failure due to lateral instability. This instability was due to Euler buckling and/or a fabrication induced prestress in the specimen.

## RECOMMENDATIONS

Hercules recommends that investigations and testing of traversing launch beams should be continued. However, any beams fabricated for such testing should be made with integral end connectors. This would make it easier to introduce the moment and shear loads to the beam and eliminate several of the problems encountered in this program.

Hercules also recommends that if it is necessary to use a half-scale design in order to save material and fabrication costs, that the scaling be on the basis of the load carrying capability of the full scale design rather than geometry.

Further testing on specimens which more accurately represent the full scale beam joints should also be conducted. These tests should precede beam testing. This would insure that an adequate joint design could be developed to transfer the required loads to the beam without premature failure in the joint region.

#### REFERENCES

1. Jones, R. M., "Mechanics of Composite Materials", McGraw-Hill Book Company, 1975.
2. AFML-TR-74-266, "Development of Engineering Data on Mechanical and Physical Properties of Advanced Composite Materials", February 1975.
3. DuPont Kevlar Handbook.
4. Roark, R. J., "Formulas for Stress and Strain", McGraw-Hill Book Company, 1954.
5. Lekhnitskii, S. G., "Anisotropic Plates", Gordon and Breach Science Publishers, Inc., Ch. 14, 1968.

APPENDIX A

MATHEMATICAL BOX BEAM ANALYSIS

EXAMPLE ANALYSIS PROCEDURE

1. Select the flange and web construction. The flange will consist of ( $0^\circ$ ,  $\pm 45^\circ$ ) construction with the  $\pm 45^\circ$  windings carried through the webs.

 0.6362"	4 layers @ $\pm 45^\circ$	0.0704"
	10.5 layers @ $0^\circ$	0.1861"
	7 layers @ $\pm 45^\circ$	0.1232"
	10.5 layers @ $0^\circ$	0.1861"
	4 layers @ $\pm 45^\circ$	0.0704"

2. Determine the flexural rigidity for this construction:

$$EI = \sum_{i=1}^n E_i I_i$$

$$I_{\text{flange}} = Ad^2 = (12.11 \times 0.6363)(12.5 - 0.6362/2)^2 = 1143 \text{ in.}^4$$

$$E_{\text{flange}} = 11.9 \times 10^6 \text{ psi}$$

$$I_{\text{web}} = (0.264)(23.73)^3/12 = 294 \text{ in.}^4$$

$$E_{\text{web}} = 2.91 \times 10^6 \text{ psi}$$

$$\therefore EI = 2(11.9 \times 10^6)(1143) + 2(2.91 \times 10^6)(294) = 2.89 \times 10^{10} \text{ lb-in.}^2$$

3. Determine linear weight:

$$WT = [A_{\text{flange}} + A_{\text{web}}] \rho (12 \text{ in./ft})$$

$$= 2[(12.11)(0.6362) + (0.264)(23.73)](0.054)(12) = 18.1 \text{ lb/ft}$$

4. Determine the average bending stress for the flange:

$$N_x = \frac{F}{b} = \frac{M}{bEI} \int_0^{A_i} E_i Y dA = \frac{M}{bEI} \sum_{i=1}^n E_i Y_i A_i$$

$$N_x = \frac{5.52 \times 10^6}{(12.11)(2.89 \times 10^6)} \left[ (11.9 \times 10^6)(0.6362)(12.11)(11.23) \right] = 16,236 \text{ lb/in.}$$

Now from laminate analysis, using this value for  $N_x$  yields:

$$\pm 45^\circ \text{ In Layers } \begin{cases} \sigma_{11} = 7842 \text{ psi} \\ \sigma_{22} = 705 \text{ psi} \\ \tau_{12} = 2940 \text{ psi} \end{cases} \quad MS = \frac{6800}{2940} - 1 = 1.31$$

$$0^\circ \text{ In Layers } \begin{cases} \sigma_{11} = 38,480 \text{ psi} \\ \sigma_{22} = 975 \text{ psi} \\ \tau_{12} = 0 \end{cases}$$

5. Determine Critical Flange Buckling Load (Ref. 1)

From computer program

$$m = 16, n = 1 \text{ (buckling modes)}$$

$$\therefore N_{x_{cr}} = 42,680 \text{ lb/in.}$$

$$MS = \frac{N_{x_{cr}}}{N_x} = \frac{42,680}{16,236} - 1 = 1.63$$

6. Determine the In-Plane Loading on the Web

$$\sigma = \frac{My}{I} = \frac{MEy}{EI} = \frac{(5.52 \times 10^6)(2.91 \times 10^6)(11.90)}{2.89 \times 10^{10}} = 6614 \text{ psi}$$

$$N_x = (6615)(0.264) = 1746 \text{ lb/in.}$$

Now from laminate analysis, again:

$$\sigma_{11} = 6076 \text{ psi}$$

$$\sigma_{22} = 545 \text{ psi}$$

$$\tau_{12} = 3300 \text{ psi} \quad MS = \frac{6800}{3300} - 1 = 1.06$$

7. Determine Maximum Shear Stress in the Web

$$\tau_{\max} = \frac{VQ}{Ib} = \frac{VEQ}{EIb} = \frac{V}{bEI} \sum_{i=1}^n E_i Y_i A_i$$

$$\begin{aligned} \sum_{i=1}^n E_i Y_i A_i &= (11.9 \times 10^6) \left(12.5 - \frac{0.6362}{2}\right) (0.6362 \times 12.11) \\ &\quad + (2.91 \times 10^6) \left(\frac{12.5 - 0.6362}{2}\right) (2) (0.264) \\ &= 1.126 \times 10^9 \text{ lb-in.} \end{aligned}$$

$$\tau_{\max} = \frac{(20,000)(1.126 \times 10^9)}{(2)(0.264)(2.89 \times 10^{10})} = 1476 \text{ psi}$$

8. Determine Critical Shear Buckling Load of Web (Ref. 5)

$$\tau_{\text{cr}} = \frac{2\pi^2 \sqrt{D_{11} D_{22}}}{b^2 t} \left[ 4 + \frac{3 \sqrt{D_{11} D_{22}}}{D_3} + \frac{D_3}{\sqrt{D_{11} D_{22}}} \right]^{1/2}$$

$$D_{11} = D_{22} = 9.011 \times 10^3$$

$$D_{12} = 6.405 \times 10^3$$

$$D_{66} = 7.167 \times 10^3$$

$$D_3 = D_{12} + 2D_{66} = 2.074 \times 10^4$$

$$\tau_{\text{cr}} = \frac{2\pi^2 (9.011 \times 10^3)}{(25)^2 (0.264)} \left[ 4 + \frac{3 (9.011 \times 10^3)}{2.074 \times 10^4} + \frac{2.074 \times 10^4}{9.011 \times 10^3} \right]^{1/2}$$

$$= 2973 \text{ psi}$$

$$MS = \frac{2973}{1476} - 1 = 1.01$$

9. Check Web Compressive (In-plane) Buckling (Ref. 5)

$$\sigma_{x_{cr}} = \frac{\pi^2 \sqrt{D_{11} D_{22}}}{b^2 t} k$$

$$k = 2.78 \sqrt{a_1 a_2}$$

$$a_1 = \sqrt{\frac{D_{11}}{D_{22}}} \left(\frac{M}{C}\right)^2 + \frac{2D_3}{\sqrt{D_{11} D_{22}}} + \sqrt{\frac{D_{22}}{D_{11}}} \left(\frac{C}{M}\right)^2$$

$$a_2 = \sqrt{\frac{D_{11}}{D_{22}}} \left(\frac{M}{C}\right)^2 + \frac{8D_3}{\sqrt{D_{11} D_{22}}} + 16 \sqrt{\frac{D_{22}}{D_{11}}} \left(\frac{C}{M}\right)^2 \quad \text{where: } C = a/b$$

From computer program:

$$M_{\min} = 14 \Rightarrow a_1 = 6.50, a_2 = 20.4$$

$$\therefore k = 32.0$$

$$\sigma_{x_{cr}} = \frac{\pi^2 (9.011 \times 10^3)}{(25)^2 (0.264)} (32) = 17,255 \text{ psi}$$

$$MS = \frac{17,255}{6,614} - 1 = 1.61$$

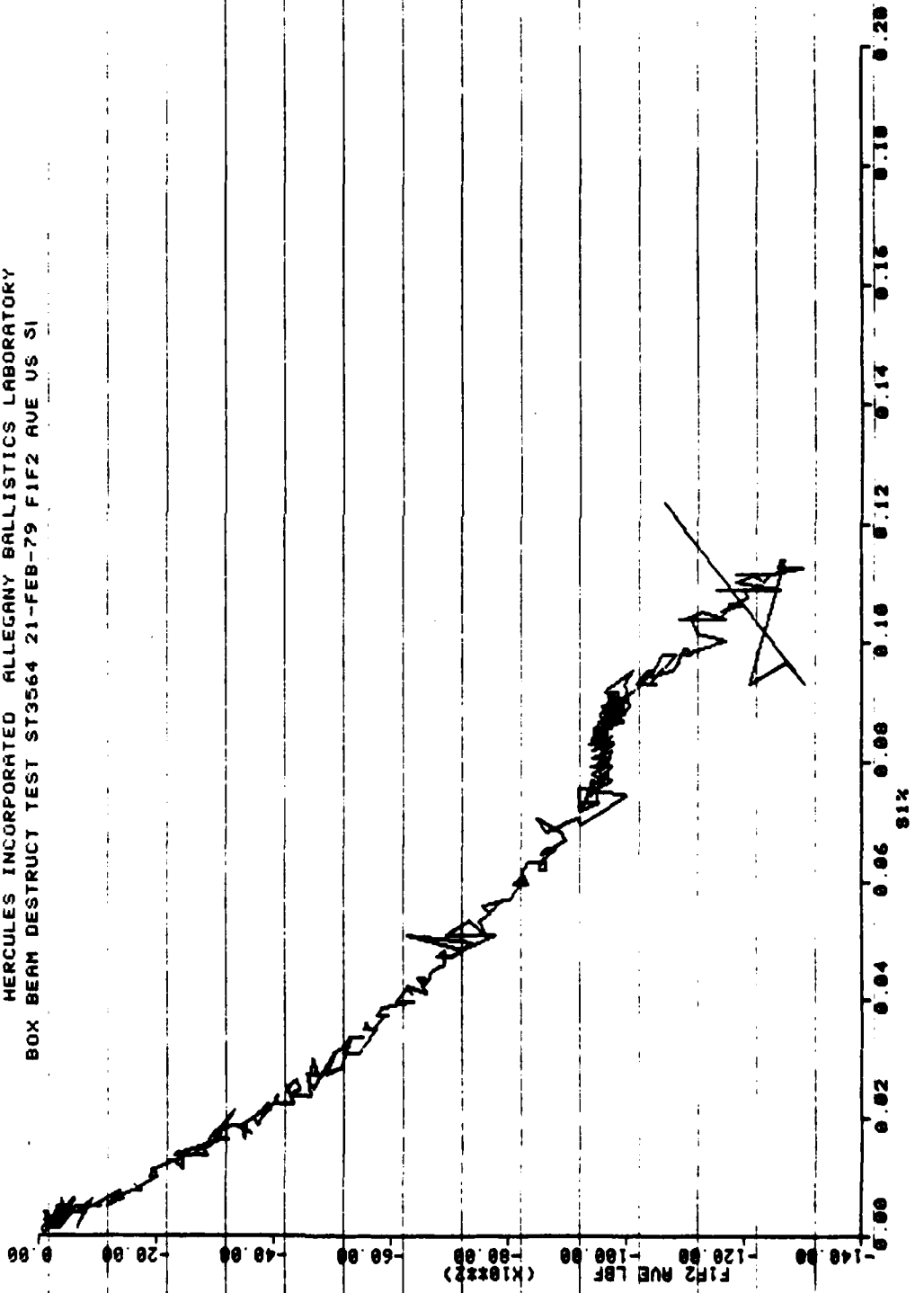


APPENDIX B

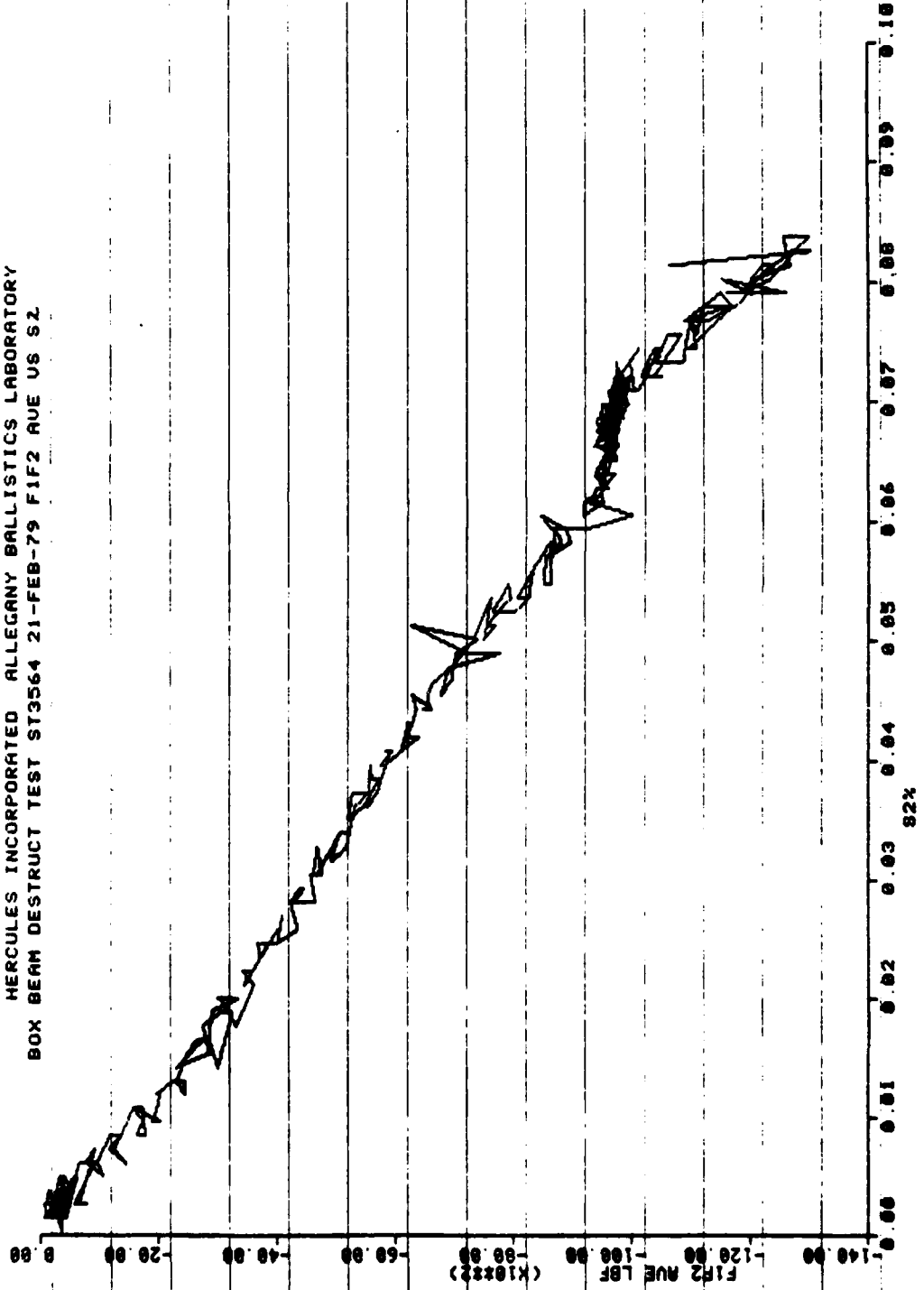
LOAD VS. STRAIN CURVES FOR GAGES S1 THROUGH S20

LOAD VS. DEFLECTION CURVES FOR GAGES L1 → L5

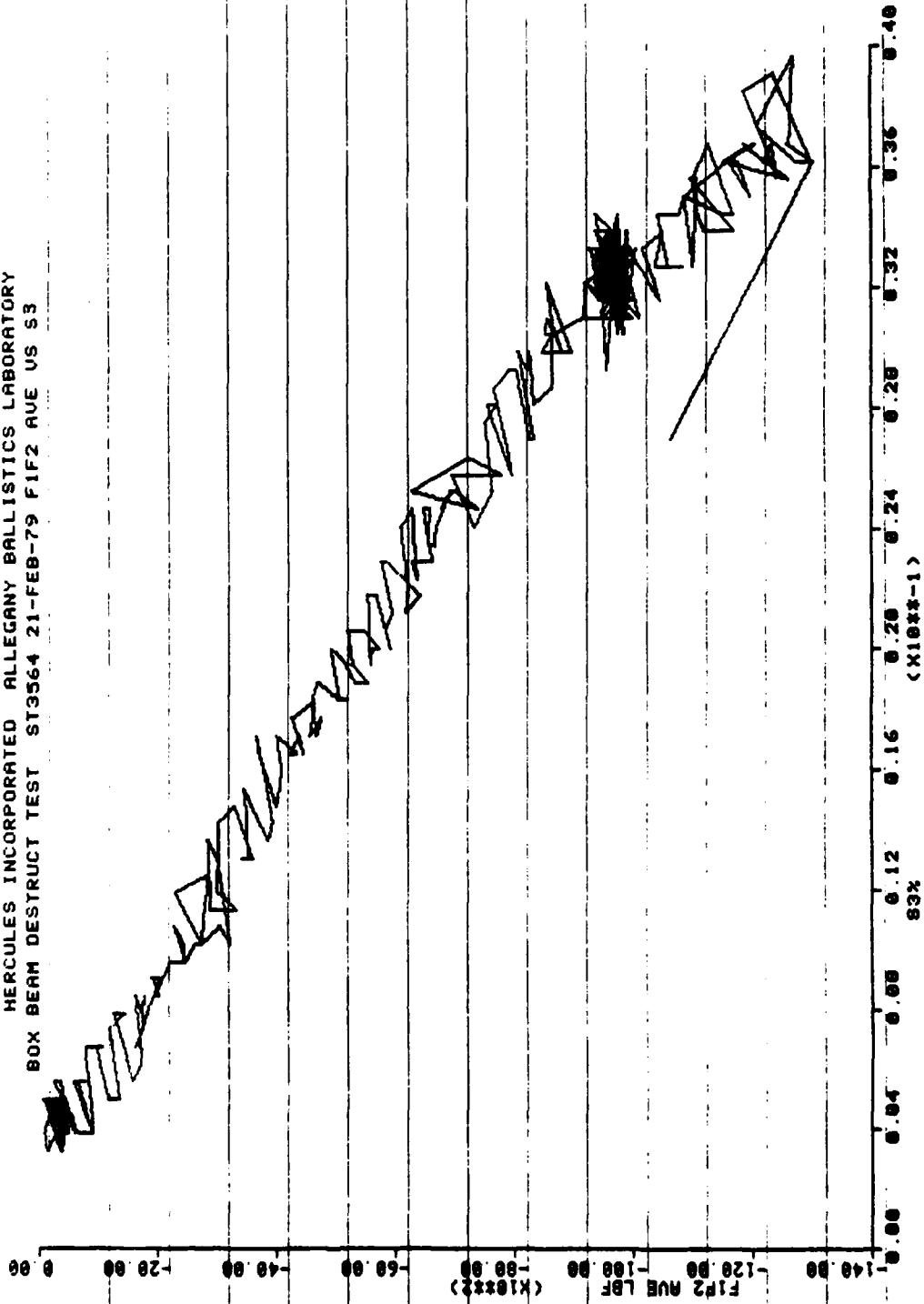
MERCULES INCORPORATED ALLEGANY BALLISTICS LABORATORY  
BOX BEAM DESTRUCT TEST ST3564 21-FEB-79 FIF2 AVE US SI



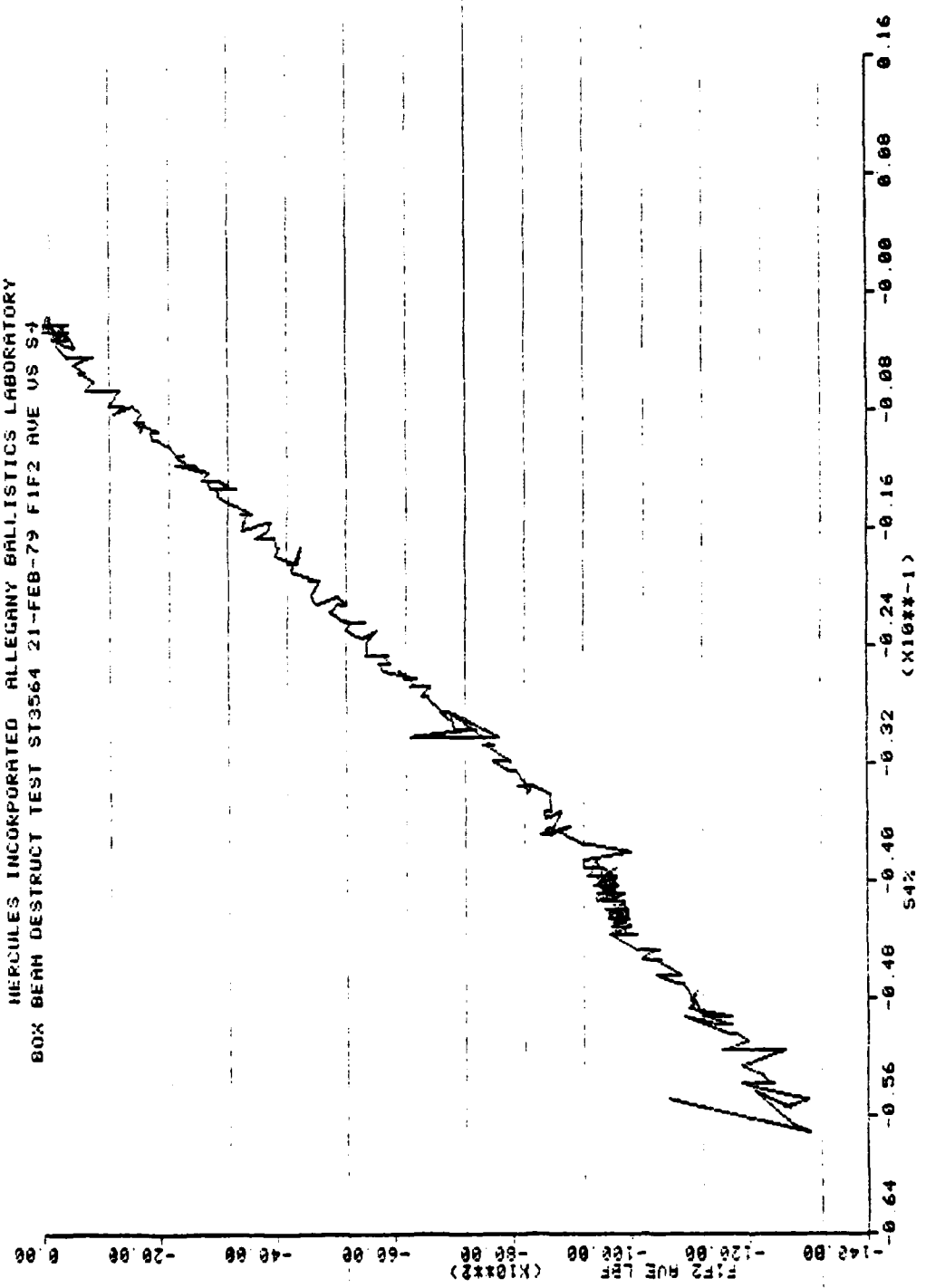
MERCULES INCORPORATED ALLEGANY BALLISTICS LABORATORY  
BOX BEAM DESTRUCT TEST ST3564 21-FEB-79 FIF2 AVE US S2



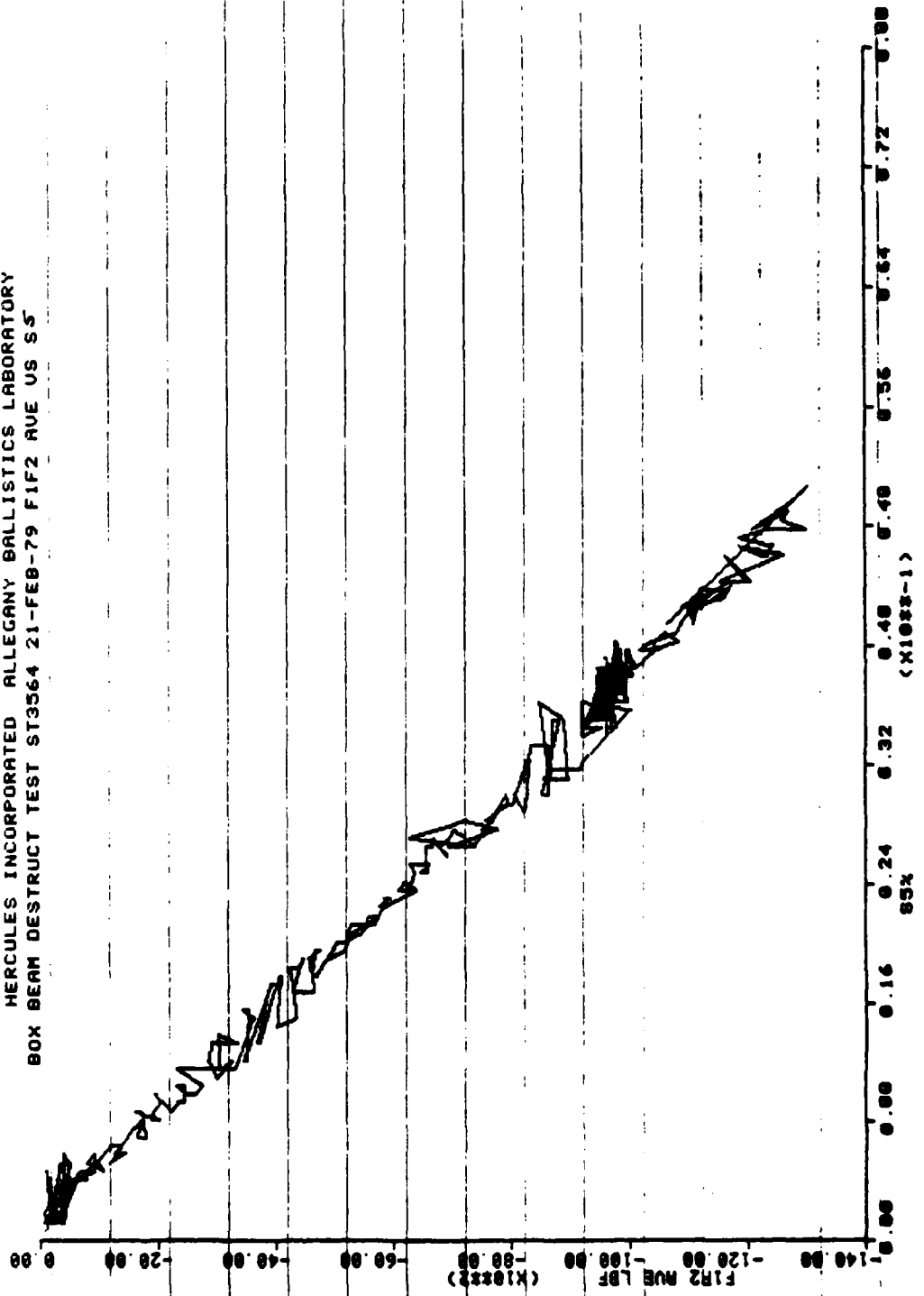
HERCULES INCORPORATED ALLEGANY BALLISTICS LABORATORY  
BOX BEAM DESTRUCT TEST ST3564 21-FEB-79 F1F2 AVE US S3



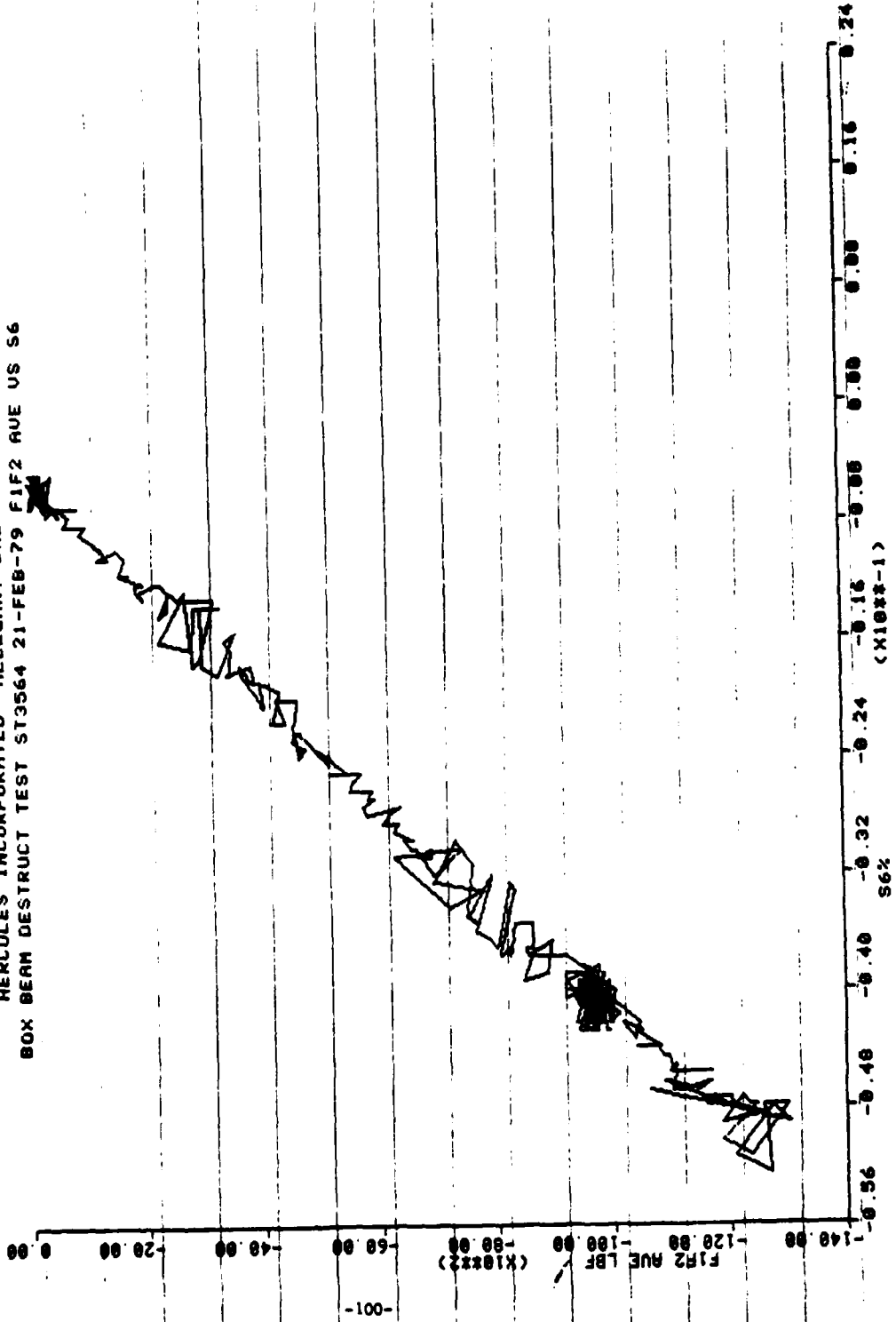
MERCULES INCORPORATED ALLEGANY BALLISTICS LABORATORY  
BOX BEAH DESTRUCT TEST ST3564 21-FEB-79 FIF2 AVE US S4



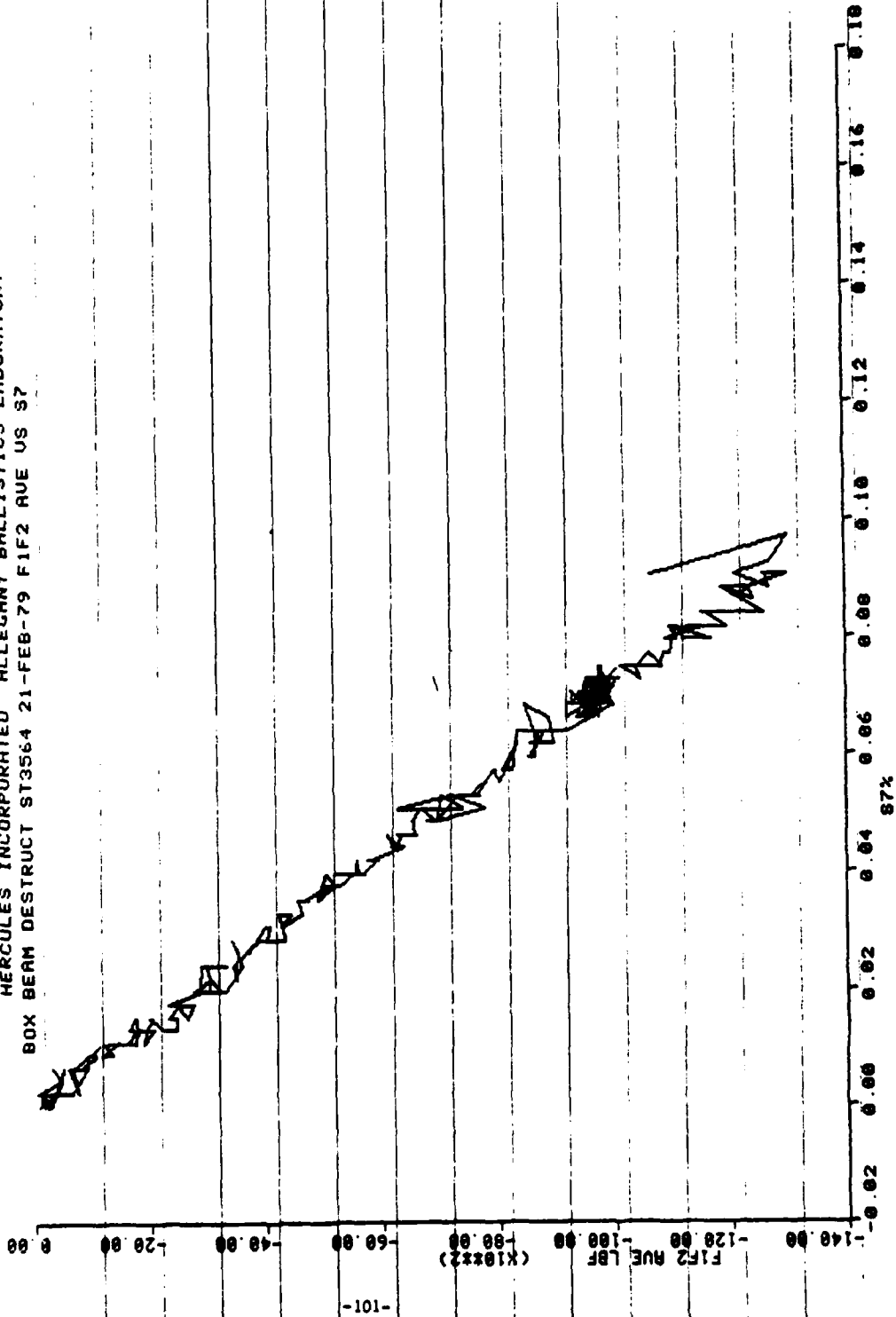
MERCULES INCORPORATED ALLEGANY BALLISTICS LABORATORY  
BOX BEAM DESTRUCT TEST ST3564 21-FEB-79 FIF2 AVE US S 5



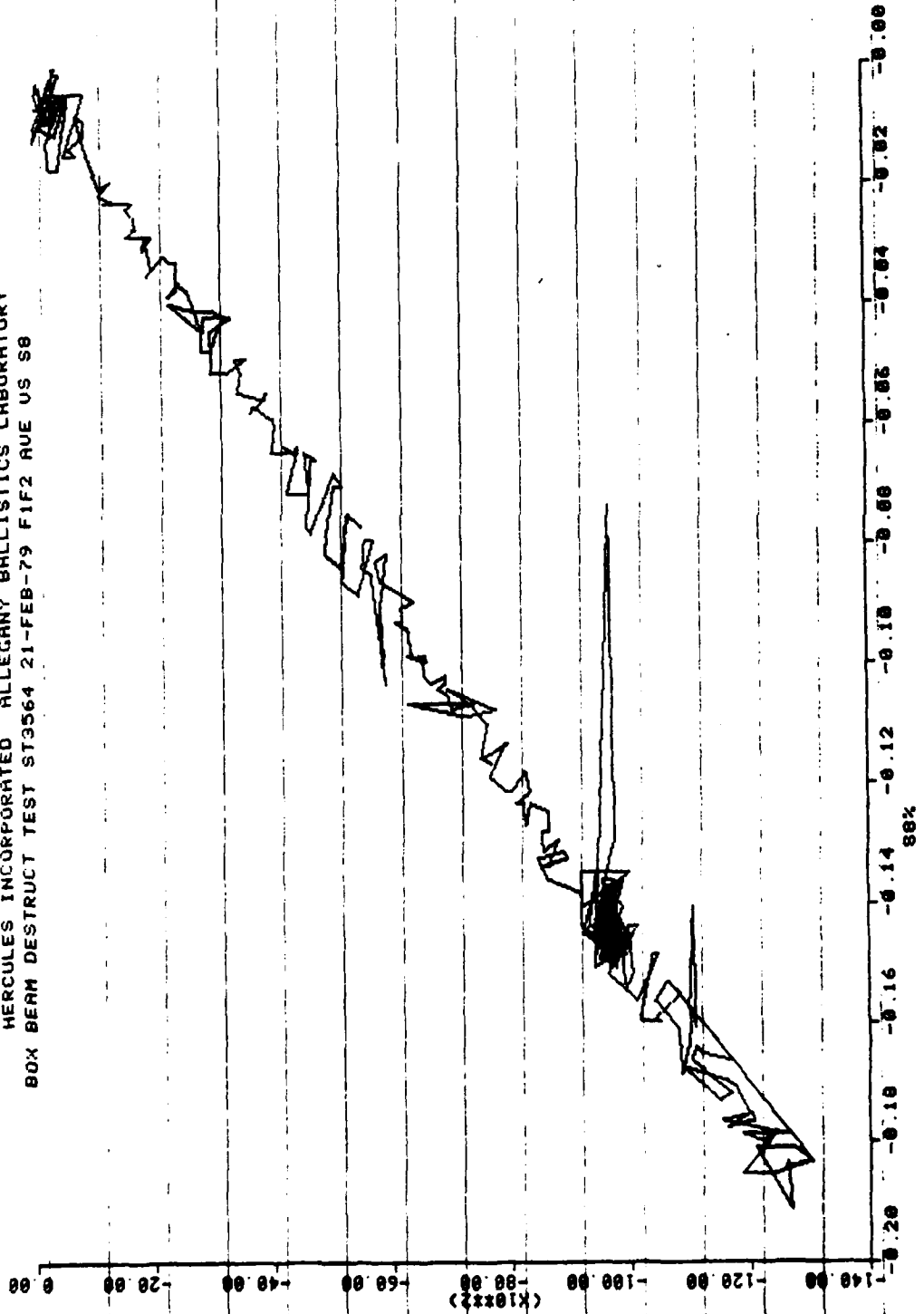
MERCULES INCORPORATED ALLEGANY BALLISTICS LABORATORY  
BOX BEAM DESTRUCT TEST ST3564 21-FEB-79 F1F2 AVE US S6



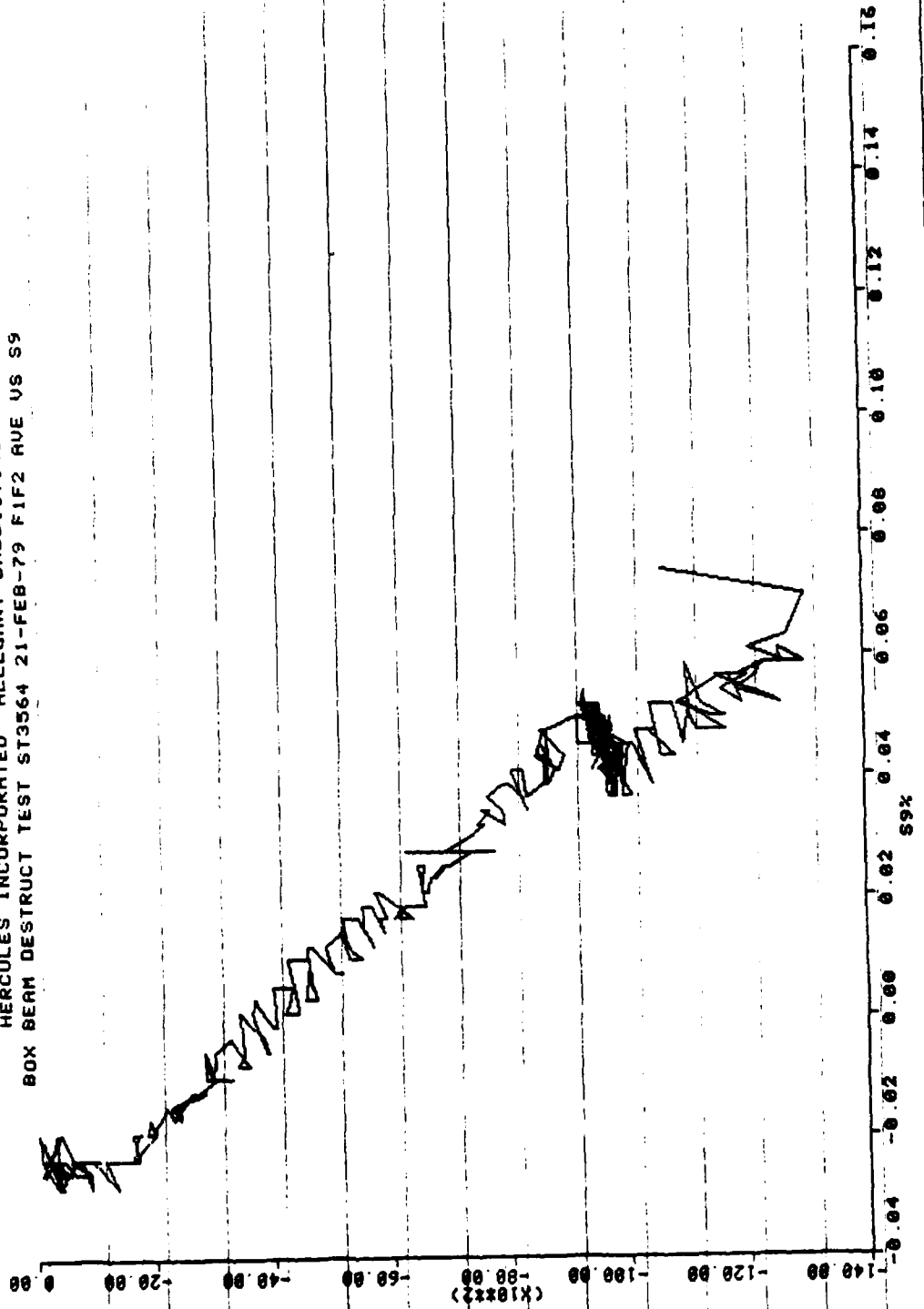
HERCULES INCORPORATED ALLEGANY BALLISTICS LABORATORY  
BOX BEAM DESTRUCT ST3564 21-FEB-79 F1F2 AVE US S7



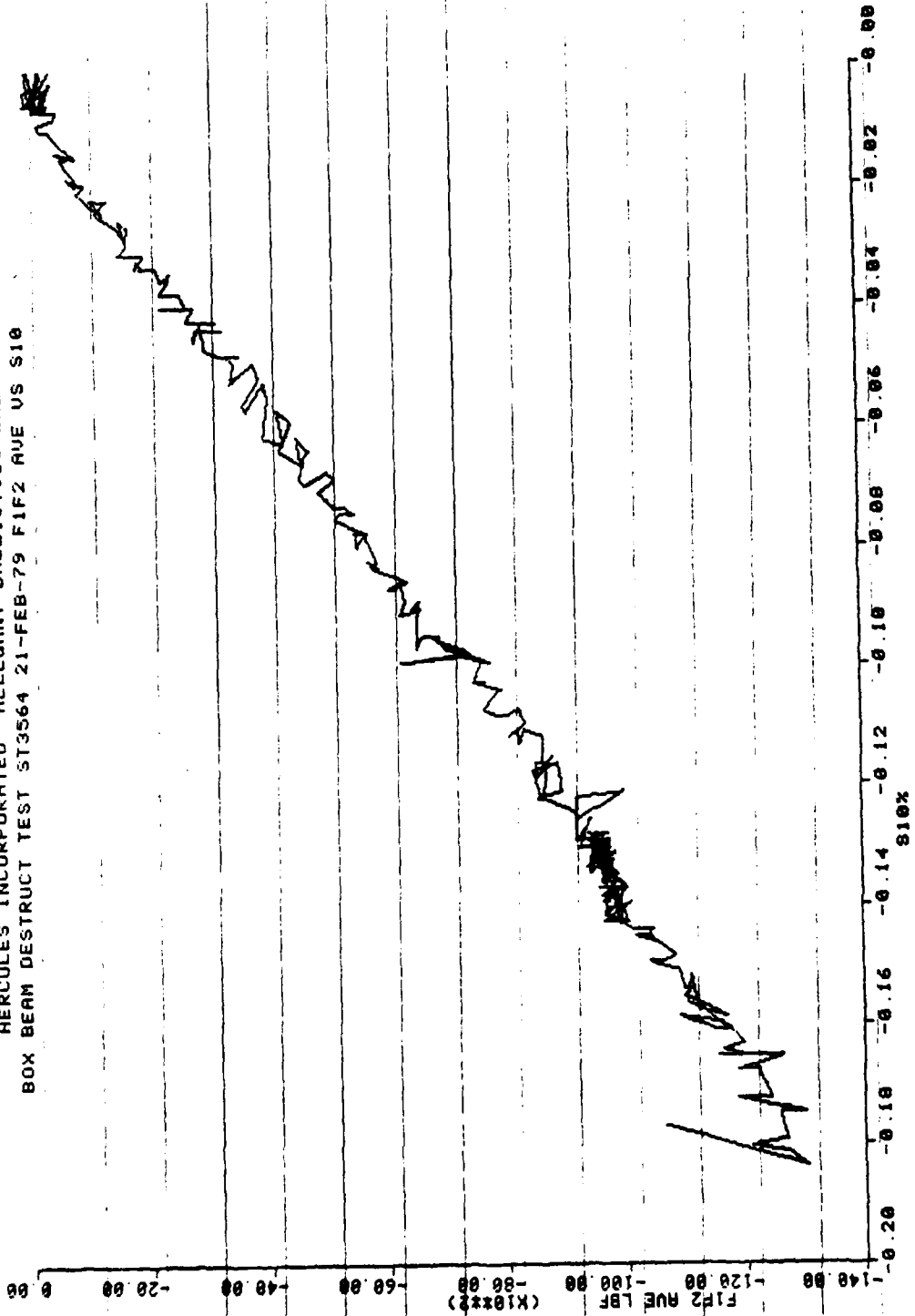
HERCULES INCORPORATED ALLEGANY BALLISTICS LABORATORY  
BOX BEAM DESTRUCT TEST ST3564 21-FEB-79 F1F2 AVE US S8



HERCULES INCORPORATED ALLEGANY BALLISTICS LABORATORY  
BOX BEAM DESTRUCT TEST ST3564 21-FEB-79 F1F2 AVE US S9

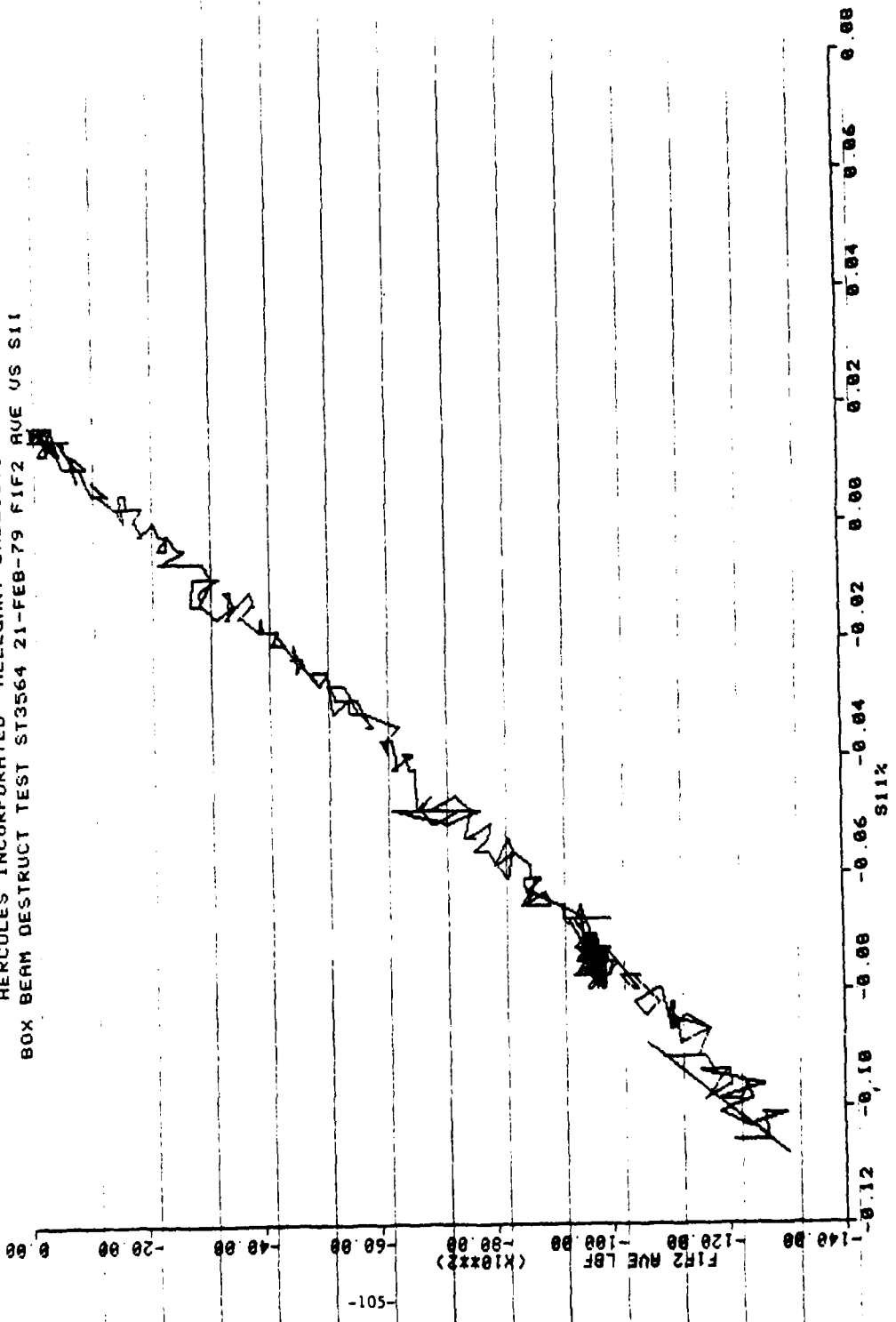


HERCULES INCORPORATED ALLEGANY BALLISTICS LABORATORY  
BOX BEAM DESTRUCT TEST ST3564 21-FEB-79 FIF2 AVE US S10

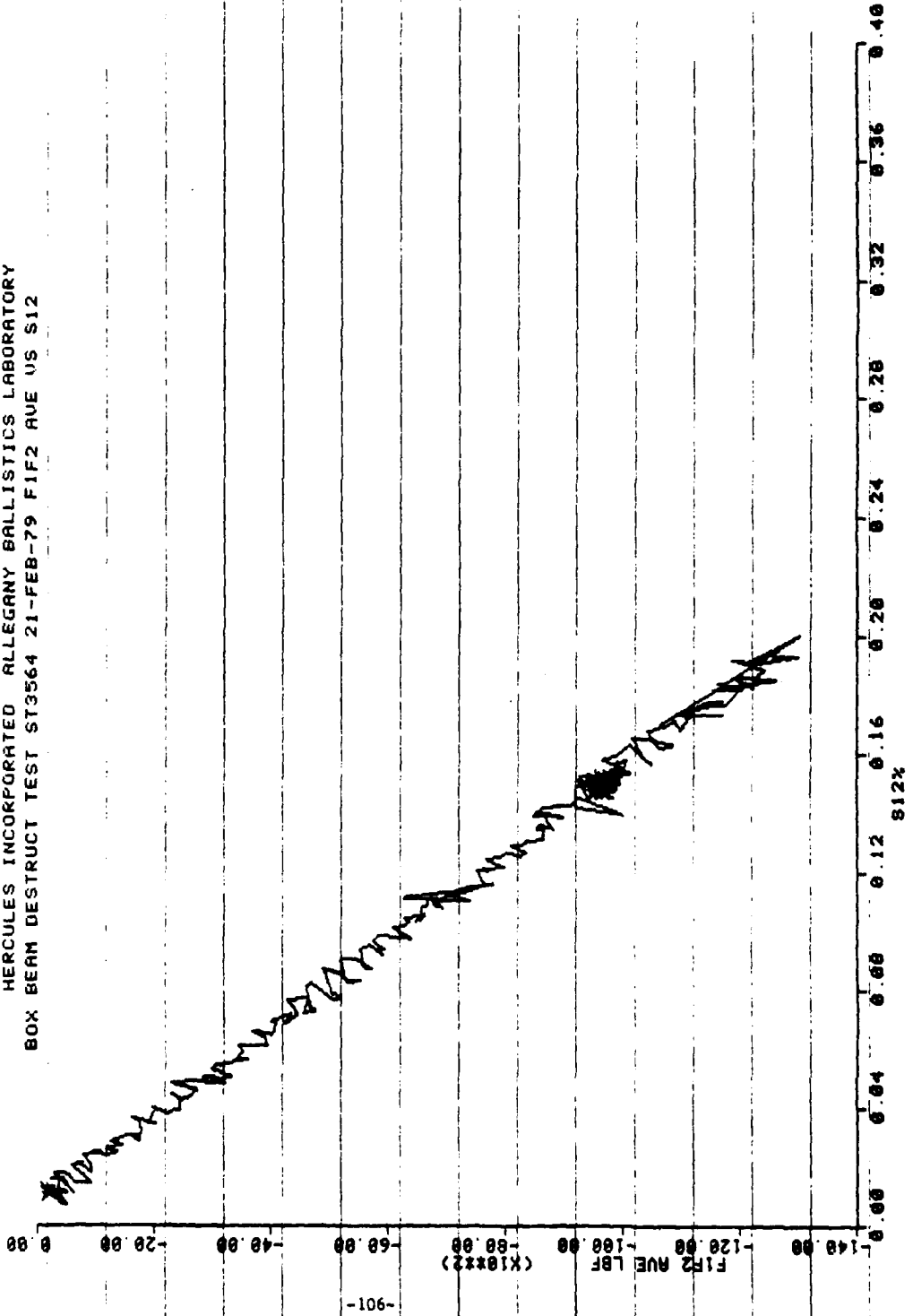


-101-

HERCULES INCORPORATED ALLEGANY BALLISTICS LABORATORY  
BOX BEAM DESTRUCT TEST ST3564 21-FEB-79 FIF2 AVE US S11

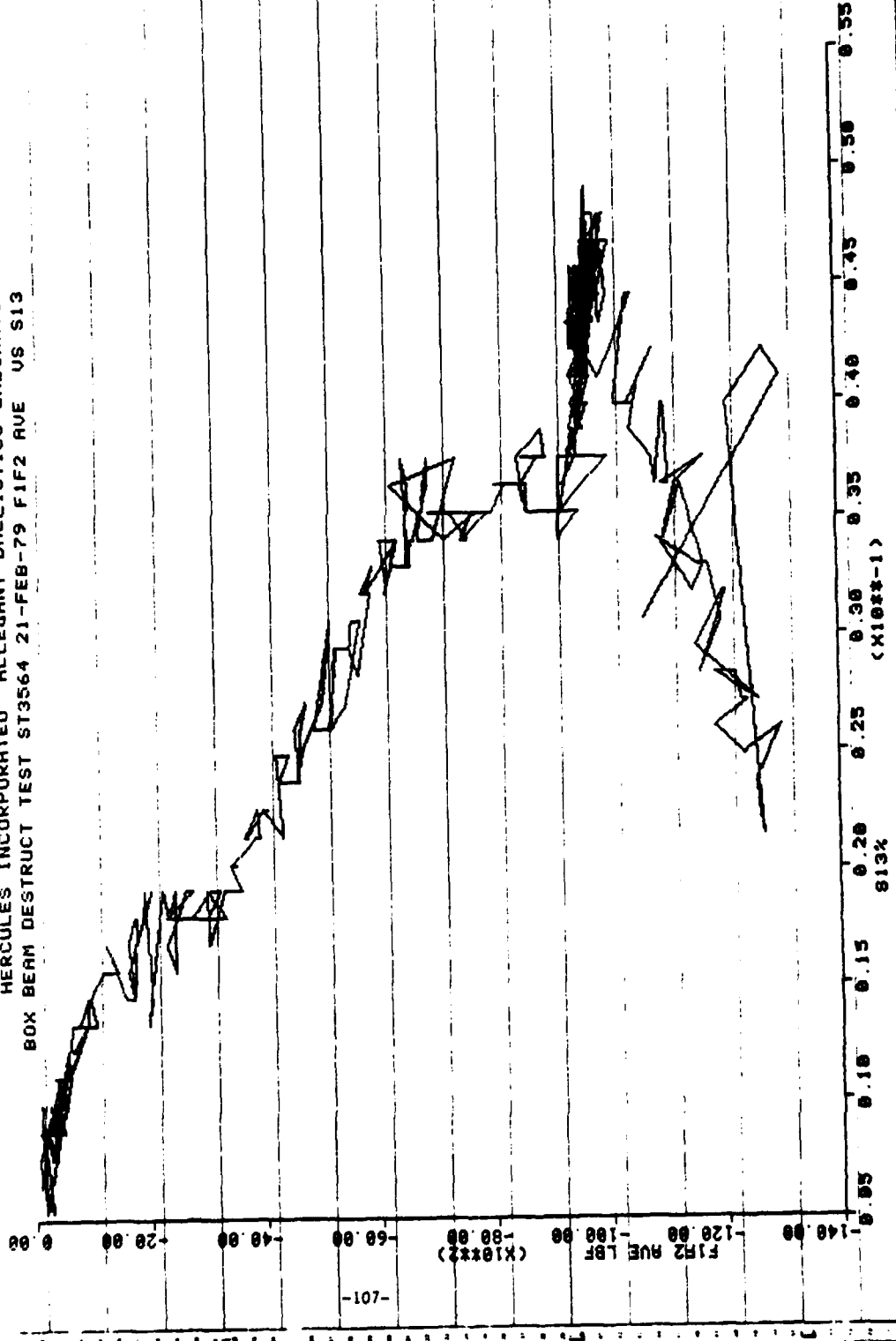


HERCULES INCORPORATED ALLEGANY BALLISTICS LABORATORY  
BOX BEAM DESTRUCT TEST ST3564 21-FEB-79 FIF2 AVE US S12



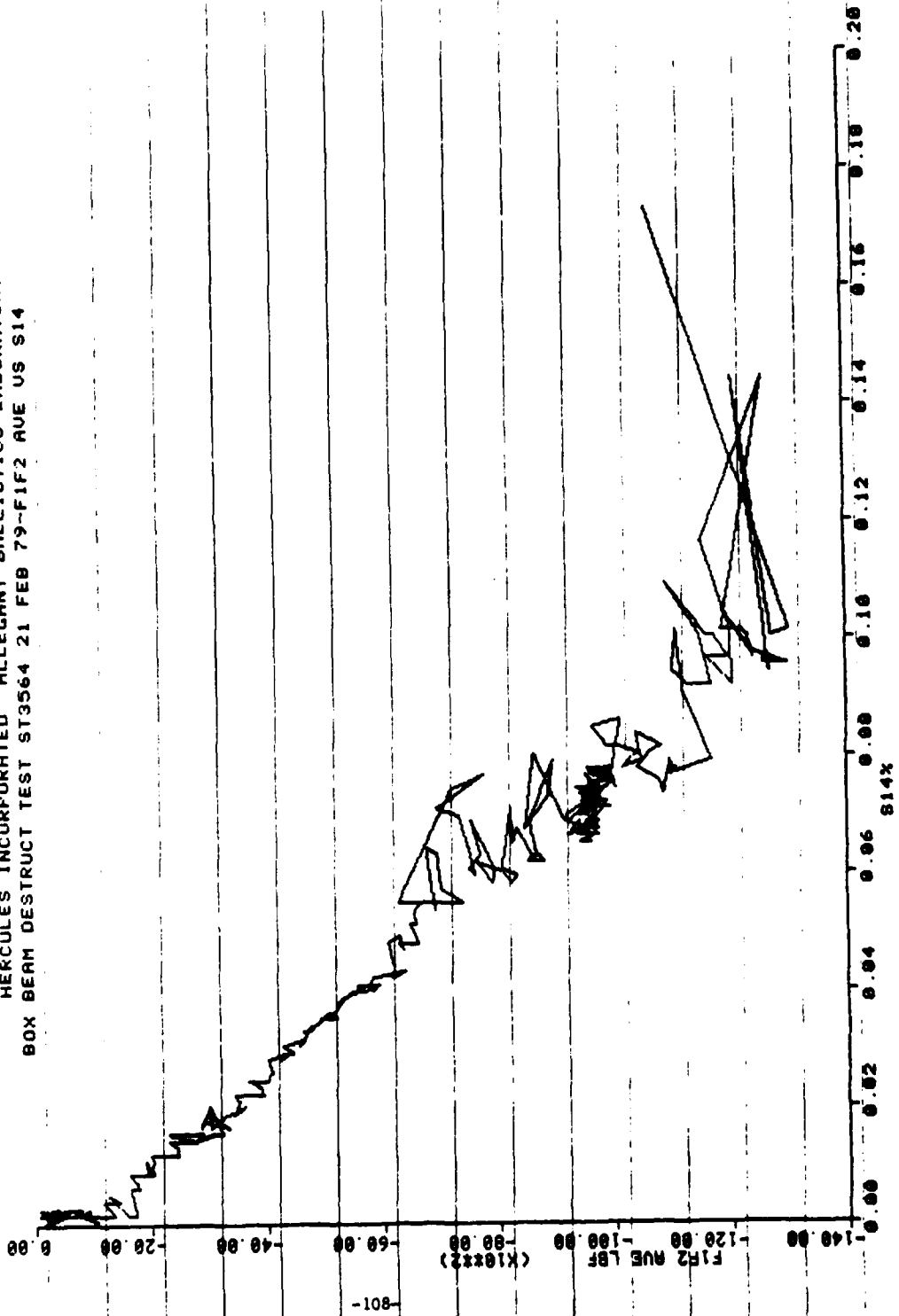
-901-

HERCULES INCORPORATED ALLEGANY BALLISTICS LABORATORY  
BOX BEAM DESTRUCT TEST ST3564 21-FEB-79 FIF2 AVE US S13

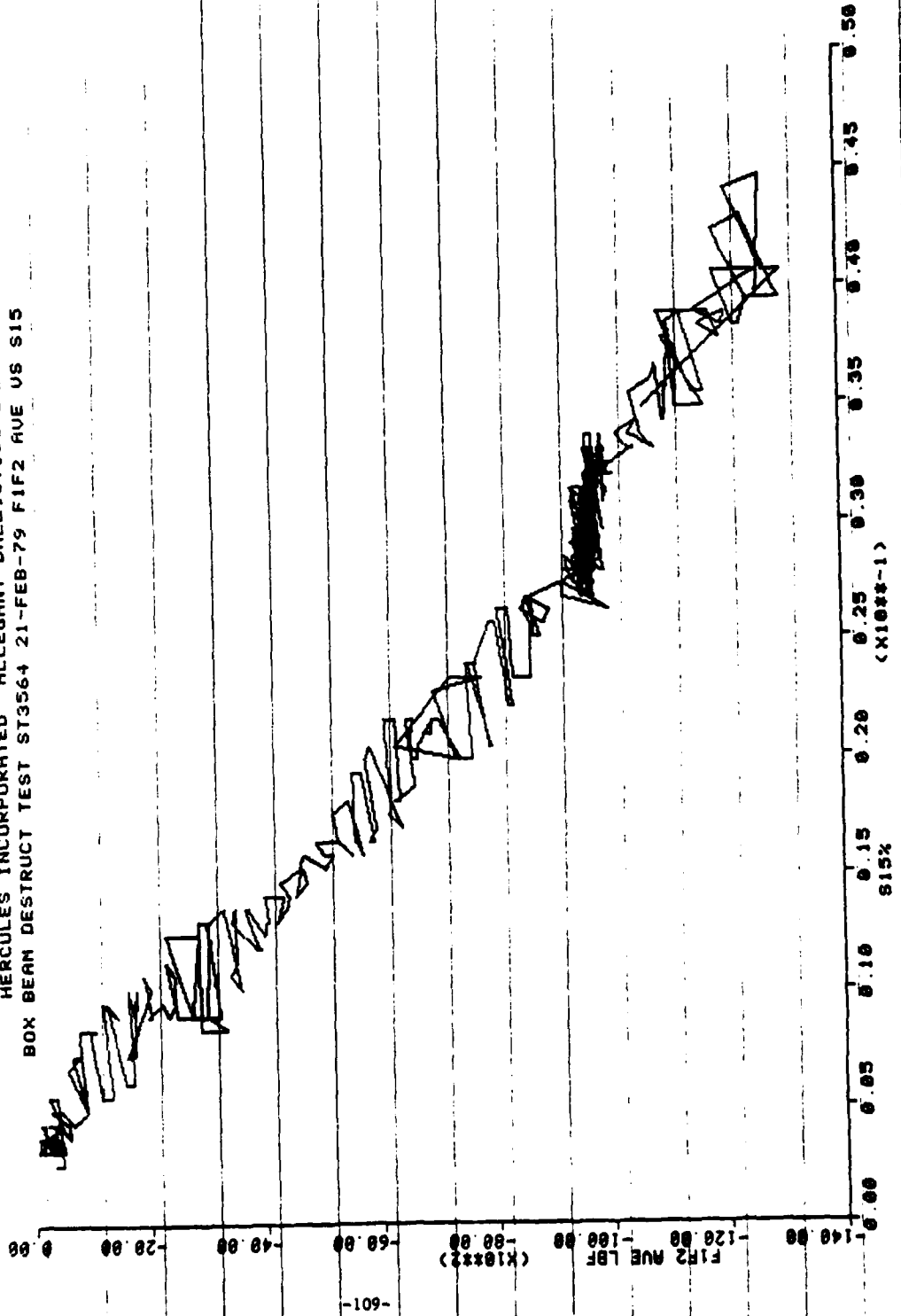


-107-

HERCULES INCORPORATED ALLEGANY BALLISTICS LABORATORY  
BOX BEAM DESTRUCT TEST ST3564 21 FEB 79-F1F2 AVE US S14

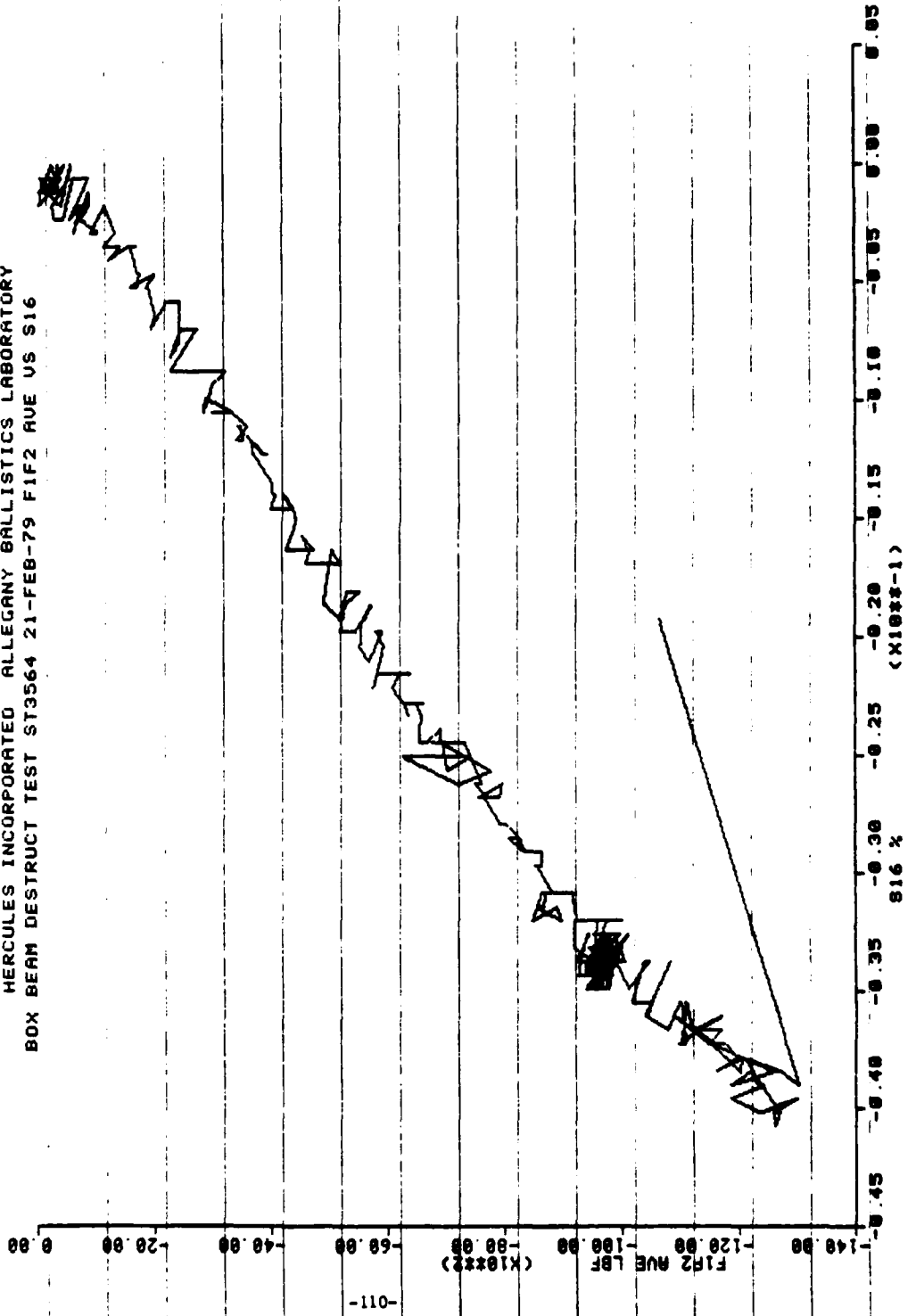


HERCULES INCORPORATED ALLEGANY BALLISTICS LABORATORY  
BOX BEAM DESTRUCT TEST ST3564 21-FEB-79 FIF2 AVE US S15

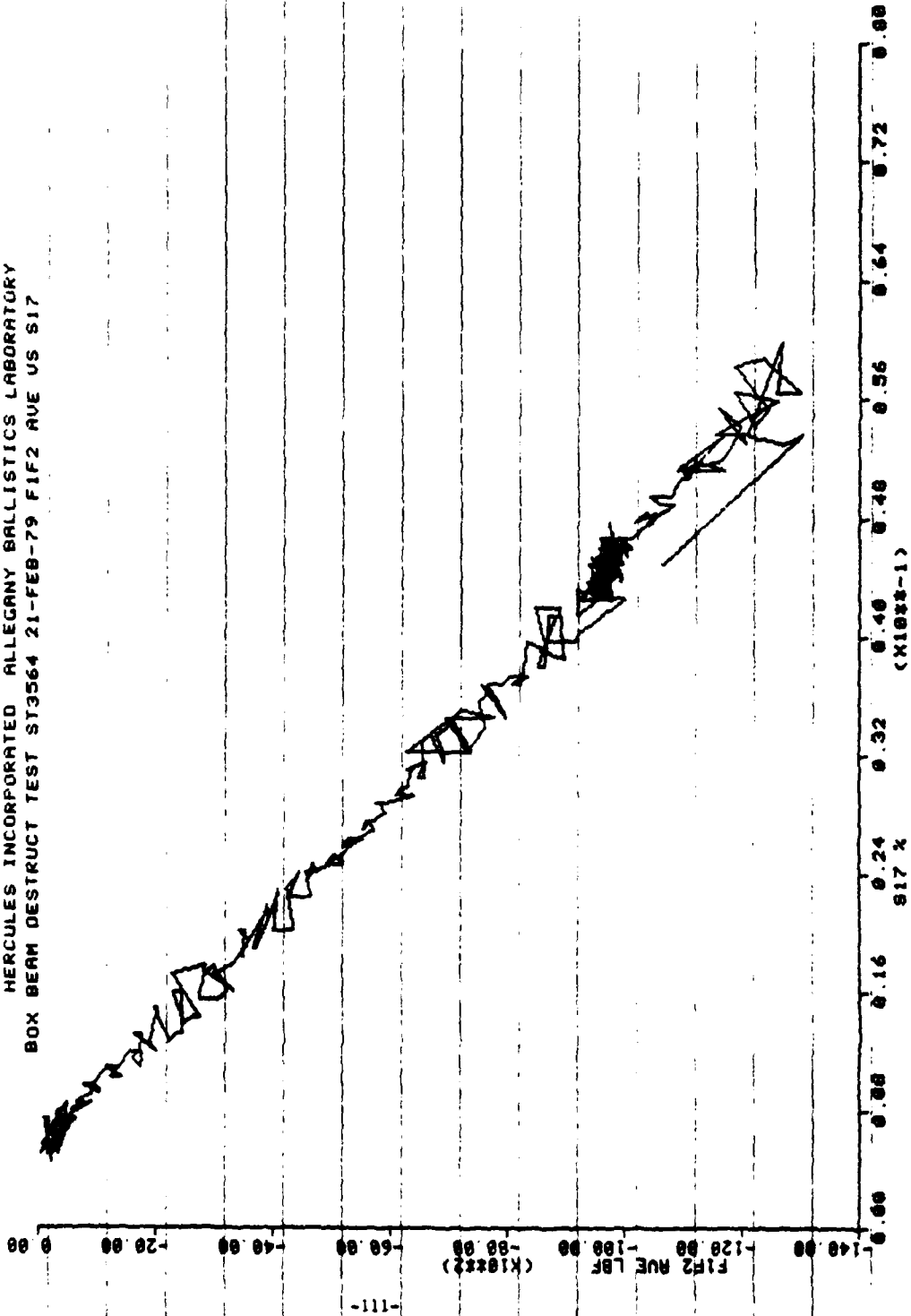


-601-

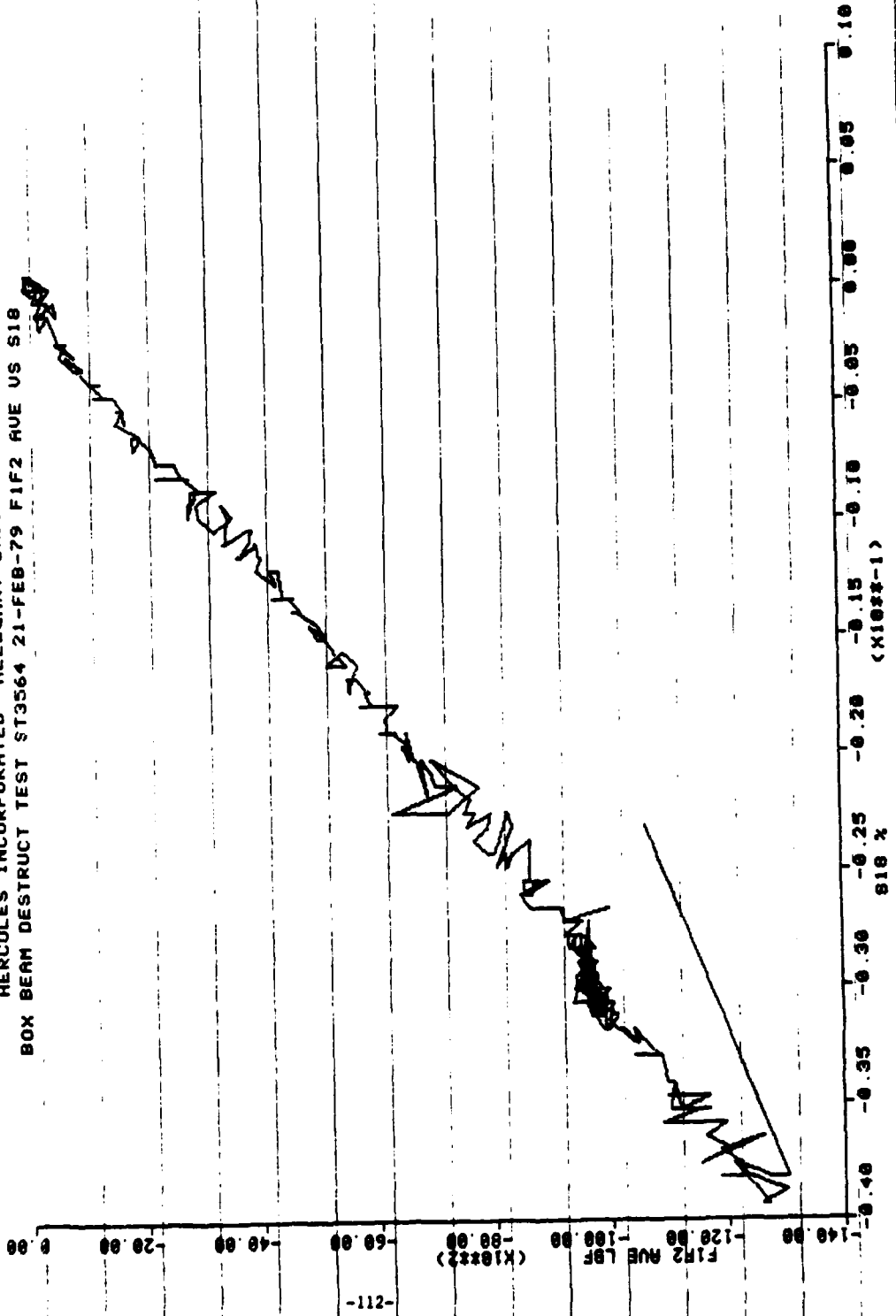
HERCULES INCORPORATED ALLEGANY BALLISTICS LABORATORY  
BOX BEAM DESTRUCT TEST ST3564 21-FEB-79 F1F2 AVE US S16



HERCULES INCORPORATED ALLEGANY BALLISTICS LABORATORY  
BOX BEAM DESTRUCT TEST ST3564 21-FEB-79 F1F2 AVE US S17

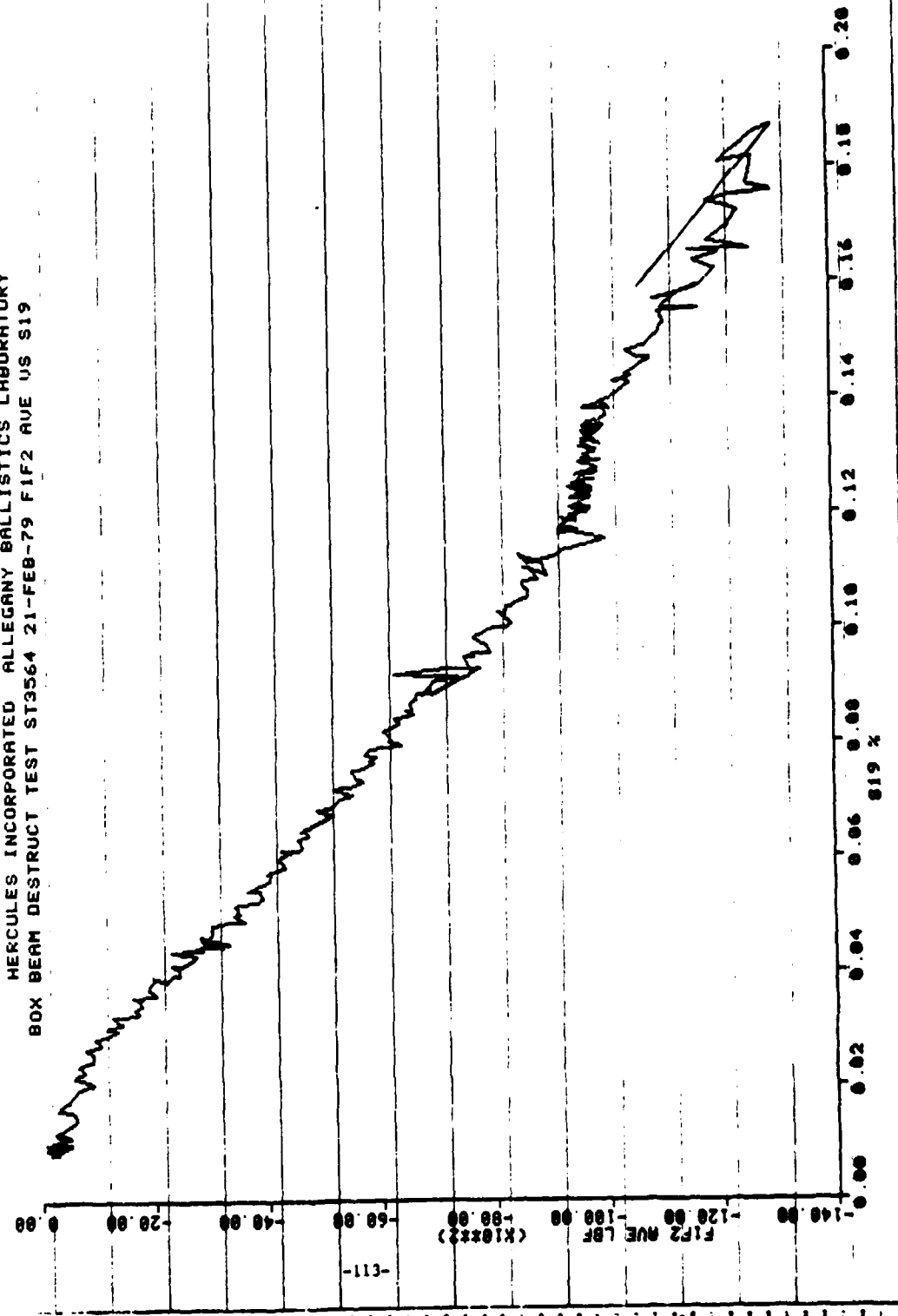


HERCULES INCORPORATED ALLEGANY BALLISTICS LABORATORY  
BOX BEAM DESTRUCT TEST ST3564 21-FEB-79 FIF2 AUE US S18



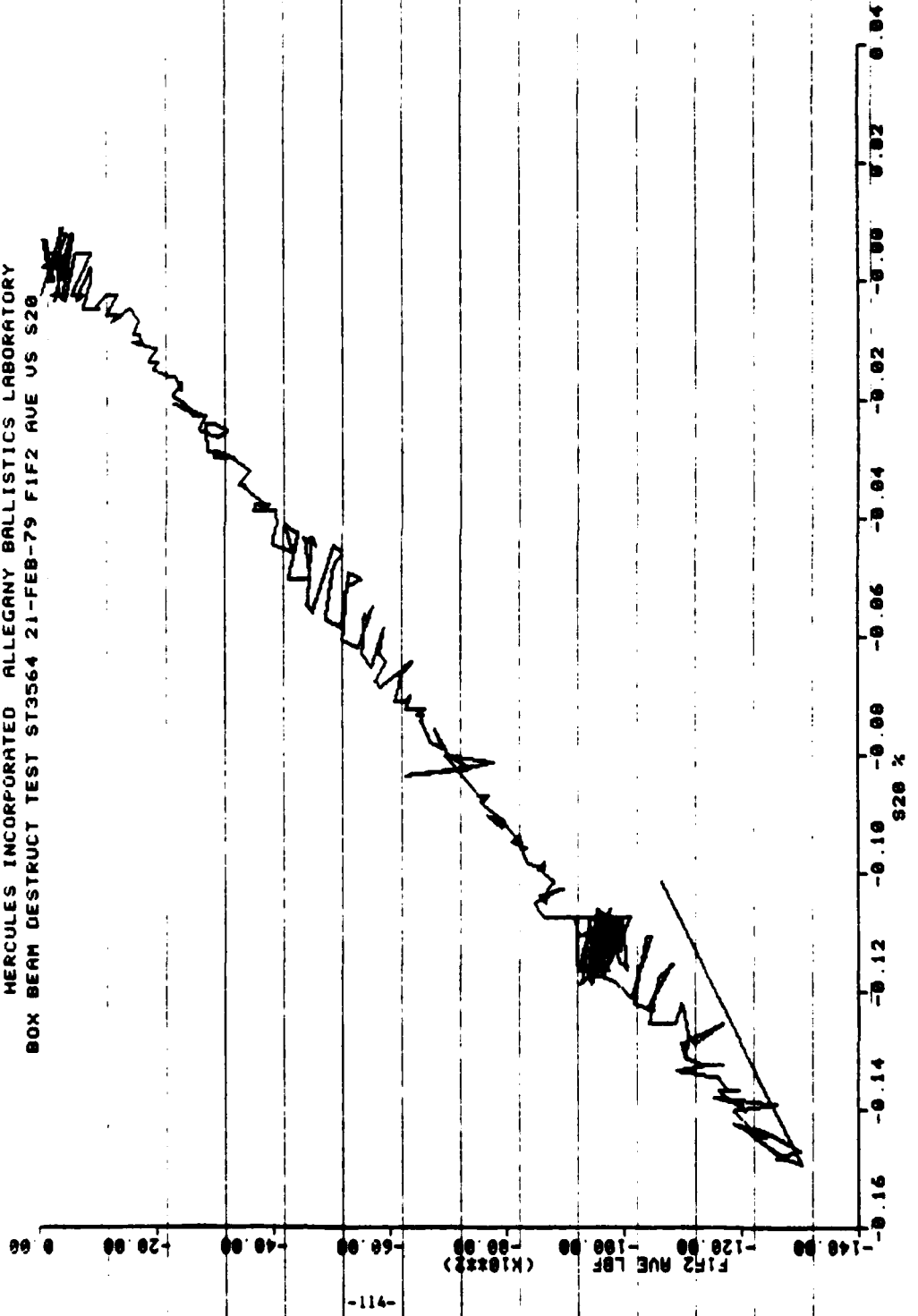
-211-

HERCULES INCORPORATED ALLEGANY BALLISTICS LABORATORY  
BOX BEAM DESTRUCT TEST ST3564 21-FEB-79 FIF2 AVE US S19



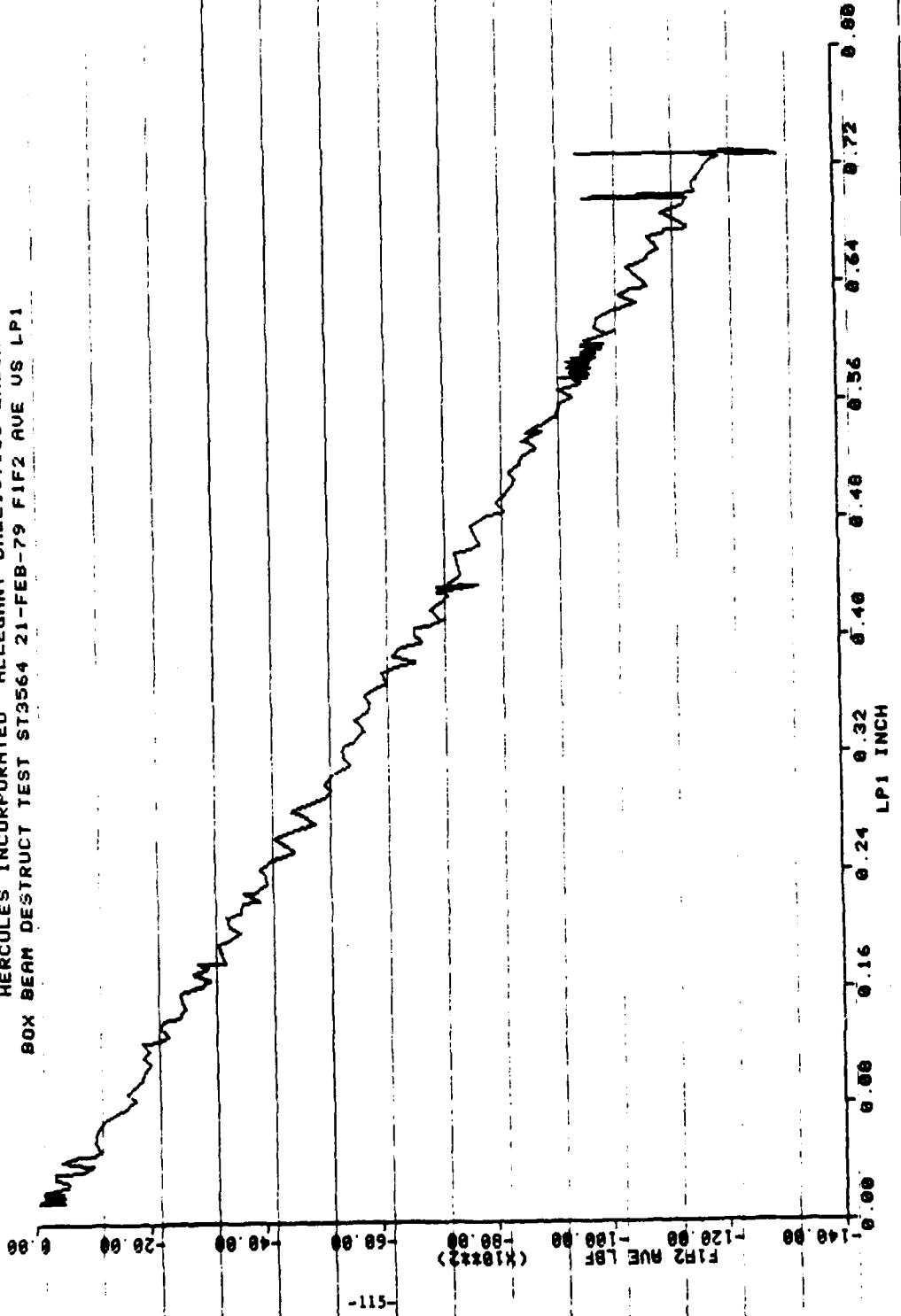
-11-

MERCULES INCORPORATED ALLEGANY BALLISTICS LABORATORY  
BOX BEAM DESTRUCT TEST ST3564 21-FEB-79 FIF2 AVE US S20



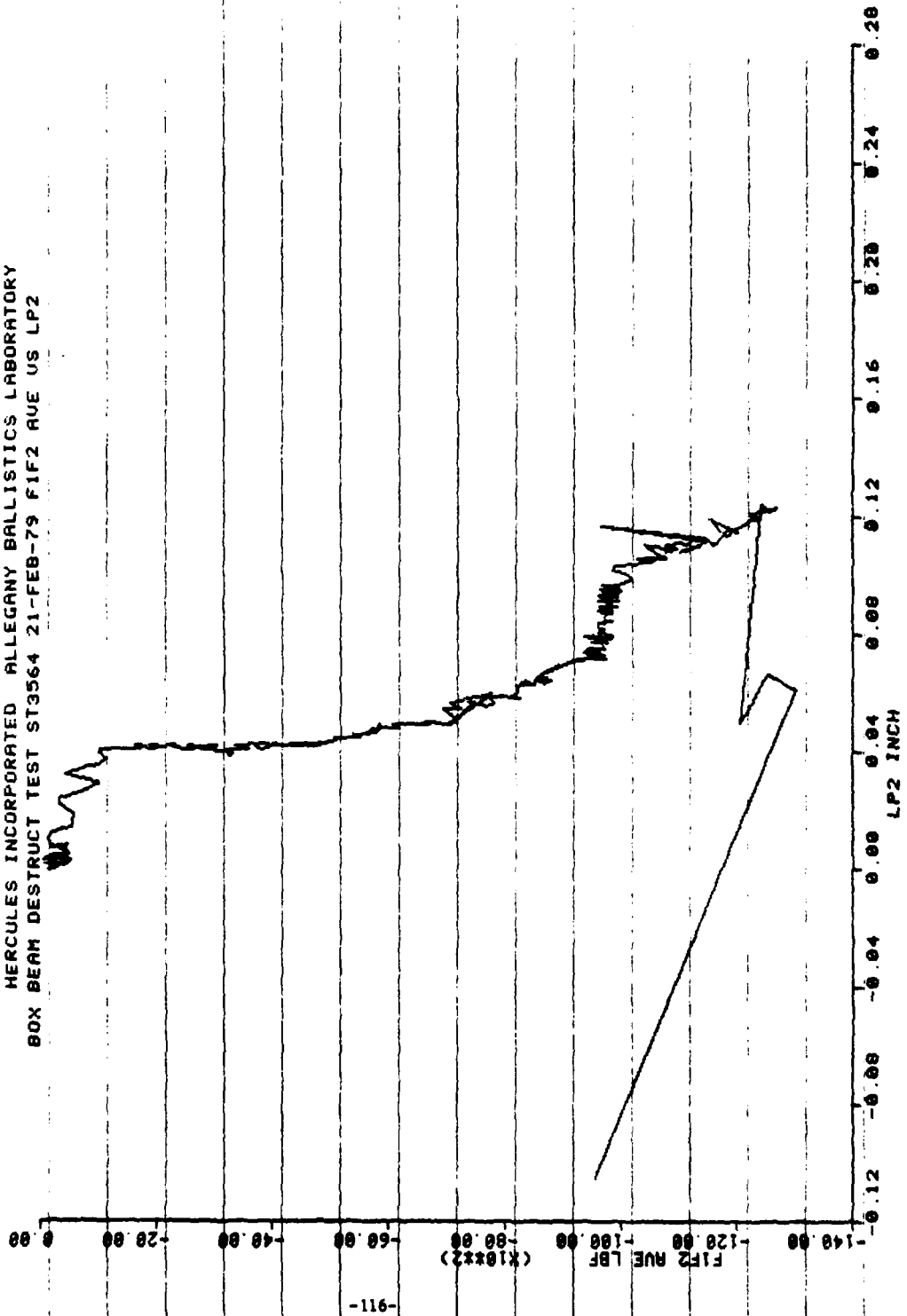
-411-

HERCULES INCORPORATED ALLEGANY BALLISTICS LABORATORY  
BOX BEAM DESTRUCT TEST ST3564 21-FEB-79 FIF2 AVE US LP1

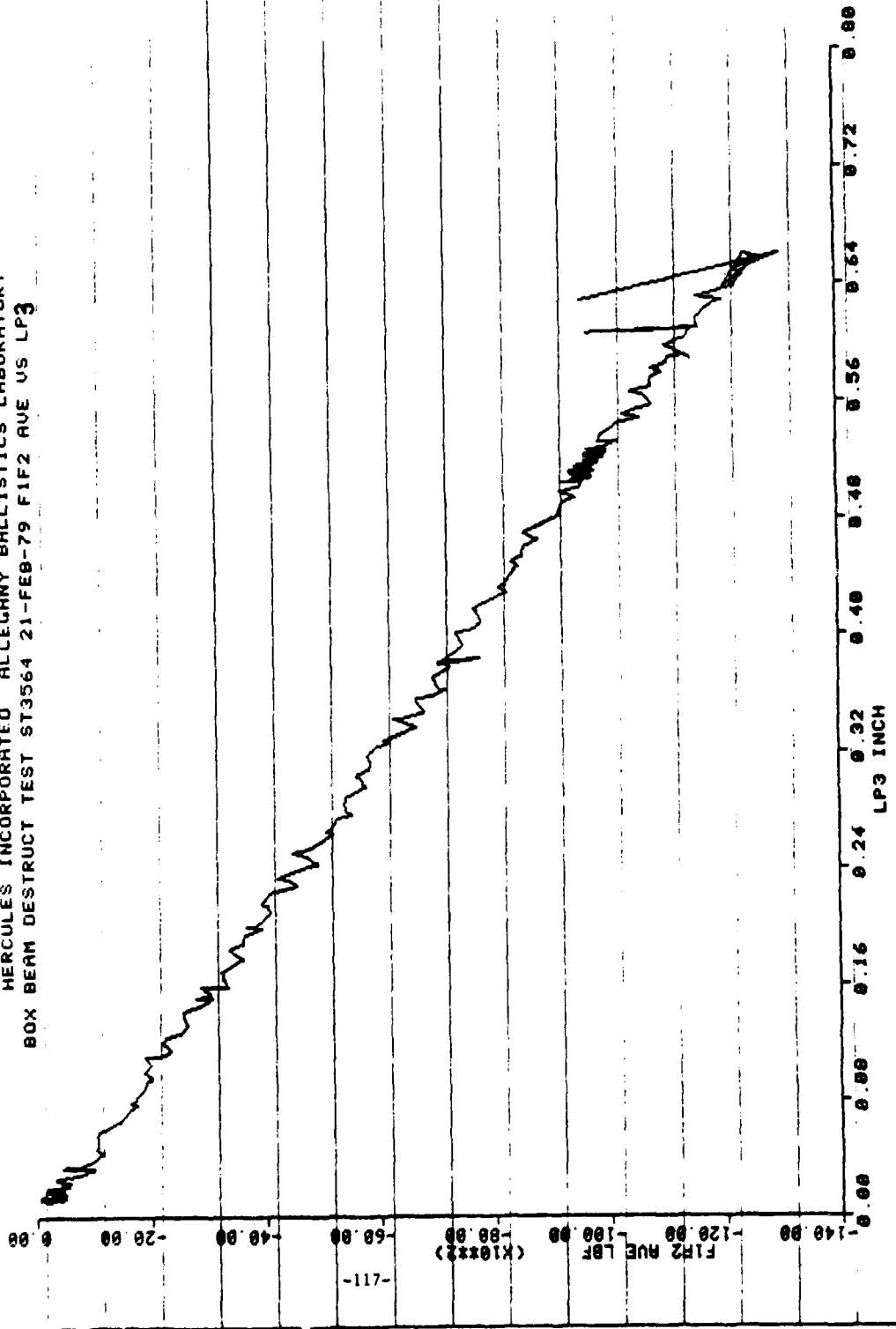


-511-

HERCULES INCORPORATED ALLEGANY BALLISTICS LABORATORY  
BOX BEAM DESTRUCT TEST ST3564 21-FEB-79 FIF2 AVE US LP2

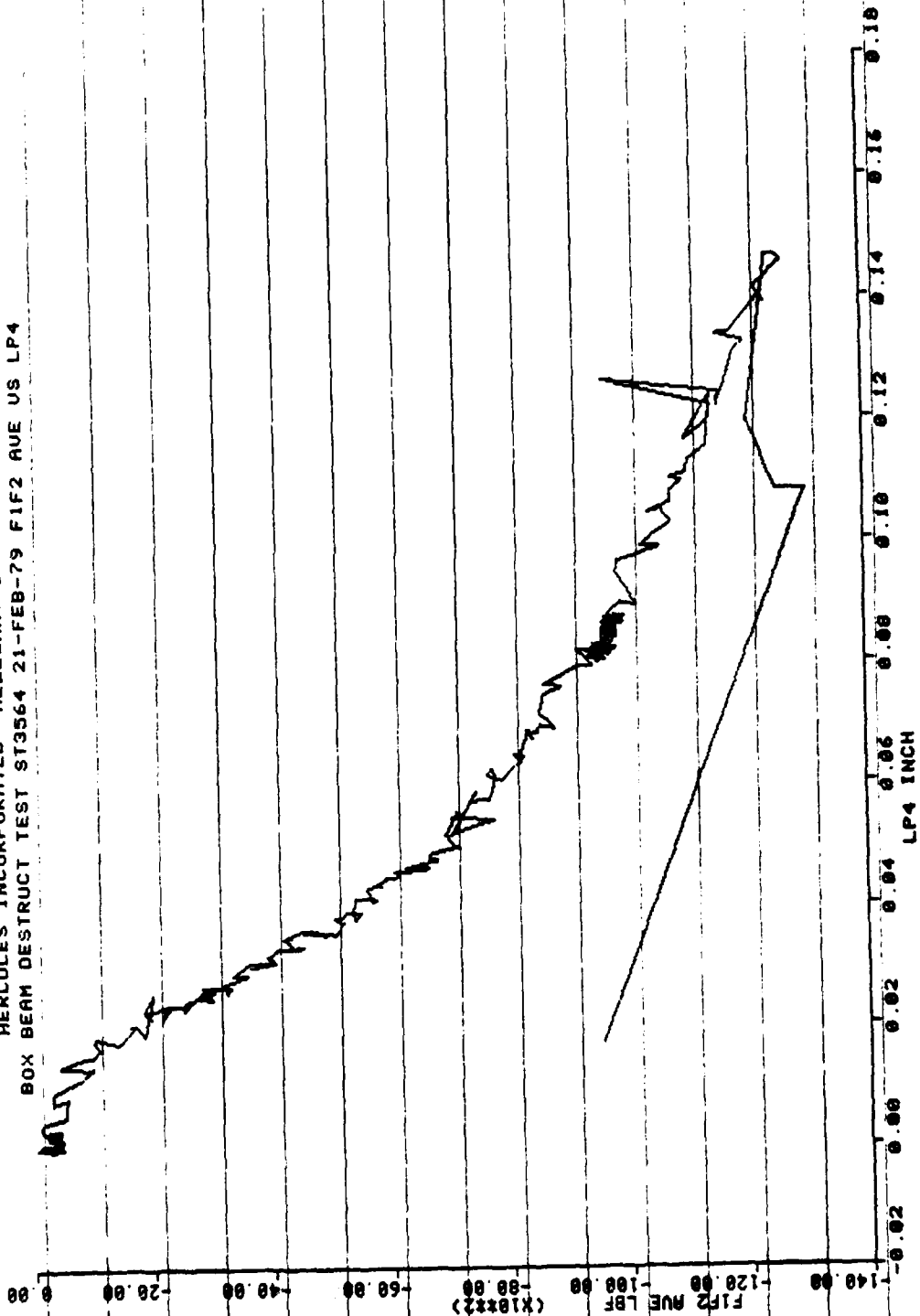


HERCULES INCORPORATED ALLEGANY BALLISTICS LABORATORY  
BOX BEAM DESTRUCT TEST ST3564 21-FEB-79 F1F2 AVE US LP3



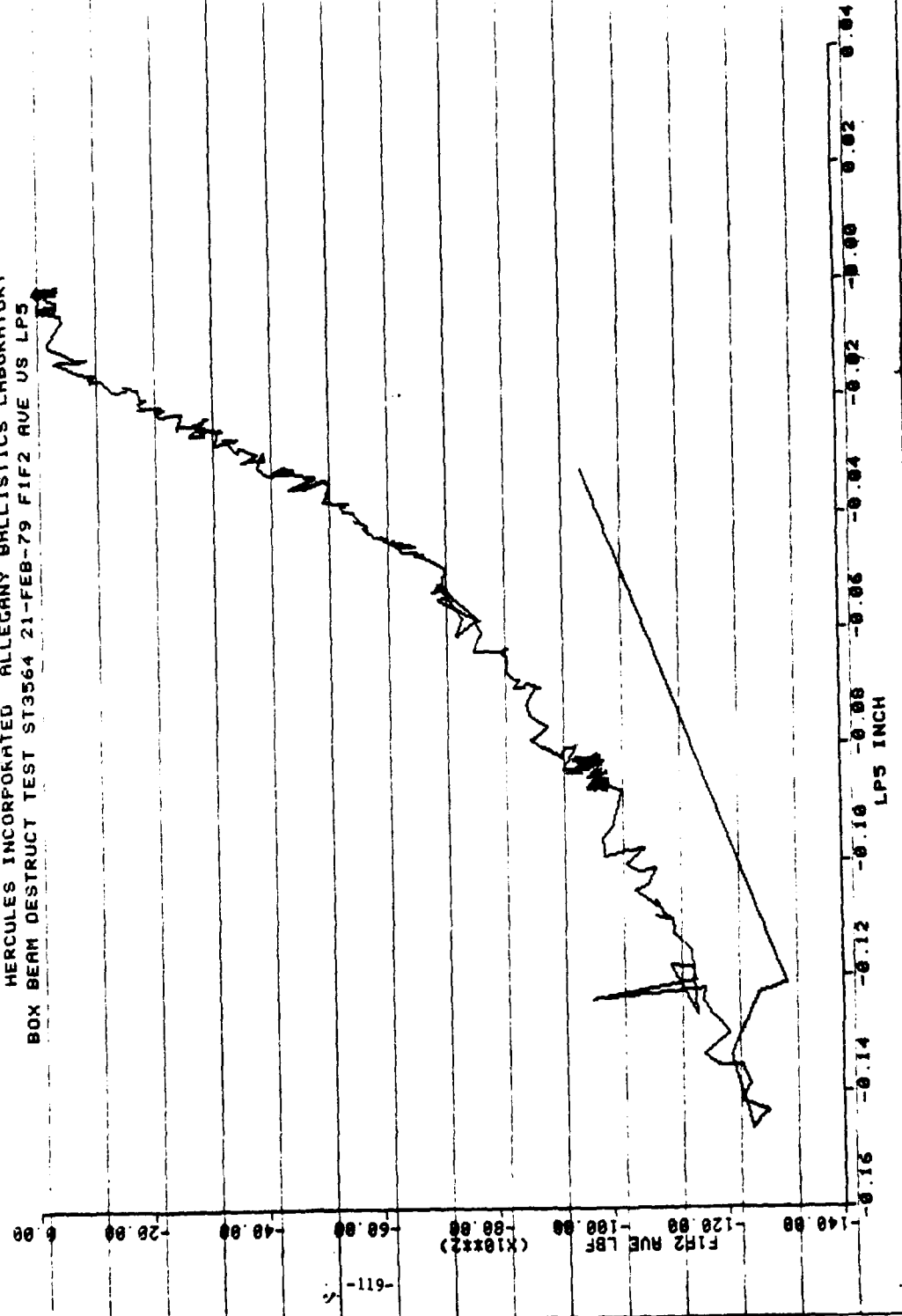
-117-

HERCULES INCORPORATED ALLEGANY BALLISTICS LABORATORY  
BOX BEAM DESTRUCT TEST ST3564 21-FEB-79 FIF2 AVE US LP4



-811-

HERCULES INCORPORATED ALLEGANY BALLISTICS LABORATORY  
BOX BEAM DESTRUCT TEST ST3564 21-FEB-79 F1F2 AVE US LP5



DISTRIBUTION

No. of Copies	To
1	Office of the Under Secretary of Defense for Research and Engineering, The Pentagon, Washington, D.C. 20301
12	Commander, Defense Documentation Center, Cameron Station, Building 5, 5010 Duke Street, Alexandria, Virginia 22314
	Metals and Ceramics Information Center, Battelle Columbus Laboratories, 505 King Avenue, Columbus, Ohio 43201
1	ATTN: Mr. Harold Mindiin, Director
1	Mr. James Lynch, Assistant Director
2	Mr. Daniel Maykuth
1	Advanced Research Projects Agency, The Pentagon, Washington, D.C. 20315
	Commander, U. S. Army Foreign Science and Technology Center, 220 Seventh Street, N.E., Charlottesville, Virginia 22901
1	ATTN: DRXST-SD3
	Deputy Chief of Staff, Research, Development, and Acquisition, Headquarters Department of the Army, Washington, D. C. 20310
1	ATTN: DAMA-ARZ-E
1	DAMA-CSS
	Commander, Army Research Office, P. O. Box 12211, Research Triangle Park, North Carolina 27709
1	ATTN: Dr. G. Mayer
1	Mr. J. J. Murray
	Commander, U. S. Army Materiel Development and Readiness Command, 5001 Eisenhower Avenue, Alexandria, Virginia 22353
1	ATTN: DRCQA-E
1	DRCQA-P
1	DRCDE-D
1	DRCDMD-FT
1	DRCLDC
1	DRCMT
1	DRCMM-M
	Commander, U. S. Army Electronics Research and Development Command, Fort Monmouth, New Jersey 07703
2	ATTN: DELSD-E, Mr. Stan Alster
	Commander, U. S. Army Missile Command, Redstone Arsenal, Alabama 35809
2	ATTN: DRSMI-TB, Redstone Scientific Information Center
1	Chief Scientist, Dr. W. W. Carter
1	Directorate of R&D
1	Dr. B. Steverding

No. of  
Copies

To

Commander, U. S. Army Troop Support and Aviation Materiel Readiness Command,  
4300 Goodfellow Boulevard, St. Louis, Missouri 63120  
1 ATTN: DRSTS-PLE, Mr. J. Corwin

Commander, U. S. Army Natick Research and Development Command,  
Natick, Massachusetts 01760  
1 ATTN: Technical Library  
1 Dr. E. W. Ross  
1 DRDNA-EM

Commander, U. S. Army Satellite Communications Agency, Fort Monmouth,  
New Jersey 07703  
1 ATTN: Technical Document Center

Commander, U. S. Army Tank-Automotive Research and Development Command,  
Warren, Michigan 48090  
1 ATTN: DRDTA-RKA  
2 DRDTA-UL, Technical Library

Commander, U. S. Army Tank-Automotive Materiel Readiness Command,  
Warren, Michigan 48090  
2 ATTN: DRSTA-Q

Commander, U. S. Army Armament Research and Development Command,  
Dover, New Jersey 07801  
1 ATTN: DRDAR-LC, Mr. E. Kelly  
2 DRDAR-TSS (STINFO)

Commander, White Sands Missile Range, New Mexico 88002  
1 ATTN: STEWS-WS-VT

Commander, U. S. Army Mobility Equipment Research and Development Command,  
Fort Belvoir, Virginia 22060  
1 ATTN: DRDME-D  
1 DRDME-E  
1 DRDME-G  
1 DRDME-H  
1 DRDME-M  
1 DRDME-T  
1 DRDME-TQ  
1 DRDME-V  
1 DRDME-ZE  
1 DRDME-N

Commander, U. S. Army Mobility Equipment Research and Development Command,  
4300 Goodfellow Boulevard, St. Louis, Missouri 63120  
1 ATTN: DRDME-PLC, Mr. J. Murphy

No. of  
Copies

To

Commander, U. S. Army Armament Materiel Readiness Command,  
Rock Island, Illinois 61201  
2 ATTN: DRSAR-QA

Commander, Rock Island Arsenal, Rock Island, Illinois 61299  
1 ATTN: SARRI-EN, Mr. W. M. Kisner

Commander, Chemical Systems Laboratory, Aberdeen Proving Ground,  
Maryland 21010  
1 ATTN: DRDAR-CLD, Mr. W. E. Montanary

Commander, ARRADCOM, Product Assurance Directorate, Aberdeen Proving Ground,  
Maryland 21010  
1 ATTN: DRDAR-QAC-E, Dr. W. J. Maurits

Commander, Watervliet Arsenal, Watervliet, New York 12189  
1 ATTN: DRDAR-LCB, Mr. T. Moraczewski  
1 Dr. T. Davidson

Commander, U. S. Army Aviation Research and Development Command,  
St. Louis, Missouri 63166  
1 ATTN: DRDAV-EXT  
1 DRDAV-ER, Dr. I. Peterson

Director, U. S. Army Industrial Base Engineering Activity,  
Rock Island, Illinois 61201  
1 ATTN: DRXPE-MT, Mr. D. Brim

Commander, Harry Diamond Laboratories, 2800 Powder Mill Road,  
Adelphi, Maryland 20783  
1 ATTN: DELHD-EDE, Mr. B. F. Willis  
1 Technical Information Office

Director, U. S. Army Ballistic Research Laboratory, Aberdeen Proving Ground,  
Maryland 21005  
1 ATTN: DRDAR-TSB-S (STINFO)  
1 Dr. D. Eichelberger

Commander, Picatinny Arsenal, Dover, New Jersey 07801  
1 ATTN: Feltman Research Laboratories

Chief, Benet Weapons Laboratory, LCWSL, USA ARRADCOM, Watervliet Arsenal,  
Watervliet, New York 12189  
1 ATTN: DRDAR-LCB-TL

Director, Eustis Directorate, U. S. Army Air Mobility Research and  
Development Laboratory, Fort Eustis, Virginia 23604  
1 ATTN: Mr. J. Robinson, DAVDL-E-MOS (AVRADCOM)

No. of Copies	To
1	Commander, U. S. Army Engineer School, Fort Belvoir, Virginia 22060 ATTN: Library
1	Commander, U. S. Army Engineer Waterways Experiment Station, Vicksburg, Mississippi 39180 ATTN: Research Center Library
1	Commander, U. S. Army Materiel Systems Analysis Activity, Aberdeen Proving Ground, Maryland 21005 ATTN: DRXSU-MP, H. Cohen
1	DRXSU-D, Dr. J. Sperazza
1	Commander, U. S. Army Research and Engineering Directorate, Warren, Michigan 48090 ATTN: SMOTA-RCM.1, Mr. Edward Moritz
1	Chief, Bureau of Ships, Department of the Navy, Washington, D.C. 20315 ATTN: Code 341
1	Chief of Naval Research, Arlington, Virginia 22217 ATTN: Code 471
1	Director, Structural Mechanics Research, Office of Naval Research, 800 North Quincy Street, Arlington, Virginia 22203 ATTN: Dr. N. Perrone
1	David Taylor Naval Ship Research and Development Laboratory, Annapolis, Maryland 21402 ATTN: Dr. H. P. Chu
1	Naval Research Laboratory, Washington, D.C. 20375 ATTN: C. D. Beachem, Head, Adv. Mat'ls Tech Br. (Code 6310)
1	Headquarters, U. S. Air Force/RDPI, The Pentagon, Washington, D.C. 20330 ATTN: Major Donald Sponberg
1	Headquarters, Aeronautical Systems Division, 4950 TEST W/TZHM (DH 2-5 Mgr), Wright-Patterson Air Force Base, Ohio 45433 ATTN: AFML-MATB, Mr. George Glenn
1	Dr. S. Tsai
1	Air Force Flight Dynamics Laboratory, Wright-Patterson Air Force Base, Ohio 45433 ATTN: AFFDL (FBE), G. D. Sendeckyj
1	National Aeronautics and Space Administration, Washington, D.C. 20546 ATTN: AFSS-AD, Office of Scientific and Technical Information

No. of  
Copies

To

- National Aeronautics and Space Administration, Marshall Space Flight Center,  
Huntsville, Alabama 35812  
1 ATTN: R. J. Schwinghamer, EHO1, Dir., M&P Lab
- National Aeronautics and Space Administration, Langley Research Center,  
Hampton, Virginia 23665  
1 ATTN: Mr. H. F. Hardrath, Mail Stop 188M
- Defense Materials Service, General Services Administration,  
Washington, D.C. 20405  
1 ATTN: Mr. Clarence A. Fredell, Director, Technical R&D Staff
- Lockheed-Georgia Company, 86 South Cobb Drive, Marietta, Georgia 30063  
1 ATTN: Materials & Processes Eng. Dept. 71-11, Zone 54
- 1 Dr. J. Charles Grosskreutz, Asst. Dir. for Research, Solar Energy Research  
Institute, 1536 Cole Boulevard, Golden, Colorado 80401
- Virginia Polytechnic Institute and State University, Department of  
Engineering Mechanics, 230 Norris Hall, Blacksburg, Virginia 24061  
1 ATTN: Prof. R. M. Barker
- 1 Southwest Research Institute, 8500 Culebra Road, San Antonio, Texas 78284
- IIT Research Institute, Chicago, Illinois 60616  
1 ATTN: Dr. I. M. Daniel
- 1 Dr. George R. Irwin, Department of Mechanical Engineering,  
University of Maryland, College Park, Maryland 20742
- Battelle Columbus Laboratories, 505 King Avenue, Columbus, Ohio 43201  
1 ATTN: Dr. E. Rybicki
- General Electric Company, Schenectady, New York 12010  
1 ATTN: Mr. A. J. Brothers, Materials & Processes Laboratory
- Westinghouse Research and Development Center, 1310 Beulah Road,  
Pittsburgh, Pennsylvania 15235  
1 ATTN: Mr. E. T. Wessel  
1 Mr. M. J. Manjoine
- Brown University, Providence, Rhode Island 02912  
1 ATTN: Prof. J. R. Rice
- Carnegie-Mellon University, Department of Mechanical Engineering,  
Schenley Park, Pittsburgh, Pennsylvania 15213  
1 ATTN: Dr. J. L. Swedlow

No. of  
Copies

To

---

1 Prof. J. Dvorak, Civil Engineering Department, University of Utah,  
Salt Lake City, Utah 84112

George Washington University, School of Engineering and Applied Sciences,  
Washington, D.C. 20052

1 ATTN: Dr. H. Liebowitz

Lehigh University, Bethlehem, Pennsylvania 18015

1 ATTN: Prof. G. C. Sih

Massachusetts Institute of Technology, Cambridge, Massachusetts 02139

1 ATTN: Prof. F. J. McGarry

University of Delaware, Department of Aerospace and Mechanical Engineering,  
Newark, Delaware 19711

1 ATTN: Prof. B. Pipes

1 Prof. D. Drucker, Dean of School of Engineering, University of Illinois,  
Champaign, Illinois 61820

1 Mr. Charles D. Roach, U. S. Army Scientific and Technical Information Team,  
6000 Frankfurt/Main, I. G. Hochhaus, Room 750, West Germany (APO 09710, NY)

State University of New York at Stony Brook, Stony Brook, New York 11790

1 ATTN: Prof. Fu-Pen Chiang, Department of Mechanics

E. I. Du Pont de Nemours and Company, Wilmington, Delaware 19898

1 ATTN: Dr. Alan R. Champion, Industrial Fibers Division,  
Textile Fibers Department

Lawrence Livermore Laboratory, Livermore, California 94550

1 ATTN: Dr. E. M. Wu

Director, Army Materials and Mechanics Research Center,  
Watertown, Massachusetts 02172

2 ATTN: DRXMR-PL  
1 DRXMR-PR  
1 DRXMR-PD  
1 DRXMR-AP  
6 DRXMR-TM, J. M. Slepetz